Evaluating Visual Field Phenotypes in Glaucomatous Patients with Cardiovascular Disease

Qingyun Wen
Faculty of Medicine and Health
The University of Sydney
2026

A thesis submitted to fulfill the requirements of the degree of Master of Philosophy.
This research was supported by an Australian Government Research Training Program (RTP) Scholarship.

Table of Contents

Evaluating Visual Field Phenotypes in Glaucomatous Patients with Cardiovascular Disease ***1***

Statement of Originality 3
Acknowledgements 4
Authorship Attribution Statement 5
Gen AI Attribution Statement 6
List of abbreviations 7
Abstract 9
Chapter 1. Cardiovascular Disease and Primary Open Angle Glaucoma 10
Chapter 2. Evaluating Visual Field Phenotypes in Glaucomatous Patients with Cardiovascular Disease 24
Chapter 3. Predicting Cardiovascular Disease from Glaucomatous Visual Fields Using Artificial Intelligence 39
Chapter 4. Artificial Intelligence Classification of 24-2 Visual Field Patterns in Glaucoma Rapid Progressors 50
Chapter 5. Concluding Thoughts 65
References 69
Appendices 101

Statement of Originality

This is to certify that the content of this thesis is my own work. This thesis has not been submitted for any other degree or purpose. I certify that the intellectual content of this thesis is the product of my own work, and that all assistance received in preparing this thesis and all sources have been acknowledged.

Qingyun Wen
28 November 2025

Acknowledgements

The completion of this thesis would not be possible without the support, guidance, and encouragement of many individuals, to whom I owe my deepest gratitude.

I would like to express my sincere appreciation to my supervisor, Associate Professor Andrew White, for his invaluable mentorship, patience, and unwavering support throughout this journey. I am truly grateful for the opportunities he has provided me and for believing in my potential.

I would also like to thank my co-supervisor Dr Gerald Liew for his expertise and time reviewing manuscripts.

I would like to extend my thanks to Yichuan Liang, who provided tremendous assistance with his time reviewing visual fields with me in Chapter 2 and his expertise on archetypal analysis in Chapter 4. I would also like to thank Dr Maitreyee Roy and MD Hasnat Riaz, who provided their expertise in constructing the artificial intelligence models in Chapters 3.

To Dr Thomas Chan and Anna Siu, many thanks for assisting with the data collected in this thesis.

Dr Karen Byth and Dr Sabrina Naz, many thanks for your guidance and assistance with the statistical analysis in Chapter 2.

Finally, I would like to acknowledge my parents, siblings, my partner and friends, for their endless understanding and encouragement through this journey. This achievement would not be possible without all of you.

Authorship Attribution Statement

Chapter 2 of this thesis has been presented as a poster at the Westmead Association Hospital Research Day in 2023 and at the Royal Australian and New Zealand College of Ophthalmologists Conference in 2024.

Chapter 3 has been presented as a poster at the Westmead Association Hospital Research Day in 2024 and at the Australian and New Zealand Glaucoma Society in 2026.

Chapter 4 has been presented as a poster at the Australian and New Zealand Glaucoma Society in 2025.

Gen AI Attribution Statement

During the preparation of the thesis, the author used Perplexity and Claude AI for the purposes of minimal copyediting. The use of these generative AI tools includes spelling and grammar checks, ensuring standardisation of abbreviations throughout and minor sentence restructuring to improve readability. The author confirms that where text was modified by generative AI, the content was reviewed for possible errors, inaccuracies, and bias. The author takes full responsibility for the submitted thesis, confirms the work is their own, and has used generative AI in accordance with University guidelines and policies.

List of abbreviations

Abbreviation	Full Term
AA	Archetypal analysis
AT	Archetype
AUC	Area under the curve
BMI	Body mass index
BP	Blood pressure
CCT	Central corneal thickness
CDR	Cup to disc ratio
CI	Confidence interval
CNN	Convolutional neural network
CVD	Cardiovascular disease
DBP	Diastolic blood pressure
DL	Deep learning
DM	Diabetes mellitus
EBS	Enlarged blind spot
HFA	Humphrey field analyser
HTG	High tension glaucoma
HTN	Hypertension
HVF	Humphrey visual field
IA	Inferior arcuate
IHD	Ischaemic heart disease
INS	Inferior nasal step
IOP	Intraocular pressure
LVH	Left ventricular hypertrophy
MAP	Mean arterial pressure
mGCIPL	Macular ganglion cell inner plexiform layer
MD	Mean deviation
ML	Machine learning
NTG	Normal tension glaucoma
OCT	Optical coherence tomography
ONH	Optic nerve head
OPP	Ocular perfusion pressure
OR	Odds ratio
PCA	Principal component analysis
PSD	Pattern standard deviation
POAG	Primary open angle glaucoma
pRNFL	Peripapillary retinal nerve fibre layer
RF	Random forest
RGC	Retinal ganglion cell
ROC	Receiver operating characteristic
ROS	Reactive oxygen species
RR	Relative risk
RSS	Residual sum of squares
SA	Superior arcuate
SAP	Standard automated perimetry
SBP	Systolic blood pressure
SD	Standard deviation

SITA	Swedish interactive thresholding algorithm
SNS	Superior nasal step
SVM	Support vector machine
VFI	Visual field index

Abstract

Although glaucoma is a leading cause of irreversible blindness, the pathophysiology of primary open angle glaucoma (POAG) is poorly understood. Emerging evidence points towards an association between cardiovascular disease (CVD) and POAG, with CVD reported as an independent risk factor for rapid disease progression. This thesis aims to further understand this relationship and to determine how baseline visual field characteristics relate to CVD and subsequent glaucoma progression.

First, existing literature on the relationship between CVD and POAG was reviewed. Further original studies were conducted: the exploration of baseline Humphrey Visual Field (HVF) phenotypes in POAG patients with CVD and other vascular risk factors, the use of artificial intelligence models to predict CVD status from HVFs, and the use of unsupervised archetypal analysis in identifying baseline HVF patterns in rapid and non-rapid POAG progressors.

CVD and other vascular risk factors may be associated with specific HVF phenotypes in POAG patients such as superior arcuate and central defects. Machine learning models outperformed deep learning models in predicting CVD status from HVF input. Archetypal analysis successfully identified clinically relevant HVF patterns in rapid and non-rapid progressors.

Chapter 1. Cardiovascular Disease and Primary Open Angle Glaucoma

1.1 INTRODUCTION

Glaucoma is the leading cause of irreversible blindness worldwide, affecting 3.54% of people aged 40-80. It is defined as a group of optic neuropathies that lead to damage of the optic nerve head (ONH) and characteristic patterns of vision loss. Within this group of optic neuropathies, POAG is the most common subset. Approximately 68.5 million individuals are affected by POAG and it is predicted that this will increase to 79.76 million by 2040 (Tham et al., 2014; Zhang et al., 2021).

The hallmark of glaucoma is the degeneration of retinal ganglion cells (RGCs) and their axons, with subsequent thinning of the retinal nerve fibre layer (RNFL), particularly in the peripapillary region which leads to cupping of the ONH (Kwon et al., 2009). The macula is also affected with thinning of the macular ganglion cell inner plexiform layer (mGCIPL) being equally diagnostic as pRNFL thickness for POAG (Mwanza et al., 2011). These structural changes eventually translate into functional disease with distinct patterns of vision loss, which are assessed in clinical practice using standard automated perimetry (SAP) on the Humphrey Visual Analyser (HFA), most commonly with 24-2 SITA strategies (McKendrick & Turpin, 2024).

Unfortunately, the underlying pathophysiology of POAG remains poorly understood. Elevated intraocular pressure (IOP) is the only established modifiable risk factor for glaucoma and is hypothesised to induce mechanical stress at the lamina cribrosa, disrupting axoplasmic flow and resulting in RGC apoptosis (Jonas et al., 2017; Weinreb et al., 2014). Even in patients with normal tension glaucoma (NTG), where the baseline IOPs are in the normal range, reducing IOP has been shown to slow disease progression (Collaborative Normal-Tension Glaucoma Study Group, 1998). Current glaucoma treatment therefore focuses on lowering IOP through pharmacological or surgical interventions. However, some patients continue to progress despite maximal IOP control, implying that there must be an alternate mechanism of RGC damage (Chan et al., 2017).

Vascular dysregulation has been raised as a key factor in the pathogenesis of POAG and NTG, with both in vitro and in vivo studies describing changes to the retinal microcirculation (Chan et al., 2017). Reduced ocular perfusion pressures (OPP) and impaired vascular autoregulation have been associated with an increased risk of OAG (Hulsman et al., 2007) and may exacerbate RGC vulnerability through ischaemia-reperfusion injury, even at IOP levels considered normal (Cherecheanu et al., 2013).

There is a growing body of literature that describes associations between POAG, NTG and systemic cardiovascular risk factors and disease, such as hypertension, dyslipidaemia, diabetes, ischaemic heart disease and vascular disease including

migraines and peripheral vasospasm. New technologies have also enabled better characterisation of the retinal microcirculation and ocular blood flow in POAG, as well as cellular processes such as oxidative stress and metabolomic biomarkers. This review aims to provide an overview of the systemic cardiovascular risk factors and localised vascular processes that have been described in POAG.

The next section summarises how glaucoma is diagnosed and monitored using structural imaging of the optic nerve and macula, alongside functional assessment with standard automated perimetry. Subsequent sections examine in detail how systemic CVD, ocular vascular changes, and cellular pathways may modulate glaucomatous damage. It is important to further understand these relationships to elucidate the role of CVD in the pathogenesis of POAG and identify potential therapeutic targets.

1.2 DIAGNOSIS AND MONITORING OF GLAUCOMA

Glaucoma diagnosis is based on the integration of patients' clinical profile, IOP measurements, characteristic structural damage to the ONH and RNFL and corresponding visual field defects. Clinicians assess the ONH for neuroretinal rim thinning, notching, enlarged cup-to-disc ratio (CDR) and evaluate structural loss using optical coherence tomography (OCT) scans of the peripapillary RNFL and macular ganglion cell complex. Functional vision loss is measured with SAP, which is the current gold standard for both diagnosis and longitudinal monitoring of glaucoma as it is standardised and has well-characterised diagnostic performance and progression algorithms.

Standard Automated Perimetry

SAP estimates differential light sensitivity at a grid of predefined test locations, and threshold values are compared against age-matched normative data. This generates probability maps to highlight locations with statistically significant visual field loss, along with global indices such as visual field index, mean deviation (MD) and pattern standard deviation (PSD). Automated static perimetry was originally developed with the Full Threshold strategy which required relatively long examinations of around 15 minutes per eye. This subsequently evolved to Swedish Interactive Threshold Algorithm (SITA) tests which shorten test time without sacrificing diagnostic performance. SITA tests use Bayesian priors and adaptive stopping rules to reduce test duration by up to half, though there is some trade-off in measurement variability, particularly in regions of existing glaucomatous damage and in more advanced disease (Artes et al., 2002; Chauhan et al., 2008; Rai et al., 2024; Tan et al., 2025). Modern devices such as the HFA use white-on-white static perimetry with Goldmann size III stimuli, typically presented on a 30-2 or 24-2 grid, and provide several SITA thresholding strategies (SITA Standard, SITA Fast, and SITA Faster). All visual field analyses in this thesis use 24-2 SITA-based HFA fields.

Limitations of SAP

There are some known limitations to SAP. Test-retest variability is minimal at normal or near-normal sensitivities but increases once sensitivities fall below the 19 dB range such as in areas of glaucomatous damage, which can obscure true progression and limit the usefulness of pointwise analyses in these areas (Gardiner et al., 2014). While physiological fluctuation can be a contributing factor, other causes include technical factors such as undersampling and fixation instability, even from small eye movements (Horani et al., 2007; Maddess, 2011, 2014).

In addition, SAP samples the field at relatively sparse locations and relies on a single white-on-white stimulus to estimate differential light sensitivities. This stimulus activates multiple RGC pathways at each test point (magnocellular, parvocellular and koniocellular), so the measured threshold at any location represents a composite response from all three pathways. If at least one pathway is relatively preserved and can compensate for damage in the others, this overlap can introduce redundancy and mask early loss of RGC function. This limits the ability of SAP to detect and localise subtle defects, or to identify selective vulnerability of each RGC pathway, and thus a significant amount of RGCs may be lost prior to any functional loss manifesting on SAP (Rai et al., 2024).

SAP is a subjective psychophysical test and is susceptible to patient fatigue, inattention and learning burden, which can all affect the accuracy of the test. Perimetric devices provide reliability indices including fixation losses, false-positive rates and false-negative rates. These provide a pragmatic indication of test quality to help clinicians interpret a test result, though it is important to acknowledge that the recent consensus on visual field assessment indicates that tests with poor reliability indices could still contain useful information on why the indices were poor National Academies of Sciences, Engineering, and Medicine, 2025). In this thesis, SITA fields were considered unreliable and excluded if fixation losses exceeded 20% or false positives exceeded 15%, based off the manufacturer's suggestion and off previous published work (Chan et al., 2017; Heijl, 2012).

A further limitation, highlighted by newer perimetric approaches, is that SAP primarily measures sensitivity and provides limited information about response timing, or 'delay'. Objective and eye-movement-based perimetry have shown that substantial delays in response can occur in areas with apparently normal SAP sensitivity, and that sensitivity and delay can show different spatial patterns and progression over time in optic neuropathies including glaucoma and multiple sclerosis, and other visual diseases such as diabetic retinopathy (Carle et al., 2011; Sabeti et al., 2024; Thepass et al., 2021; Yibekal et al., 2026). This suggests that sensitivity-only SAP may not fully capture all relevant aspects of functional vision loss.

Alternative Perimetric Methods

Alternative perimetric techniques have been developed to address limitations of SAP such as patient fatigue, test-retest variability and redundancy. Selective perimetry aims to focus on specific RGC subsets to identify functional loss earlier; short-wavelength automated perimetry uses a blue stimulus on a yellow background to bias responses toward the koniocellular/short-wavelength sensitivity pathway and has been reported to detect glaucomatous defects years before conventional SAP, though it is limited by longer test times and susceptibility to media opacities such as early cataract. Frequency-doubling technology perimetry targets magnocellular cells using stimuli at high temporal and low spatial frequency and can predict functional progression on SAP. There are several other subjective approaches including high-pass resolution perimetry, motion-based perimetry. Microperimetry incorporates SAP and a non-mydriatic fundus camera which tracks fundal landmarks to correct for any shifts in gaze to localise macular sensitivity to structural changes on OCT. Though these techniques offer valuable insights in specific clinical or research contexts, particularly in early or macular-predominant disease, their use is restricted by equipment availability and the lack of universally adopted normative and progression databases compared to SAP (Rai et al., 2024).

Objective perimetric methods attempt to circumvent the subjectivity and learning effects inherent to SAP by deriving functional information from electrophysiological or pupillary responses. Multifocal electroretinography and multifocal visual evoked potentials can map localised dysfunction in retinal and cortical responses, and multifocal pupillographic objective perimetry simultaneously tests both eyes and derives regional sensitivity and latency from pupil responses to multifocal stimuli (Di Russo et al., 2002; Hood et al., 2012; Maddess et al., 2024; Sabeti et al., 2017). Similarly, saccadic perimetry and related approaches such as the Standardised Oculomotor and Neurological Disorders Assessment measure visual sensitivities by analysing the latency and accuracy of eye movements towards briefly presented stimuli and provides information on both sensitivities and response delay. This has shown promising diagnostic performance in glaucoma and other retinal and neuro-ophthalmic diseases, with rapid protocols that can assess both eyes within 90 seconds, but they are not yet as widely standardised or embedded in routine glaucoma care as SAP (Vrijling et al., 2023, 2025).

Monitoring Glaucoma Progression

Monitoring glaucoma requires longitudinal structural and functional data. Detecting visual field progression is important because the goal of treatment is to preserve visual function, and OCT parameters can reach a measurement ‘floor’ in advanced disease. Event-based progression compares SAP tests such as HVFs and flags ‘possible’ or ‘likely’ progression when predefined criteria are exceeded, whereas trend-based methods model longitudinal change with global or pointwise indices, typically using linear regression on MD values. Both approaches are limited by test-retest variability, which is typically small at locations with near-normal sensitivities

but greater in locations with advanced disease. This can arise from patient factors such as learning, fatigue, or variability in the test administration and algorithmic features including Bayesian priors and special neighbourhood logic. Typically speaking, at least one SAP examination per year is required in routine glaucoma care to monitor progression with rapid commonly defined as a rate of change in MD of -1dB/year (Chauhan et al., 2014).

Archetypal Analysis

Beyond global indices, there is increasing interest in modelling glaucomatous visual field loss as combinations of recurring spatial patterns, or 'archetypes'. Archetypal analysis and related clustering approaches decompose SAP fields into weight sums of prototypical defect patterns, capturing the heterogeneity of glaucomatous damage and allowing more nuanced description of phenotype and progression than single global metrics (Cutler & Breiman, 1994; Elze et al., 2015; Thakur et al., 2020). These pattern-based methods can be integrated with event- and trend-based analyses and could provide a framework for analysing how systemic cardiovascular disease and other factors may associate with particular visual field archetypes, which will be a focus in *Chapter 4* of this thesis.

1.3 SYSTEMIC CARDIOVASCULAR RISK FACTORS AND GLAUCOMA

Cardiovascular Abnormalities

Glaucoma has been reported as an independent risk factor for incident CVD including coronary artery disease, myocardial infarct and ischaemic stroke. Choi et al. reported an increased risk of CVD in younger individuals with glaucoma – similarly, the Blue Mountains Eye Study had previously reported an association between glaucoma and increased CVD mortality in patients younger than 75. A large retrospective cohort study in Taiwan reported a significantly higher cumulative prevalence of ischaemic heart disease (IHD), heart failure and atrial fibrillation in patients with POAG than those without, with a hazard ratio of 2.32 for IHD (Chen et al., 2016).

Another study assessing vascular risk factors in patients with NTG described two phenotypes of patients: a) the Flammer syndrome, which tends to affect females with lower body mass index (BMI) and features nocturnal hypotension, migraines, Raynaud's, and reduced blood flow with cold provocation and b) metabolic syndrome, which tends to affect males and features higher BMI, hypertension, diabetes and obstructive sleep apnoea (Funk et al., 2022). Both phenotypes are thought to lead to reduced ocular perfusion pressures and subsequently retinal ischaemia. Interestingly, the Flammer syndrome has been found to be more common in NTG patients with lower IOPs, suggesting a role for autonomic dysregulation in these patients (Kim et al., 2014; Lee et al., 2017). Bariatric surgery has been associated with a reduced risk of POAG (RR 0.36) and use of IOP lowering medications (RR 0.565) (Russell et al., 2024).

CVD is not only associated with POAG prevalence, but is also a risk factor for disease progression (Leske et al., 1999; Dascalu et al., 2021; Chan et al., 2017; Marshall et al., 2021). Patients in a prospective study who had IHD had an odds ratio of 5.826 (p<0.01) for progression of their glaucomatous disease (Dascalu et al., 2021). Another study demonstrated that CVD was associated with rapid progression of glaucoma as measured through HVF testing (≥1 dB MD/year; OR 2.33, 95% CI [1.03, 5.27]). CVD was defined as hypercholesterolaemia, hypertriglyceridemia, arrhythmias, IHD, cerebrovascular disease and peripheral vascular disease. Patients with CVD who were rapid progressors had lower IOPs at baseline, suggesting that the effect of CVD on glaucoma progression was independent of the IOP pathway (Chan et al., 2017). The presence of CVD risk factors in another cohort of POAG patients (including HTN, SBP and anti-hypertensive therapies) was also predictive of functional progression (Marshall et al., 2021). Patients with paracentral VF defects were found to have higher genetic CVD risk scores (Marshall et al., 2022).

Cardiac abnormalities such as left ventricular hypertrophy (LVH), bradycardia and atrial arrhythmias have been associated with the presence of OAG, with LVH also showing a significant association with functional disease severity (Suzuki & Kiyosawa, 2022). A Mendelian randomisation study utilising the UK Biobank data demonstrated a potential causal relationship between atrial flutter and POAG, with no effect of atrial flutter on IOP (Lee & Seo, 2024). Interestingly, a Peruvian case study showed persistent structural progression of glaucoma despite maximal IOP-lowering therapy in a patient with CVD, with subsequent improvement in her glaucoma after cardiac catheterization, further implying a role for cardiovascular health in glaucoma (Valera-Cornejo et al., 2019). Increasing physical activity reduces the risk of incident glaucoma, and exercise has been shown to lower IOP acutely, likely through reducing oxidative stress (Meier et al., 2018)**.** A survey of US patients showed that 56.7% of glaucomatous patients had inadequate cardiovascular health as measured through a quantitative metric – every 1-unit increase in this metric was significantly associated with a reduced risk of glaucoma prior to adjusting for age, sex, education and income, suggesting a role for socioeconomics in addition to demographics in the relationship between CVD and glaucoma (De La Cruz et al., 2021).

Diabetes

Diabetes has been associated with an increased risk of POAG, up to 2 times as high as non-diabetic patients (Choi et al., 2023; Funk et al., 2022; Kolli et al., 2023; Lee et al., 2022; Manz et al., 2024; Trott, 2022; Ye et al., 2024). When stratifying patients by polygenic risk scores for POAG, the difference in diabetes prevalence and HbA1c levels between POAG patients and control cases was greater in patients with lower genetic risk for POAG than those with higher risk, suggesting a considerable environmental influence due to concomitant diabetic pathology (Kolli et al., 2023). Patients diagnosed with diabetes at an earlier age (<54) were also noted to have higher IOPs (Ye et al., 2024).

The use of diabetic medications has also been studied in patients with glaucoma. Patients with untreated Type 2 diabetes had an OR of 1.5 for POAG, whereas treatment with metformin was associated with a lower risk of POAG with an OR of 0.18. Interestingly, the cumulative lifetime risk for POAG was lower in patients on metformin than patients without a diagnosis of diabetes, implying a potential protective effect of metformin (Vergroesen et al., 2022). Conversely, a large Korean cohort study reported no statistical association between metformin use and the prevalence of POAG (Kim et al., 2024).

Systematic reviews have reported significant association between diabetes and glaucoma (Aldarrab et al., 2023; Zhao & Chen, 2017; Zhao et al., 2015; Zhou et al., 2014) with a 5% increase in risk of glaucoma for each year since diabetes diagnosis. However, there was considerable heterogeneity across the included studies. It has been suggested that there is a potential comorbid relationship between the two diseases, due to the overlap in risk factors particularly with endothelial dysfunction and vascular dysregulation (Gerber et al., 2015). Diabetic patients with glaucoma have lower retrobulbar flow in the central retinal artery and a trend toward higher retinal microcirculation flow in the inferior retinal sector, suggesting that diabetes influences the ocular vasculature in patients with open-angle glaucoma (Shoshani et al., 2012). High glucose levels in the aqueous humour has also been proposed to upregulate oxidative stress, inflammation and fibrosis pathways in the trabecular meshwork, leading to trabecular meshwork dysfunction and increased IOP (Singh et al., 2024). More research, particularly well-designed longitudinal and prospective studies, is required to further explore the interaction between diabetes and POAG pathogenesis.

Dyslipidaemia

The literature on dyslipidaemia and glaucoma is variable. Studies previously discussed in *Cardiovascular Abnormalities* have reported increased prevalence of dyslipidaemia and use of lipid lowering medications in POAG patients (Chen et al., 2016; Choi et al., 2023). Interestingly, POAG cases in the UK Biobank had higher odds of dyslipidaemia, but lower cholesterol and lower low-density lipoprotein (LDL) levels compared to control cases. This association did not significantly differ between patients with lower polygenic risk scores for POAG and patients with higher genetic risk for POAG, suggesting that this relationship is independent of any genetic predisposition towards POAG (Kolli et al., 2023). Other large scale population studies have also found increased prevalence of lipoprotein metabolism disorders in POAG patients (Lee et al., 2017; Manz et al., 2024).

The most common lipid-lowering medications are statins, which have also been studied as part of this relationship. Statins have pleiotropic effects; they reduce cholesterol biosynthesis and inflammatory cells in arteriosclerotic plaques. They also reduce isoprenoid intermediate production with a resulting increase in nitric oxide,

which is known to mediate vasodilation and therefore can increase ocular blood flow. They have previously been reported as protective against glaucoma (Ueda et al., 2024), with an 8% reduction in risk of glaucoma in patients taking statins >2 years (Stein et al., 2012) and a time-dependent reduction in glaucoma conversion and progression rates in patients taking statins > 10 years (Thiermeier et al., 2021). Other studies have reported no association between statin use and glaucoma prevalence as measured by IOP, mGCIPL or RNFL thickness – an initial significant association between statin use and retinal thinning was rendered non-significant after adjustment for BMI, SBP, DM and CVD, suggesting that these are important factors in that relationship (Kim et al., 2022). A case-control study in Australia reported an increased risk of glaucoma with statin use > 3 years, though data was not available to adjust for any confounding effects of serum hypercholesterolaemia (Yuan et al., 2023).

There is evidence for a positive correlation between dyslipidaemia and IOP, which could explain its association with POAG prevalence. Hyperlipidaemia can increase blood viscosity and episcleral venous pressure, leading to a reduction in aqueous humour outflow and subsequent increase in IOP (Wang & Bao, 2019). *CAV1/2* polymorphisms have also been associated with IOP – this gene encodes caveolin 1, which is involved in regulating cholesterol metabolism (Loo et al., 2023). In a large Korean epidemiological study of patients with no diagnosis of CVD or POAG, high IOP was associated with subclinical atherosclerosis regardless of conventional CVD risk factors such as age, smoking, family history (Ye et al., 2015). Total cholesterol (TC), LDL and high density liproprotein (HDL) were positively associated with corneal-compensated IOP in two large UK cohorts even after adjusting for BMI, diabetes and statin use (Madjedi et al., 2022).

A cohort study examining Chinese, Indian and Malay adults reported no association between TC, LDL and POAG. They found a negative association between total HDL3 and POAG independent of IOP, SBP, BMI and statin use. This association was replicated in Mendelian randomization analyses between HDL3 cholesterol and POAG genetic associations, suggesting a causal relationship (Nusinovici, 2022). HDL has been described as having atheroprotective effects and is involved in cholesterol transportation. *ABCA1* polymorphism has also been associated with POAG – this study proposed that impaired *ABCA1* function could lower HDL3 levels and increase cholesterol accumulation in the retina beyond a homeostatic level, thereby potentiating RGC apoptosis. It is worth noting that these two studies varied largely in their demographics, which could contribute to the different findings.

Despite the heterogeneity within studies evaluating the relationship between lipids and glaucoma, meta-analyses have reported positive associations between hypercholesterolaemia and glaucoma (Posch-Pertl et al., 2022; S. Wang & Bao, 2019). The association between hypercholesterolaemia and IOP was re-iterated,

with a pooled increase in IOP by 0.016 mmHg with every 10 mg/dL increase in blood triglyceride levels.

Blood Pressure, IOP and Glaucoma

Research suggests a complex relationship between blood pressure (BP) and POAG. While some large population based studies have reported a significant association between hypertension and POAG prevalence (Manz et al., 2024; Mitchell et al., 2004), others have reported an association between hypotension and POAG prevalence instead (Lee et al., 2022). The Singapore Epidemiology of Eye Disease described an U-shaped relationship between systolic blood pressure (SBP) and POAG prevalence, whereas the Los Angeles Latino Eye Study found an U-shaped relationship between diastolic blood pressure (DBP) and POAG (Memarzadeh et al., 2010; Tham et al., 2018). Meta-analyses have found a J-shaped relationship between BP and POAG – however, the effect of anti-hypertensive treatment was not isolated (Zhao et al., 2014).

A US based study similarly described an U-shaped relationship between both SBP and POAG prevalence and DBP and POAG prevalence in patients not on anti-hypertensive therapy – this relationship was not observed in those with anti-hypertensives, implying that anti-hypertensives could have a protective role against POAG, which has been supported by other studies (Horwitz et al., 2017; Kim & Choi, 2019). The use of calcium channel blockers (CCBs) have been associated with a slower rate of functional progression in POAG patients (Montesano et al., 2025). A systematic review of 11 studies reported an inverse association of beta blockers with IOP and POAG (Leung et al., 2023). However, it also reported that CCBs were associated with glaucoma, which could be due to CCB-induced vasodilation causing diversion of blood flow and ischaemia in vulnerable tissue (Vergroesen et al., 2022).

Meta-analyses have reported a positive association between BP and IOP, with an average increase in IOP by 0.26 mmHg and 0.17 mmHg for every 10 mmHg increase in SBP and DBP respectively (Nislawati et al., 2021; Zhao et al., 2014). Hypertension increases ciliary artery pressure and can lead to increased IOP due to increased aqueous humour production, and reduced outflow of aqueous humour due to increased episcleral vein resistance. Independent of IOP, chronic hypertension could also lead to increased peripheral resistance and small vessel disease, thereby reducing ONH perfusion (Kim & Choi, 2019). Hypotension is thought to cause a reduction in ocular perfusion pressure (OPP), since OPP is estimated to be the difference between SBP and IOP (Cherecheanu et al., 2013). This could explain the non-linear relationship between BP and POAG described by many studies.

BP variability with extreme dipping of both SBP and DBP have also been identified as significant risk factors for glaucomatous damage (Melgarejo et al., 2018, 2023). Patients with nocturnal dips or higher standard deviation of BP are at higher risk of progression (Bowe et al., 2015; Dascalu et al., 2021) – specifically, at higher risk of

faster functional loss (Pham et al., 2025). BP variability is also associated with poor functional outcomes in various cardiovascular diseases such as ischaemic stroke. Interestingly, patients with NTG were noted to have significantly increased BP variability compared to POAG patients, suggesting that this could play a larger role in the pathogenesis of glaucomatous damage in patients with normal or low IOPs (Lindemann et al., 2018). This is in keeping with the Flammer syndrome described in NTG patients, with characteristic features of nocturnal hypotension and autonomic dysfunction.

It is evident that there is a complex interplay between BP, IOP, POAG and NTG. Mendelian randomization analysis did not find a causal relationship between BP and IOP or BP and POAG, though this analysis relied on the assumption that there are no pleiotropic horizontal relationships between these variables (Plotnikov et al., 2022). It is possible that BP variability and subsequently, unstable ocular perfusion pressure and vascular dysregulation, could explain the inconsistent results reported in the literature regarding the relationship between these variables with the prevalence and progression of glaucoma.

1.4 OCULAR VASCULAR CHANGES AND GLAUCOMA

Ocular Perfusion Pressure

Ocular perfusion pressure (OPP) is calculated as the difference between two-thirds of the mean arterial pressure and IOP (OPP = (2/3 x MAP) – IOP) and is the driving pressure for ocular blood flow. Animal models have demonstrated that ocular blood flow is the primary determinant of RGC integrity, and increased BP provides short term protection for RGC survival by increasing OPP, whereas low BP exacerbates IOP-induced ischaemia (Dascalu et al., 2021) thus supporting the vascular theory of glaucoma pathogenesis.

Lower OPP is associated with an increased prevalence of POAG as well as more severe structural and functional disease (Omodaka et al., 2020). A meta-analysis of 43 studies found significantly lower OPP in POAG patients compared to controls, with the difference most evident in patients with baseline IOP greater than 21 mmHg (Kim et al., 2020). Similarly, ocular blood flow is significantly reduced in POAG and NTG patients compared to patients with just ocular hypertension and no glaucomatous disease (Bhagat et al., 2022). POAG patients are more likely to have lower OPP than patients with NTG, possibly due to the higher IOPs in POAG patients compared to NTG patients. Beyond absolute OPP levels, the instability of OPP emerges as a critical factor – both POAG and NTG patients with unstable OPP are more likely to experience disease progression (Lee et al., 2024; Melgarejo et al., 2018, 2023), and patients with end-stage glaucoma have the greatest OPP fluctuation (Ch'ng et al., 2021).

The pathophysiological mechanisms underlying OPP dysfunction in glaucoma involve impaired vascular autoregulation and neurovascular coupling. Experimental

human studies demonstrate abnormal ONH blood flow autoregulation during isometric exercise in POAG patients, indicating a compromised ability to regulate and maintain adequate ocular blood flow (Bata et al., 2019). This autoregulatory dysfunction, combined with breakdowns in neurovascular coupling, can convert episodic OPP reductions into chronic metabolic and ischaemic stress at the neurovascular unit level, hence contributing to glaucomatous optic neuropathy (Wareham & Calkins, 2020). The Flammer theory suggests that ischaemia and reperfusion damage caused by unstable ocular perfusion may play a central role in the vascular pathophysiology of POAG, with contributing factors including insufficient ocular blood flow due to autonomic nervous system dysfunction (Shin et al., 2022), atherosclerosis or other vascular factors such as diabetes (Shoshani et al., 2012) or endothelial cell dysfunction. Glaucoma patients have increased levels of endothelin-1, a potent vasoconstrictor, and autonomic dysfunction can trigger coronary vasospasm, underscoring the broader cardiovascular implications of glaucomatous vascular pathology.

Retinal Circulation and Nerve Fibre Thickness

The narrowing of retinal vessels and blood flow deficiencies in retinal, choroidal and retrobulbar circulations have been associated with POAG (Chan et al., 2017) with reduced optic nerve head vascular density in both POAG and NTG patients when compared to controls (Arish et al., 2024). In patients with single hemifield glaucomatous changes, the hemisphere corresponding to the affected hemifield had lower blood density compared to the hemisphere corresponding to the normal hemifield (Chen et al., 2017). Vascular parameters have been shown to be comparable to visual fields for diagnosing perimetric glaucoma (Kumar et al., 2016). Total retinal blood flow and oxygen extraction has been shown to be lower in POAG and associated with worse structural and functional disease, with no significant correlation between either the total retinal blood flow and IOP or total retinal oxygen extraction and IOP, suggesting an IOP-independent process (Garhöfer et al., 2022).

Retinal vessel diameter has also been associated with CVD, HTN and DM (Dervenis et al., 2019; Mitchell et al., 2005), with individuals with coronary artery disease demonstrating significantly lower vascular densities in the macula and a larger foveal avascular zone. The retinal circulation changes seen in glaucoma are thought to support the role of vascular dysfunction. However, it remains unclear whether vascular dysfunction leads to RGC death, or if RGC death results in reduced metabolic demand and subsequent changes in retinal circulation.

A comparison of RNFL circulation on optical micro-angiography between glaucomatous eyes and non-glaucomatous eyes revealed reduced vessel density and blood flow in the glaucomatous eyes, independent of RNFL thickness and without any functional defect. Retinal arteriole narrowing is also associated with glaucoma, with the narrowing occurring prior to the development of early-stage glaucoma (Kim et al., 2012). In NTG, reduced peripapillary vessel density was

associated with subsequent functional progression (Saks et al., 2023.). A separate study evaluating retinal blood flow using Doppler Fourier-domain OCT reported >1.62 dB change in MD with each dB reduction in blood flow (Hwang et al., 2012). Increased resistive index and reduced flow velocity in ophthalmic artery and central retinal artery were associated with structural progression on retinal tomography in glaucoma suspect and early glaucoma patients (Jimenez-Aragon et al., 2013). These results suggest that defects in retinal circulation could precede functional and structural changes in glaucoma, though causality could not be confirmed.

BMI and BP are known to be negatively associated with both mGCIPL and pRNFL thickness in patients without glaucoma (Von Hanno et al., 2022). Systemic arterial stiffness has previously been associated with reduced macular vessel density in NTG patients (Lee et al., 2021). A recent study found vascular wedge defects in 16% of glaucoma patients (Saks et al., 2023). These defects had corresponding focal RNFL loss and were associated with thinner pRNFL and mGCIPL – interestingly, there was no significant association between the vascular defects and CVD, implying that these defects could either be a direct consequence of glaucomatous damage, or could precede systemic vascular conditions.

The location of vascular dysfunction and structural damage could be of importance in glaucoma pathophysiology. Vessel density loss in the macula was significantly faster in glaucomatous eyes than non-glaucomatous eyes (Shoji et al., 2017). Within glaucomatous patients, mGCIPL thinning was found to precede pRNFL loss among those with lower IOP (Marshall et al., 2019). Higher systemic arterial stiffness was more likely to be associated with mGCIPL defects than pRNFL defects at baseline, even after accounting for IOP (Lee et al., 2022). Similarly, another study reported that POAG patients with predominantly mGCIPL thinning at baseline had a higher prevalence of hypertension and previous myocardial infarction compared to glaucoma suspect patients with no mGCIPL or pRNFL changes (Marshall et al., 2021). This difference was not replicated between patients with predominantly pRNFL thinning and the same reference group. The predictive value of CVD risk factors in structural progression was also explored in this study. Higher SBP was initially associated with pRNFL structural progression, but this relationship was attenuated after adjusting for age and IOP. Hypertension was associated with mGCIPL structural progression – specifically, a faster rate of mGCIPL thinning. Faster rates of mGCIPL thinning were also seen in patients with higher genetic CVD risk scores (Marshall et al., 2022).

It appears that there is an association between CVD and glaucomatous changes in the macula compared to the peripapillary region, independent of IOP. Alternate pathways of glaucomatous damage could potentially explain the difference in CVD risk factors i.e., the vascular theory could be implicated in patients with initial

structural damage at the macula rather than initial damage at the peripapillary region.

1.5 CELLULAR PROCESSES IN GLAUCOMA

On a cellular level, oxidative stress and inflammation have been reported to contribute to glaucoma pathogenesis. Reactive oxygen species (ROS), a group of highly reactive compounds including free radicals, are produced through endogenous sources such as the mitochondria and nicotinamide adenine dinucleotide phosphate (NADPH) oxidases. ROS are implicated in a range of cellular functions including proliferation, apoptosis, inflammation and gene expression, and can be produced as a physiological response to injury. However, excessive amounts of ROS can induce cellular damage. In POAG, it is proposed that an excessive amount of ROS causes damage to the trabecular meshwork, leading to extracellular matrix remodelling, thus increasing outflow resistance and IOPs (Saccà et al., 2020; Ung et al., 2017). Mitochondrial dysfunction further generates pathologic ROS and contributes to glaucomatous neurodegeneration. RGCs are highly metabolically active and rely on mitochondrial oxidative phosphorylation and redox homeostasis. Impaired mitochondrial ATP production sensitises RGCs to stressors such as elevated IOP and ischaemia-reperfusion insults. A mouse model demonstrated that glutamate transporter dysfunction and reduced glutathione made RGCs more vulnerable to excitotoxicity and oxidative stress even without elevated IOP (Harada et al., 2007), proposing that glutamate neurotoxicity and oxidative stress are important mechanisms of RGC death in NTG.

Metabolomic and biomarker studies show disrupted antioxidant enzymes, lipid-peroxidation product, antioxidant-related amino acids and inflammatory cytokines in aqueous humour, tear fluids and serum plasma (Wang et al., 2021). These further support the role of oxidative stress and inflammation in POAG, either through IOP regulation or by exacerbating RGC vulnerability even at normal IOP levels. The measurement of oxidative markers in tears/aqueous humor (malonyldialdehyde, 4-HNE, TAC), inflammatory mediators (TNF-α, IL-6), and proteomic/metabolomic candidates (ALDH1A1, RAD23B) can form a multimodal biomarker panel to assess for glaucomatous processes at a cellular level (Benoist d'Azy et al., 2016; Tang et al., 2019).

ROS are also implicated in CVD such as heart failure (Yu et al., 2012; Zhou & Tian, 2018). Endothelial dysfunction can lead to impaired autoregulation of OPP, leading to ischaemia-reperfusion which can increase ROS production, compounding oxidative and mitochondrial stress in RGCs. CVD and CVD-adjacent risk factors such as DM and HTN, along with impaired OPP could thus further amplify ROS generation and metabolic stress, accelerating glaucoma progression. This interplay highlights the need for integrated management strategies to address cardiovascular health and optimise outcomes for patients with POAG. More studies investigating genetic and molecular pathways could also further elucidate the temporal

relationship between CVD and glaucoma, and the causality of CVD risk factors (if any) with regards to glaucomatous disease.

1.6 CONCLUSION

Glaucoma is a complex and multifactorial disease with a significant burden on both quality of life as well as healthcare costs. Due to the lack of clarity surrounding its aetiology, therapeutic intervention remains limited to IOP-lowering strategies, which can be unsuccessful in preventing progression. It is imperative to better understand the disease process and identify further therapeutic targets.

There is evidence for a relationship between CVD and glaucoma, particularly with regards to glaucomatous damage in the macular region. Furthermore, CVD has been shown to a be an independent risk factor for rapid glaucoma progression. It is possible that there are multiple pathways through which RGC loss can occur, with oxidative stress and inflammation as a key cellular process in both POAG and NTG, contributing to both IOP-dependent and IOP-independent pathways. Understanding the relationship between CVD and glaucoma is essential for developing comprehensive treatment approaches that address both conditions simultaneously.

Though there is a growing body of literature on the specifics of glaucomatous structural progression in relation to CVD, there remains a paucity in literature with regards to the specifics of functional progression. This thesis aims to utilise HVF data from POAG patients to examine the relationship between POAG and CVD as well as other vascular risk factors, and to determine how baseline visual field patterns and archetypal representations of field loss relate to the risk of rapid disease progression.

Chapter 2. Evaluating Visual Field Phenotypes in Glaucomatous Patients with Cardiovascular Disease

ABSTRACT

PURPOSE

To investigate the relationship between glaucoma and CVD, by evaluating Humphrey Visual Field (HVF) defects in glaucomatous eyes with and without CVD.

METHODS

A retrospective chart review was carried out across five ophthalmology clinics in Sydney, NSW. Patients were included if they had five or more 24-2 HVFs and if they had a documented history of vascular risk factors (CVD, hypertension and diabetes). Fields were manually screened for the first identifiable glaucomatous defect and categorised into visual field phenotypes, then analysed with multinomial logistic regression against their vascular risk factors.

RESULTS

A total of 400 eyes were included (CVD = 258 eyes; no CVD = 142 eyes). Of these, 297 eyes had single defects allowing for multinomial logistic regression (CVD = 180 eyes; no CVD = 117 eyes). Eyes with any combination of vascular risk factors had significantly high odds of a superior arcuate defect than eyes with no risk factors (Odds Ratio [OR] 5.1-6.5; $p<0.05$). Eyes with CVD only were more likely to have a superior nasal step defect (OR 36.3; $p = 0.003$). Eyes with CVD and one other vascular risk factor (hypertension or diabetes) had higher odds of an inferior arcuate defect (OR 4.7; $p = 0.001$). Initial central defects were more likely in eyes with CVD and hypertension and/or diabetes.

CONCLUSION

Our findings suggest that CVD and other vascular risk factors are associated with specific visual field phenotypes in glaucoma, particularly superior arcuate and central visual field defects. Further analysis may allow clinicians to identify patients at risk of glaucoma progression or CVD through visual field testing.

2.1 INTRODUCTION

Glaucoma is the leading cause of irreversible blindness worldwide, affecting 3.54% of people aged 40-80. It is defined as a group of optic neuropathies that lead to damage of the ONH and characteristic patterns of vision loss. POAG is the most common subset, affecting approximately 68.5 million individuals and is predicted to affect 79.76 million by 2040 (Tham et al., 2014; Zhang et al., 2021).

The pathophysiology of glaucoma is not yet well understood. A popular theory is the vascular hypothesis, which proposes that vascular dysregulation and impaired ocular perfusion pressure are implicated in the disease process. There is a growing body of literature to support this, with studies demonstrating an association between CVD and other vascular risk factors with glaucoma prevalence and progression (Chan et al., 2017; Chen et al., 2016; Choi et al., 2023; Dascalu et al., 2021; Kolli et al., 2023; Marshall et al., 2021, 2022). However, the impact of CVD on visual field defects is unclear. Previous studies have explored the location of visual field defects in POAG, often comparing the subtypes of high-tension glaucoma (HTG), where the baseline intraocular pressure (IOP) is elevated, and normal-tension glaucoma (NTG), where the maximal untreated IOP is within the normal range. A recent systematic review summarises that POAG patients are more likely to have a nasal step defect, then paracentral scotomas and arcuate-like defects, whereas central defects are more common in NTG patients (Vandersnickt et al., 2024). Paracentral defects have also been associated with higher CVD genetic risk scores, though this study did not specify if other regions of functional vision loss were evaluated (Marshall et al., 2022). Although there is a body of literature addressing systemic risk factors associated with visual field defects, this study represents the first known effort to evaluate several multiple glaucomatous visual field phenotypes with a focus on CVD.

This chapter aims to further characterize the relationship between CVD and glaucoma by investigating visual field defects in individuals with POAG, coexisting CVD and other vascular risk factors.

2.2 METHODOLOGY

Data Collection

A retrospective chart review was conducted on patients from a private ophthalmology clinic in New South Wales, Australia with ethics approval obtained from the clinic board. The review covered charts from 1991 to 2015. All data was de-identified prior to analysis. This study was conducted in accordance with the tenets of the Declaration of Helsinki.

Patients were included if they had a diagnosis of glaucoma from the treating ophthalmologist, if they had ≥ five consecutive Humphrey 24-2 Visual Fields (HVF) for either eye and if a self-reported medical history was available. The presence or absence of hypertension (HTN), diabetes mellitus (DM), and CVD was recorded. Our definition of CVD aligns with previous published work which has reported CVD as a

significant risk factor for rapid glaucoma progression. This definition is outlined in Table 1. We isolated HTN from CVD as an independent vascular risk factor due to the high prevalence of HTN in our population and the substantial body of literature reporting variable associations between HTN and POAG. Patients who were diagnosed with glaucoma due to a secondary cause such as angle closure glaucoma were excluded. If both eyes satisfied the inclusion and exclusion criteria, they were included individually. Automated perimetry was performed on the Humphrey Visual Field Analyser Zeiss Meditec 740-16054-4.1 using the SITA standard or SITA fast protocol.

Table 1. Definition of cardiovascular disease (CVD).

Cardiovascular disease (CVD) was defined as the presence of one of more of the following conditions:
• Dyslipidaemia • Ischaemic heart disease • Valvular heart disease • Arrhythmias • Heart Failure • Cerebrovascular disease, including transient ischaemic attack • Vascular disease, including peripheral vascular disease and thromboembolic disease

Demographics including age, gender, and baseline ocular characteristics such as CDR, IOP measured with Goldmann applanation tonometry and central corneal thickness (CCT) were collected for each eye. Age was recorded as age at the first visual field test. Vascular risk factors were grouped into the following categories: a) no vascular risk factors, b) CVD only, c) CVD + HTN or CVD + DM, d) HTN +/- DM, no CVD and e) all three. This categorisation was chosen to isolate the independent effect of CVD on visual field phenotypes and assess synergistic effects of multiple vascular risk factors, as this could further influence ocular perfusion pressure and contribute to vascular dysregulation in POAG. DM was combined with HTN as an 'and/or' grouping due to the low percentage of eyes with DM alone in our cohort, which would have resulted in insufficient statistical power for meaningful analysis of DM as an independent category.

Visual Field Phenotypes

Visual fields were manually evaluated by two independent reviewers for the first field with an identifiable defect. VFI, MD and PSD parameters were recorded for each included field.

A 'defect' was defined based off the Hodapp-Parrish-Anderson criteria as a cluster of three or more points on the pattern deviation map, with at least one point depressed at a probability of less than 1% of occurring in the normal population (p<1%) (Hoddap et al., 1993). To create a standardised set of visual field phenotype definitions, common glaucomatous visual field abnormalities were drawn from the Ocular Hypertension Study classifications (Keltner et al., 2003) and work describing patterns of functional vision loss in glaucoma identified through regionally condensed

stimulus arrangements and archetypal analysis (Elze et al., 2015; Schiefer et al., 2010). These definitions were further refined in consultation with a glaucoma specialist prior to visual field analysis and simplified to allow straightforward classification of fields, including by non-glaucoma clinicians (Table 2; Figure 1). Given the relatively small dataset, the number of phenotypes was intentionally kept limited after discussion with the study statisticians.

Table 2. Definitions of visual field phenotypes.

1. Arcuate: a cluster of six or more points depressed at a probability of less than 2% of occurring in the normal population (*p<2%)*. These were further classified into superior or inferior based on the affected hemifield.
2. Central: a 'defect' where most or all points fall within the central 2x4 rectangle.
3. Nasal step: a 'defect' where most or all points fall within the 3x3 nasal triangle and directly abut the horizontal meridian. These were further classified into superior or inferior based on the affected hemifield.
4. Enlarged blind spot: a 'defect' directly adjacent to the blind spot.
5. Non-specific: a 'defect' present on two consecutive fields that does not satisfy any of the above categories.
6. No defect: assigned if none of the visual fields available exhibited an identifiable defect.

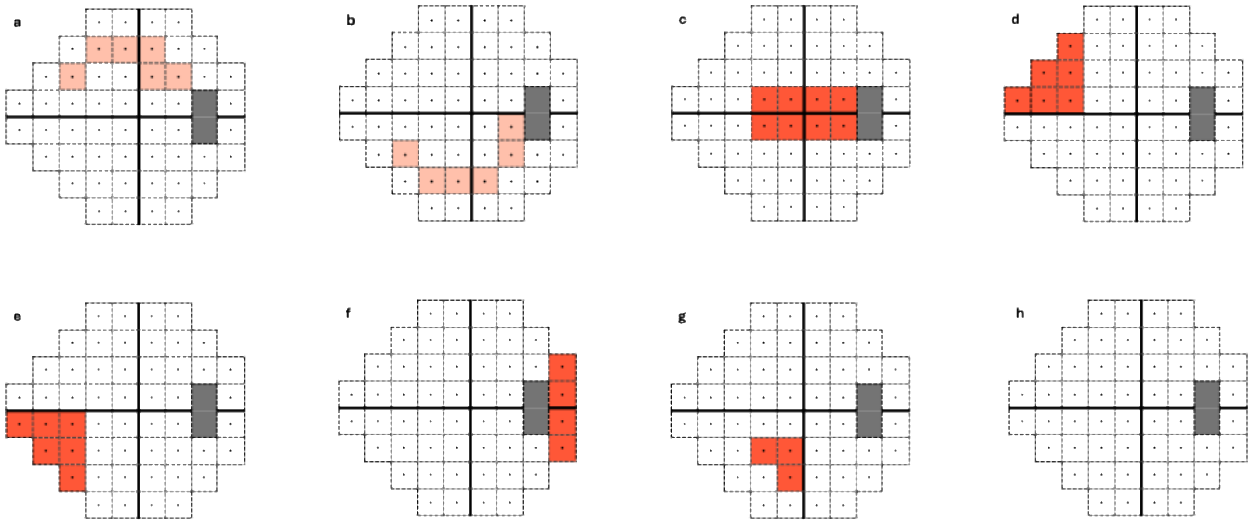

Figure 1. Schematics of visual field phenotypes with dark orange squares representing a point depressed at *p<1%* and light orange squares representing a point depressed at *p<2%.* All images are representative of a 24-2 field of the right eye, with the blue squares representing the physiological blind spot. From left to right: a) superior arcuate, b) inferior arcuate, c) central, d) superior nasal step, e) inferior nasal step, f) enlarged blind spot, g) non-specific defect and h) no defect.

If a field displayed more than one distinct defect, they were classified as a combination of all visible phenotypes e.g. superior arcuate + inferior nasal step. The exception was when these defects were contiguous in the same hemifield – for example, a contiguous superior nasal step + superior arcuate or contiguous superior arcuate + enlarged blind spot would be classified as just the superior arcuate.

Fields with fixation loss >20% or false positives >15% were considered unreliable and excluded from the screening process. These reliability indices were based on prior work, as discussed in *Chapter 1*. Any differences between the two reviewers regarding the classification of a visual field were resolved by discussion within a consensus panel.

Statistical Analysis
Statistical analyses were performed in IBM SPSS Statistics Version 29 (IBM, Armonk, NY). Demographics, baseline ocular characteristics and visual field parameters including rate of MD change in eyes with and without CVD were assessed. Eyes with a rate of MD change ≥ -1dB/year were considered rapid progressors. Normal distribution of the continuous variables (age, IOP, CDR, CCT, VFI, MD) was checked using skewness and kurtosis values, with data considered normally distributed if values were between -2 and 2. Normally distributed variables were compared using the independent samples t-test while non-normally distributed variables were compared using the Mann-Whitney test. Categorical variables were compared using the Chi-square test of proportions.

Multinomial logistic regression was used to model the relationship between the observed visual field phenotypes and the combination of systemic vascular risk factors. Specifically, the odds ratio (OR) was calculated for each observed visual field phenotype relative to 'no defect', for each combination of vascular risk factors in comparison to having no vascular risk factors. This analysis was performed on eyes with only a single observed defect. Given the small sample size, multivariable analysis adjusting for potential confounders was not feasible. Two-tailed tests with a significance level of $p<0.05$ were used throughout.

2.3 RESULTS

Approximately 5000 eyes were available for analysis. After excluding eyes with no reliable tests, no available baseline ocular characteristics or past medical history, or which demonstrated non-glaucomatous defects, a total of 400 eyes were included. 258 had a history of CVD and 142 did not have a history of CVD. Eyes with CVD were more likely to be older and have a history of hypertension or diabetes. They were also more likely to have a worse VFI and MD. There were no significant differences between gender distribution, baseline IOP, CDR or CCT between eyes with and without CVD (Table 3). Fields were mostly full-threshold SITA standard, with some SITA fast fields. The full range of observed visual field phenotypes, including the single defects defined in Figure 1, as well as phenotypes representing combinations of these defects, is presented in Figure 2.

Table 3. Demographics and ocular characteristics of eyes with and without cardiovascular disease. Note: continuous variables age, CDR and CCT analysed using independent samples t-test. IOP, VFI, MD analysed using Mann Whitney test. Figures rounded to 2 decimal points. * indicates statistical significance (*p<0.05*).

	CVD	No CVD	*p*
Total (number of eyes)	258	142	
Male (%)	108 (41.9%)	56 (39.4%)	0.64
Average age (in years)	66	61	<0.00*
Hypertension (%)	206 (79.8%)	59 (41.5%)	<0.00*
Diabetes (%)	65 (25.2%)	8 (5.6%)	<0.00*
Range of baseline IOP (mmHg)	7-36	10-30	
Average baseline IOP (mmHg ± SD)	20.5±5.0	20.4±4.0	1.0
Average baseline CDR	0.46	0.43	0.29
Average baseline CCT (µm ± SD)	531.8±35.6	537.9±39.0	0.16
Average VFI of included field	86.5	92.4	<0.00*
Average MD of included field (dB ± SD)	-6.2±5.6	-3.8±4.2	<0.00*
Rapid progressors with rate of MD loss ≥ 1dB/year	64 (24.8%)	22 (15.5%)	0.03*

A schematic of the observed visual field phenotypes is shown on the next page (Figure 2). The distribution of these phenotypes across all 400 eyes, along with the percentage of rapid progressors within each phenotype is shown in Table 4.

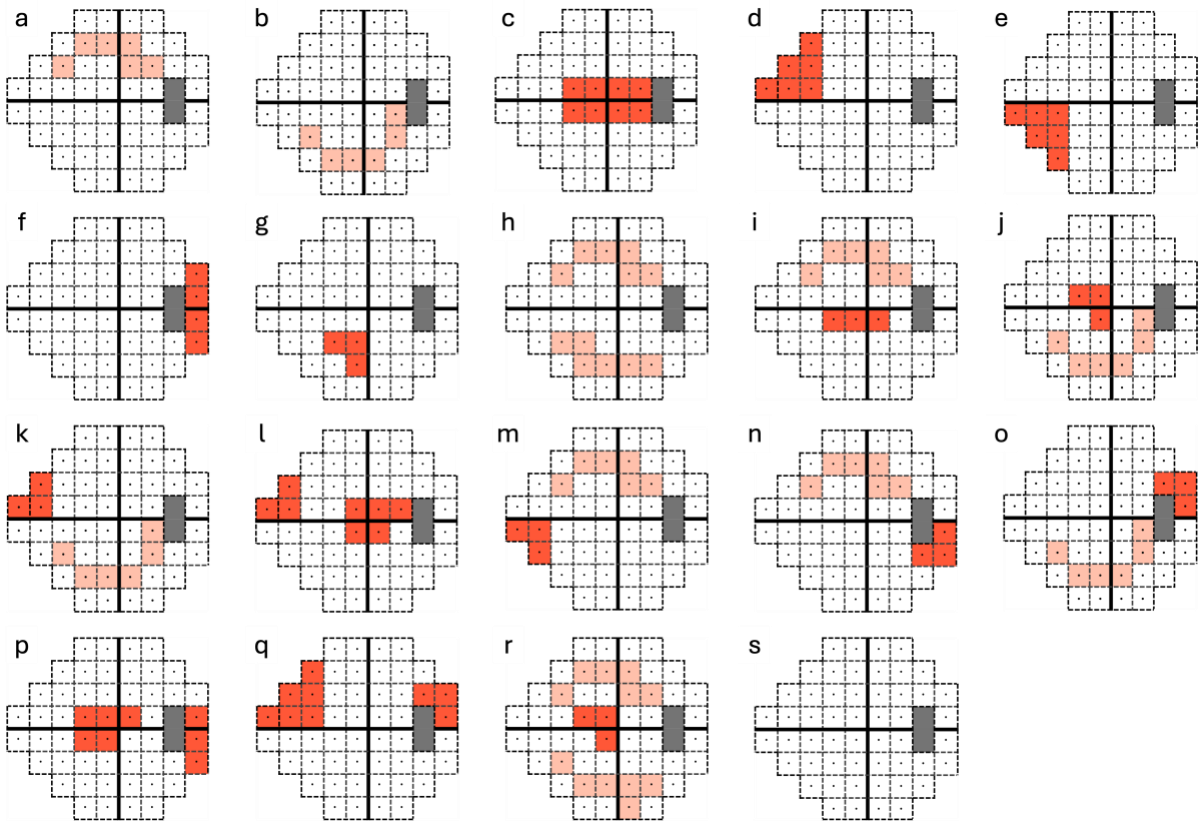

Figure 2. Schematics of visual field phenotypes observed in the 400 included eyes, with (a-g) and (s) as single defects and (h-r) as combination defects. (a-g) have previously been described in *Figure 1*. From left to right: h) superior arcuate+inferior arcuate, i) superior arcuate+central, j) central+inferior arcuate, k) superior nasal step+inferior arcuate, l) superior nasal step+central, m) superior arcuate+inferior nasal step, n) superior arcuate+enlarged blind spot, o) inferior arcuate+enlarged blind spot, p) central+enlarged blind spot, q) superior nasal step+enlarged blind spot and r) superior arcuate+inferior arcuate+central.

Table 4. Distribution of visual field phenotypes across all 400 eyes. Rapid progressors within each phenotype (defined as rate of MD loss ≥ 1dB/year) shown in the rightmost column as a percentage of eyes within the specified visual field phenotype.

Visual field phenotype	**Frequency**	**Percent**	**Rapid Progressors**
No defect	66	16.5%	3 (4.5%)
Superior arcuate (SA)	73	18.3%	23 (31.5%)
Inferior arcuate (IA)	56	14.0%	16 (28.6%)
Central	57	14.2%	9 (15.8%)
Superior nasal step (SNS)	12	3.0%	3 (25%)
Inferior nasal step (INS)	7	1.8%	1 (14.3%)
Enlarged blind spot (EBS)	19	4.8%	2 (10.5%)
Non-specific	7	1.8%	1 (14.3%)
SA+IA	14	3.5%	5 (35.7%)
SA+central	24	6.0%	14 (16.7%)
IA+central	30	7.5%	7 (23.3%)
IA+SNS	1	0.3%	0
Central+SNS	1	0.3%	0
SA+INS	1	0.3%	0
SA+EBS	1	0.3%	0
IA+EBS	1	0.3%	1 (100%)
Central+EBS	3	0.8%	1 (33.3%)
SNS+EBS	1	0.3%	0
SA+IA+central	26	6.5%	10 (38.6%)
Total	400	100%	

297 eyes (74%) had single defects only, with superior arcuate being the most common (n = 73), followed by no defect (n = 66). Nearly half of eyes (46%) in those with no CVD, HTN or DM had no defect. The most common defects in eyes with only CVD were superior arcuate (29.6%), superior nasal step (18.5%) and inferior arcuate (18.5%). In eyes with all 3 systemic risk factors (CVD, HTN and DM), 26.5% displayed a central defect, 23.5% a superior arcuate defect and 20.6% had no defect (Figure 3).

HVF Pattern	Vascular Risk Factors				
	Nil	CVD only	CVD+HTN, or CVD+DM	HTN and/or DM, no CVD	All 3
No defect	**29 (44.6%)**	4 (14.8%)	15 (12.6%)	11 (21.2%)	7 (20.6%)
Superior Arcuate	5 (7.7%)	**8 (29.6%)**	**36 (30.3%)**	**30.8%**	8 (23.5%)
Inferior Arcuate	12 (18.5%)	5 (18.5%)	29 (24.4%)	11.5%	4 (11.8%)
Central	10 (15.4%)	2 (7.4%)	25 (21.0%)	21.2%	**9 (26.5%)**
Superior Nasal Step	1 (1.5%)	5 (18.5%)	4 (3.4%)	3.8%	0 (0.0%)
Inferior Nasal Step	1 (1.5%)	1 (3.7%)	2 (1.7%)	3.8%	1 (2.9%)
Enlarged Blind Spot	5 (7.7%)	2 (7.4%)	5 (4.2%)	3.8%	5 (14.7%)
Non-specific	2 (3.1%)	0 (0.0%)	3 (2.5%)	3.8%	0 (0.0%)
Total	65 (100%)	27 (100%)	119 (100%)	52 (100%)	34 (100%)

Figure 3. Heat map detailing the distribution of observed visual field defects by combination of vascular risk factors. This heat map includes only the eyes with single defects (n = 297), which is the population on which multinomial logistic regression can be employed. The deeper the green, the more common is that defect for eyes with those risk factors.

For the 297 eyes with single defects, multinomial logistic regression was used to model the relationship between the observed visual field defect and the combination of vascular risk factors (Table 5). Non-specific defects were excluded from this analysis as there was no data for more than one category of vascular risk factors. A summary of demographics for this subgroup of eyes can be found in Appendix 1.

Eyes with CVD only were more likely to have a superior arcuate defect than patients with no vascular risk factors (OR 11.6; 95% confidence interval [CI] 2.5-53.6; p = 0.002). They were also more likely to have a superior nasal step defect (OR 36.3; 95% CI 3.3-395; p = 0.003). Eyes with CVD, HTN and/or DM were more likely to display a superior arcuate defect (OR 13.9; 95% CI 4.5-42.8; p < 0.001), an inferior arcuate defect (OR 4.7; 95% CI 1.9-11.7; p = 0.001) or a central defect (OR 4.8; 95% CI 1.8-12.7; p = 0.001) compared to the reference group. Eyes with HTN and/or DM but no history of CVD had higher odds of a superior arcuate defect (OR 8.4; 95% CI 1.9-11.7; p = 0.001). Eyes with all three vascular risk factors were more likely to show a superior arcuate defect (OR 6.6; 95% CI 1.7-26.6; p = 0.001) or a central defect (OR 3.7; 95% CI 1.1-12.6; p = 0.035).

Table 5. Odds ratios (ORs) as calculated using multinomial logistic regression for each observed visual field phenotype relative to 'no defect', for each combination of vascular risk factors compared to eyes with no risk factors. Note: "na" not applicable because there were zero patients in the 'All 3" risk group.

Visual Field Phenotype	Vascular Risk Factors	Odds Ratio	95% CI for OR		p-value
			Lower	Upper	
Superior Arcuate 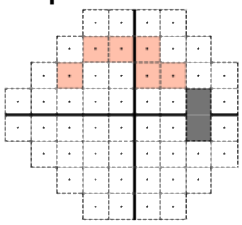	**All 3 vs Nil**	6.6	1.7	26.6	**0.01***
	(HTN and/or DM, no CVD) vs Nil	8.4	2.5	28.6	**0.01***
	(CVD+HTN or CVD+DM) vs Nil	13.9	4.5	42.8	**<0.01***
	(CVD only) vs Nil	11.6	2.5	53.6	**<0.01***
	Nil (reference)	1	reference category		
Inferior Arcuate 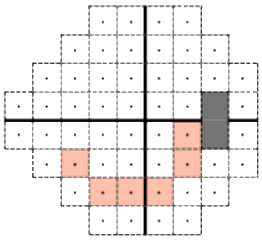	**All 3 vs Nil**	1.4	0.3	5.6	0.65
	(HTN and/or DM, no CVD) vs Nil	1.3	0.4	4.4	0.65
	(CVD+HTN or CVD+DM) vs Nil	4.7	1.9	11.7	**<0.01***
	(CVD only) vs Nil	3.0	0.7	13.2	0.14
	Nil (reference)	1	reference category		
Central 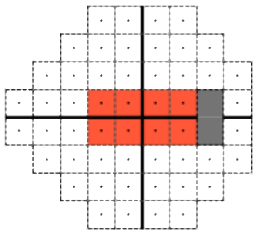	**All 3 vs Nil**	3.7	1.1	12.6	**0.04***
	(HTN and/or DM, no CVD) vs Nil	2.9	1.0	8.7	0.06
	(CVD+HTN or CVD+DM) vs Nil	4.8	1.8	12.7	**<0.01***
	(CVD only) vs Nil	1.5	0.2	9.2	0.69
	Nil (reference)	1	reference category		
Superior Nasal Step 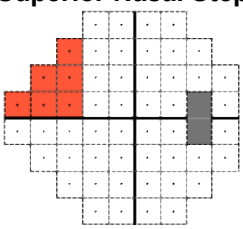	**All 3 vs Nil**	na	na	na	Na
	(HTN and/or DM, no CVD) vs Nil	5.3	0.4	64	0.19
	(CVD+HTN or CVD+DM) vs Nil	7.7	0.8	75	0.078
	(CVD only) vs Nil	36.3	3.3	395	**<0.01***
	Nil (reference)	1	reference category		
Inferior Nasal Step 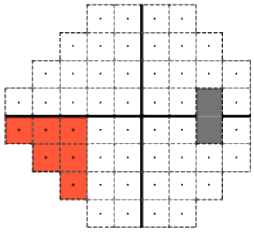	**All 3 vs Nil**	4.1	0.2	75	0.34
	(HTN and/or DM, no CVD) vs Nil	5.3	0.4	64	0.19
	(CVD+HTN or CVD+DM) vs Nil	3.9	0.3	46	0.29
	(CVD only) vs Nil	7.3	0.4	140	0.19
	Nil (reference)	1	reference category		
Enlarged Blind Spot	**All 3 vs Nil**	4.1	0.9	18.4	0.06
	(HTN and/or DM, no CVD) vs Nil	1.1	0.2	6.3	0.95
	(CVD+HTN or CVD+DM) vs Nil	1.9	0.5	7.7	0.35

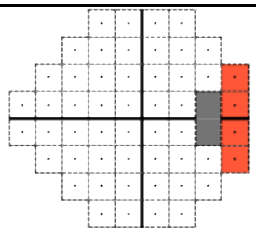	**(CVD only) vs Nil**	2.9	0.4	20.3	0.28
	Nil (reference)	1	reference category		

In supplementary analyses, the distribution of VF defects was also evaluated at a 'per defect' level instead of a 'per eye' level. This meant that an eye with a combination of visual field patterns such as 'SA+central' was classified into both 'Any SA' and 'Any Central'. A total of 525 defects were observed. 'No defect' remained the most common phenotype in patients with no vascular risk factors. 'Any Central' remained the most common pattern in patients with all three vascular risk factors and 'Any SA' remained the most common pattern in all other risk factor combination groups. Multinomial logistic regression was used to calculate the odds ratios for our 'per defect' analysis for interest, though the lack of independence means this is an inherently flawed analysis and not reliable (Appendix 2). Similar results were obtained compared to our 'per eye' analysis.

2.4 DISCUSSION

In this study, we identified common patterns of visual field defects in glaucomatous eyes in relation to underlying vascular risk factors. In the population studied, eyes with CVD tended to be older, have co-existing hypertension or diabetes and had worse VFI and MD parameters on their baseline visual field relative to eyes without a history of CVD. There was also a greater number of rapid progressors in eyes with CVD than eyes without.

Vascular risk factors including ischaemic cardiac disease and arterial hypertension have been associated with glaucoma progression (Dascalu et al., 2021), with systolic blood pressure exhibiting comparable effects to IOP on structural progression (Marshall et al., 2021). CVD has also been reported as an independent risk factor for rapid progression (Chan et al., 2017), which our results confirm. The poorer baseline VFI and MD in CVD eyes without any significant difference in baseline IOP further supports this association.

We found that eyes with any combination of vascular risk factors – CVD alone, HTN and/or DM without CVD, CVD and HTN or DM, and all three – had significantly higher odds of an initial superior arcuate defect. Eyes with CVD alone were also more likely to have an initial superior nasal step defect, with an odds ratio of 36.3. Eyes with CVD and HTN and/or DM had higher odds of demonstrating an initial inferior arcuate or initial central defect. Eyes with all three risk factors were also more likely to have an initial central defect.

Superior Visual Field Defects

Glaucoma typically affects one hemifield initially (Germano et al., 2022), with several studies reporting that superior visual field defects are more common(Jiang et al., 2021; Singh & Rijal, 2020; Vandersnickt et al., 2024; Yousefi et al., 2018), particularly superior nasal step or superior arcuate patterns (Ballae Ganeshrao et al., 2019). In our study, superior defects were more common. Eyes with any vascular risk factor had significantly higher odds of a superior arcuate defect than eyes without any risk factors. This aligns with previous work reporting that arcuate defects were associated with HTN (Kosior-Jarecka et al., 2017).

Eyes with CVD alone showed remarkably high odds (OR 36.3) for an initial superior nasal defect, but there was no significant relationship between a superior nasal step and HTN or DM. In contrast, a previous study reported that superior nasal step patterns were more likely to have HTN and DM and progress centrally (Kim et al., 2015). This may reflect methodological differences, as we classified any superior nasal steps contiguous with a superior arcuate as a superior arcuate phenotype. Alternatively, this suggests that nasal fibre bundles are more vulnerable to CVD than HTN or DM. Park et al. found initial nasal step defects were associated with higher IOP compared to initial central scotomas – in our study, CVD included dyslipidaemia, which has been reported to have a positive association with IOP (Posch-Pertl et al., 2022; S. Wang & Bao, 2019). This relationship may contribute to the presence of an initial nasal step in eyes with CVD alone, though we found no significant difference in baseline IOPs between CVD and non-CVD eyes.

The predominance of superior visual field defects could be explained by the vulnerability of the inferotemporal ONH (Singh & Rijal, 2020), which corresponds retinotopically to superior visual field regions (Garway-Heath et al., 2000). The lamina cribrosa experiences maximal shear strain in the inferior and temporal quadrants (Midgett et al., 2017), and most commonly has focal defects in the inferotemporal region with corresponding RNFL thinning (Tatham et al., 2014). This area also has the highest prevalence of choroidal microvasculature dropout, which is thought to indicate reduced optic nerve perfusion (Jo et al., 2019; A. Lee et al., 2022). The shear strain on the lamina cribrosa is a key factor in the mechanical theory of glaucomatous damage – the mechanical vulnerability of the inferotemporal ONH may be further exacerbated by vascular dysfunction, thus leading to the relationship between superior visual field defects in our study and cardiovascular risk factors.

Other studies have reported no significant difference in HTN or DM prevalence between superior and inferior hemifield defects (Takeuchi et al., 2019), or between nasal steps and parafoveal scotomas (Kang et al., 2015; Park et al., 2011). These discrepancies may arise from different study methods, patient selection criteria, glaucoma subtype classifications, or because IOP-dependent and independent

factors may not operate exclusively in the development of visual field patterns. Our study design is unique as a) we compared each defect pattern to 'no defect' rather than comparing between defects, and b) we focused on defect patterns by vascular risk factor status rather than examining the differences between glaucoma subtypes.

Central Defects

Central visual field loss within 5-10 degrees of fixation can occur early in glaucoma (Germano et al., 2022; Singh & Rijal, 2020). Patients with central visual field defects are more likely to have NTG with a lower maximal IOP (Thonginnetra et al., 2010; Vandersnickt et al., 2024), thinner RNFL, lower ocular perfusion pressures, and systemic vascular factors including hypotension, migraine, autonomic dysfunction (Chen et al., 2025) and Raynaud's phenomenon (Park et al., 2011). They are at higher risk of rapid progression (Garg et al., 2018; Jackson et al., 2023) and have greater longitudinal decline in their quality of life (Abe et al., 2016).

We found that patients with CVD and at least one other vascular risk factor (HTN or DM) have significantly higher odds of a central defect compared to patients with no risk factors or with CVD alone. Similarly, Jung et al. demonstrated that parafoveal scotomas were significantly linked to systemic vascular disease, including HTN and cerebrovascular disease (p <0.05). Central visual field progression has been associated with HTN and DM in early glaucoma (Kim et al., 2015) and systemic antihypertensive use in advanced glaucoma (Sugisaki et al., 2022). Marshall et al. demonstrated that paracentral visual field defects in POAG are associated with higher CVD genetic risk scores (OR 1.85, p = 0.01) (Marshall et al., 2022).

Vascular risk factors preferentially affect the macular region. Patients with predominant mGCIPL thinning are older, have higher CVD genetic risk scores with lower IOP (Marshall et al., 2022), or larger vertical CDR without any significant difference in IOP (Park et al., 2023), suggesting an IOP-independent mechanism of damage. mGCIPL thinning has been associated with arterial stiffness (OR 7.48) (Lee et al., 2022), and rapid macular ganglion cell complex thinning correlates directly with faster rates of central visual field decline (Mahmoudinezhad et al., 2023), establishing a clear structure-function relationship in glaucomatous damage.

Vascular density in the parafoveal retina is decreased in POAG patients (Tao et al., 2020). Narrower retinal arteriolar diameter (Yoo et al., 2017) and impaired parapapillary choroidal perfusion is significantly associated with an initial parafoveal scotoma (Lee et al., 2018), subsequent functional progression, and higher rates of functional loss (Lee et al., 2021). Hypoperfusion to the optic nerve head is implicated, however further research is required to establish whether vascular insufficiency to the ONH causes cell death or if reduced metabolic demands lead to vascular dropout.

Other studies have reported conflicting findings: no significant difference in arrhythmias, orthostatic hypotension and DM between patients with parafoveal and nasal step scotomas (Park et al., 2011), or inverse relationships between central visual field defects, DM (Kosior-Jarecka et al., 2017) and HTN (Kim et al., 2015). These results were obtained by comparing central defects to peripheral defects, whereas our study compared each defect pattern against no defect. Kim et al. propose that early-stage HTN increases ocular perfusion pressure, preserving macular blood flow and initial central function. As HTN duration increases, the macular becomes more vulnerable, which is supported by the significant relationship between HTN and central progression.

We isolated HTN from CVD, whereas other studies reporting associations between CVD, macula thinning, and glaucoma progression have included HTN within their CVD definitions (Marshall et al., 2021, 2022). Our analysis reveals that the established CVD combined with additional vascular risk factors creates a synergistic effect that particularly predisposes to central visual field involvement. This patient population may experience IOP-independent mechanisms such as ischaemia and reperfusion damage caused by unstable ocular perfusion pressures, which could preferentially damage the macula and result in a central visual field defect.

Strengths and Limitations
To our knowledge, this is the first study to characterise multiple visual field phenotypes in glaucomatous patients with a primary focus on CVD. Patients were recruited from a real-world clinical setting, reflecting a spectrum of disease severity at baseline, thereby enhancing the study's clinical relevance and translational potential.

Study limitations include the retrospective design, small sample size, lack of structural data and reliance on self-reported medical history. Details on ethnicity, history of migraines, family history of glaucoma and OCTs were not available for a portion of patients. Exclusion of low reliability fields may have affected the initial included defect. Information on the duration of vascular risk factors, HTN severity, blood pressure parameters and systemic medications were not available. The lack of significance and wide confidence intervals in our multinomial logistic regression can be attributed to small sample size for some of the observed visual field phenotypes, which limits the statistical power of the analyses. The small sample size precluded multivariable analysis to adjust for possible confounders such as age, gender, and baseline IOP.

Finally, it should be noted that this analysis only demonstrates an association between visual field phenotype and CVD and vascular risk status but does not prove causality.

Future directions should use a larger prospective cohort with multivariable analysis, integrate structural data, and verify medical history with general practitioners or using genetic risk scores to increase the accuracy of the ‘CVD’ label. Additional analyses could examine differences between HTG and NTG subgroups, differentiate superior and inferior central defects, and include 10-2 fields. Receiver operating characteristic (ROC)-based performance metrics can be incorporated to formally assess the predictive utility of visual field phenotypes in CVD status.

2.5 CONCLUSION

In summary, patients with cardiovascular risk factors are more likely to show an initial superior arcuate, superior nasal step or central defect on 24-2 HVF testing. Distinguishing these visual field phenotypes may allow clinicians to identify patients at risk of rapid progression and who may benefit from further workup for CVD risk factors.

Chapter 3. Predicting Cardiovascular Disease from Glaucomatous Visual Fields Using Artificial Intelligence

ABSTRACT

PURPOSE

This study aims to evaluate the performance of machine learning (ML) and deep learning (DL) models in predicting underlying CVD from HVFs of POAG patients.

METHODS

Patients were recruited if they had a diagnosis of POAG and at least five 24-2 HVFs per eye. CVD history was documented for each patient. The earliest HVF with a detectable glaucomatous defect was selected per eye, and PD maps were extracted. These were used to train two ML models Random Forest (RF) and Support Vector Machine (SVM) and two DL models (ResNet, custom CNN) to classify eyes as CVD-positive or CVD-negative. The dataset (393 eyes from 200 patients: 252 CVD-positive, 141 CVD-negative) was split into training and testing sets (3:1 ratio), with data balancing applied to the training set.

Additional OCT data was available for a subset of patients. HVF-OCT data was processed as a single fused-input and as parallel inputs to train ML model RF and DL model FusionNet. The dataset (135 eyes: 82 CVD, 53 non-CVD) was split into training (64%: 53 CVD, 33 non-CVD), validation (16%: 13 CVD, 9 non-CVD) and testing (20%: 16 CVD, 11 non-CVD) sets.

RESULTS

Model performance for the HVF only data, as summarised by the area under curve (AUC) of the receiver operating characteristics (ROC) curve, was as follows: SVM (0.73), custom CNN (0.70), RF (0.69) and ResNet 18 (0.60). The ML model SVM had the best overall performance.

For the HVF-OCT data, RF produced an AUC of 0.64 for the single fused input and 0.60 for parallel inputs. FusionNet had an AUC of 0.66 for parallel inputs.

CONCLUSION

Artificial intelligence can detect CVD signals from HVF at above-chance levels (AUC>0.5). The traditional ML model SVM outperformed DL approaches. Multimodal input with OCT ONH data did not improve model performance. These findings suggest that HVF data contain information related to CVD status, but current performance is insufficient for standalone clinical screening and should be viewed as proof-of-concept only. Future studies should assess if model performance can be improved with larger datasets.

3.1 INTRODUCTION

Artificial intelligence is an emerging field across all healthcare domains, including ophthalmology. Both machine learning and deep learning models have been trained to assess HVFs and detect glaucoma, grade disease severity, classify visual field patterns, and even predict future HVFs (AlShawabkeh et al., 2024; Chen et al., 2023; Huang et al., 2023; Tian et al., 2023; Wen et al., 2019). These tools are valuable in reducing clinicians' workload, in a field where the patient population grows exponentially each year (Tham et al., 2014).

Deep learning models have also been trained to detect CVD risk from retinal images, demonstrating that systemic vascular health can be screened for using non-invasive ocular imaging (Hu et al., 2025; Kamalzadeh et al., 2025). These results support the idea that the retinal microvasculature is related to broader systemic vascular disease. This allows identification and risk-stratification of patients who may a) experience rapid glaucoma progression (Chan et al., 2017) and/or b) CVD and cardiovascular events. However, to our knowledge, the use of machine learning or deep learning models in detecting CVD directly from HVF data has not been previously explored.

We previously identified patterns of functional vision loss which were more common in specific vascular risk factor profiles in *Chapter 2*, which aligns with increasing evidence that CVD and vascular health is implicated in POAG pathophysiology. These findings raise the possibility that the severity and/or spatial configuration and visual field loss in POAG may carry latent signatures of underlying systemic vascular disease.

The aim of this chapter is to therefore explore whether artificial intelligence can predict CVD from HVF data, and whether combining functional HVF data with structural OCT data of the retinal nerve fibre layer (RNFL) at the ONH can improve model performance. This provides a proof-of-concept analysis of whether HVFs contain systemic vascular information beyond their traditional role of monitoring functional visual data.

3.2 METHODOLOGY

Study Design and Participant Recruitment

A retrospective review was conducted on patients from a private glaucoma clinic in New South Wales, Australia, between the period 1991 to 2015. Ethics approval was granted by the clinic board, and the study was conducted in accordance with the tenets of the Declaration of Helsinki. Patients were included if they had a diagnosis of POAG from a glaucoma specialist, at least five 24-2 HVF tests per eye, and a documented history of CVD (as defined in *Chapter 2*; see Textbox 1) in their clinic notes. HVF data in this chapter were drawn from the same cohort and testing protocol as *Chapter 2*: automated perimetry was performed on the HFA (Zeiss Meditec 740-16054-4.1) using the SITA Standard or SITA Fast protocol in a 24-2

grid, and the same reliability criteria (fixation losses ≤20%, false positives ≤15%) were applied.

Textbox 1. Definition of cardiovascular disease (CVD).

Cardiovascular disease (CVD) was defined as the presence of one or more of the following conditions: dyslipidaemia, ischaemic heart disease, valvular heart disease, arrhythmias, heart failure, cerebrovascular disease (including transient ischaemic attack) and vascular disease including peripheral vascular disease and thromboembolic disease.

This study comprised two phases. Phase 1 analysed HVF data exclusively to assess if CVD status could be predicted from HVF data alone. Phase 2 examined a subset of patients who had OCT ONH scans in addition to HVF data, to determine whether integrating functional (HVF) and structural (OCT) measures could improve classification performance.

Phase 1: HVF analysis

Data Collection and Preprocessing

For each eligible eye, the earliest reliable HVF test with a glaucomatous defect was selected to capture the patient's baseline function at disease onset. If there was no glaucomatous defect across all fields, the most recent HVF was included instead. Pattern deviation values were extracted using *Matlab2023b*. Numeric pattern deviation values were used instead of pattern deviation plots to capture the exact decibel deviation at each test location for use as model input features. This produced 52-element vectors, each containing the threshold sensitivities at the 52 test locations in the 24-2 HVF protocol.

All blank spots, including locations outside the test region and the blind spot, were represented as NaN values to pad the 52-element vector to an 80-element vector corresponding to an 8x10 matrix (Figure 1). During training, NaN entries were replaced with the sentinel value '9999'. This value was chosen to be distinct from physiologically plausible sensitivity values (0–40 dB). The matrices were then flattened into a one-dimensional vector of length 80 in sequential order, preserving the spatial ordering of test locations for compatibility with machine learning algorithms. Each HVF vector was assigned a binary label: 1 for eyes with CVD and 0 for eyes without CVD. HVF data were processed as vectorised feature vectors rather than explicit spatial image tensors; consequently, horizontal flipping of left-eye HVFs was not performed.

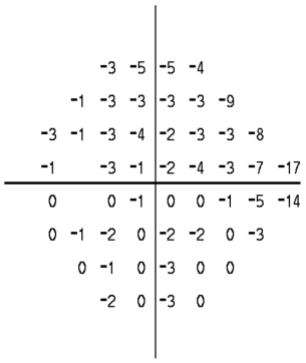


```
NaN,NaN,NaN,−3,−5,−5,−4,NaN,NaN,NaN
NaN,NaN,−1,−3,−3,−3,−3,−9,NaN,NaN
NaN,−3,−1,−3,−4,−2,−3,−3,−8,NaN
NaN,−1,NaN,−3,−1,−2,−4,−3,−7,−17
NaN,0,NaN,0,−1,0,0,−1,−5,−14
NaN,0,−1,−2,0,−2,−2,0,−3,NaN
NaN,NaN,0,−1,0,−3,0,0,NaN,NaN
NaN,NaN,NaN,−2,0,−3,0,NaN,NaN,NaN
```

Figure 1. Construction of 80-element visual field vectors. The 52-pattern deviation (PD) values from the 24-2 test grid were first mapped to their corresponding locations within an 8×10 matrix representing the overall test region. All blank spots, including positions outside the test region and the blind spot, were assigned NaN values.

Dataset partitioning was performed in two stages. First, the original dataset (393 eyes: 252 CVD, 141 non-CVD) underwent stratified random sampling using a 3:1 training-to-test split, applied independently within each class. This produced an initial training set with class imbalance and a test set of 79 eyes (51 CVD, 28 non-CVD). Second, to address class imbalance in the training set, the non-CVD group was balanced to the CVD group using class-weighted loss functions in classical ML models and Convolutional Neural Network (CNN)-based models (class_weight="balanced" in scikit-learn and pos_weight in BCEWithLogitsLoss). This produced a final balanced training set of 402 VFs (201 CVD, 201 non-CVD). A random state of 42 was fixed across all experiments for reproducibility. To avoid introducing artificial data artifacts, no synthetic sample generation or data augmentation was performed.

Model Training

Four classification models were trained to predict CVD status from HVF data: two traditional ML models Random Forest (RF) and Support Vector Machine (SVM) and two DL models ResNet18 and custom CNN. The models were selected to compare established ML and DL approaches across a spectrum of complexity and interpretability. RF and SVM served as traditional ML models with proven performance on high-dimension clinical data, with RF additionally enabling inspection of feature importance. A pre-trained ResNet18 was used as a widely adopted DL model, whereas the custom CNN was specifically designed for the 8x10 matrix representation to better capture the spatial structure of the test.

The ML models were implemented in Python using scikit-learn with feature standardisation (StandardScaler) and Principal Component Analysis (PCA). DL models were developed in PyTorch using a pretrained ResNet18 backbone and custom multimodal fusion architectures. Training, calibration, and evaluation employed class-weighted optimisation, probability calibration, and ROC-based performance metrics. The performance of each model was summarised using key

measures of accuracy, precision, recall, F1-score, AUC, and a confusion matrix. Analysis of feature importance using RF was conducted; however, since the features were transformed using PCA, the importance scores corresponded to the principal components instead of specific locations of pattern deviations.

Phase 2: Multimodal Fusion with Optical Coherence Tomography Data
Data Collection and Preprocessing
Eligible eyes were identified retrospectively by manually locating OCT ONH scans in the clinic's Cirrus HD-OCT 5000 (Carl Zeiss Meditec, Dublin, CA) device database. For eyes with available OCT ONH scans, the closest in-time scan with the included HVF was selected to approximate contemporaneous structural-function relationships. Each case was assigned a binary label: CVD (1) or no CVD (0).

OCT scans with a signal strength <7 were excluded to minimise noise from poor-quality acquisitions. No manual grading for other artefacts was undertaken, reflecting real-world clinical workflow. En face RNFL thickness maps centred on the optic disc were exported from the Cirrus device, converted to grayscale, trimmed to remove dark borders, centre-cropped to 90% of the field and resized to 224x224 pixels. They were then converted to RGB and normalised with ImageNet standards. Left-right orientation standardisation was applied to OCT images, where spatial structure is explicitly modelled by convolutional networks. During training, light augmentation such as horizontal flips, small rotations, and mild brightness or contrast variations were applied. Tensors were then fed to a frozen ResNet-18 feature extractor.

For HVF matrices, NaN values were removed without replacement. Each remaining vector was scaled between 0 and 1 and zero-padded to a consistent length between cases to facilitate batch processing. The training set was used to fit standardisation and dimensionality reduction with StandardScaler and PCA. The same transformation was then applied to both validation and testing data to avoid leakage. Minor random variations, like slight noise and gentle scaling changes, were added to the HVF data during training to make the model more stable and less sensitive to minor fluctuations in the input.

Single Fused Input for HVF-OCT Data
The OCT-HVF paired dataset (135 eyes: 82 CVD, 53 non-CVD) was partitioned using a nested stratified split strategy into training (64%: 53 CVD, 33 non-CVD), validation (16%: 13 CVD, 9 non-CVD) and testing (20%: 16 CVD, 11 non-CVD) sets.

A pretrained ResNet-18 was used to extract a 512-dimensional feature vector from each OCT image. The HVF data were reduced in dimension using PCA, and these features were then combined with the OCT features to create a single, fused input used for the traditional ML classifiers.

Three traditional ML models (logistic regression, SVM, RF) were chosen to facilitate a balanced comparison across linear and non-linear classifiers. They were trained on the fused features with the following parameters in scikit-learn to address class imbalance:

- Logistic Regression (class_weight="balanced", max_iter=5000)
- Support Vector Machine (class_weight="balanced") with probability calibration (Platt scaling via CalibratedClassifierCV)
- Random Forest (900 trees, class_weight="balanced_subsample", min_samples_leaf=2)

Class_weight="balanced" was applied in Logistic Regression and linear SVM to weight classes inversely proportional to their frequencies in the training data, while max_iter=5000 was set to ensure optimisation convergence for these high-dimensional feature inputs. In addition, RF models used class_weight="balanced_subsample", which applies class balancing at the level of each bootstrap sample during tree construction.

The validation set was used for model selection (based on AUC) and decision threshold tuning to maximize balanced accuracy. Random forest was the final selected model. After tuning its threshold on the validation set, the model was tested once on the unseen test set and key measures were recorded.

Parallel Inputs for HVF-OCT Data
A separate method to assess the combined structure-function data was explored. We combined information from two parallel branches. The OCT branch used a pretrained ResNet18 network, where the early layers remained fixed and only the deeper layers were fine-tuned to capture domain-specific patterns. This produced a 512-dimensional feature representation of each OCT image. In parallel, the HVF branch used a simple two-layer neural network to process the PCA-reduced HVF data, extracting key statistical features. The feature outputs from both branches were then merged and passed through a final fully connected layer that generated the overall prediction. The data was partitioned as in the single fused input.

The RF model and a deep learning model FusionNet were trained using a weighted loss to address class imbalance and an adaptive optimiser with separate learning rates for the backbone and fusion layers. Early stopping was used to reduce overfitting. Because the dataset was relatively small, the training set was expanded to 1,000 samples per class through carefully controlled augmentation of both OCT images and HVF data. OCT image augmentation was performed in tensor space and included horizontal flipping, small in-plane rotations, and mild intensity perturbations (brightness and contrast jitter). These transformations were applied stochastically during training using tensor-level operations (e.g., torch.flip, affine transformations via torch.nn.functional.affine_grid and grid_sample, and linear intensity jitter),

following standard preprocessing steps including border trimming and centre cropping (OpenCV), resizing to 224×224 (cv2.resize), and ImageNet normalisation (torchvision.transforms.Normalize).

HVF data augmentation was implemented directly on the numeric pattern deviation vectors using NumPy-based operations. This included the addition of low-variance Gaussian noise (numpy.random.normal), minor multiplicative scaling (numpy.random.uniform), and limited value smoothing at randomly selected locations. All augmented HVF vectors were subsequently standardised and transformed using the same StandardScaler and PCA objects, which were fitted exclusively to the original training data, ensuring consistent feature representation and preventing data leakage.

After training, the prediction threshold was fine-tuned on the validation set to achieve the best balance between sensitivity and specificity. The final evaluation was carried out on the unseen test set. Class distributions were reviewed throughout to confirm that the data remained balanced and that no leakage occurred between splits.

3.3 RESULTS

Phase 1: HVF-Only Classification Performance

Four models were evaluated using identical training (n=402; 201 per class) and test sets (n=79; 51 CVD, 28 non-CVD). Performance metrics are summarized in Table 1 and receiver operating characteristic (ROC) curves are represented in Figure 2 for all models.

Table 1. Summary metrics of HVF-only model performance. Models analysed were two machine learning models, Random Forest (RF) and Support Vector Machine (SVM), and two deep learning models, ResNet18 and Custom Convolutional Neural Network (CNN). Key parameters summarised are accuracy, precision, recall, F1-score and AUC. Confusion matrices are included as the rightmost column with true negative (TN), false positive (FP), false negative (FN) and true positive (TP) rates.

Model	**Accuracy**	**Precision**	**Recall**	**F1-Score**	**AUC**	**Confusion Matrix (TN, FP FN, TP)**
RF	0.65	0.73	0.71	0.72	0.69	15, 13, 15, 36
SVM	0.67	0.84	0.61	0.70	0.73	22, 6, 20, 31
ResNet18	0.53	0.77	0.39	0.52	0.60	22, 6, 31, 20
Custom CNN	0.67	0.79	0.67	0.72	0.71	19, 9, 17, 34

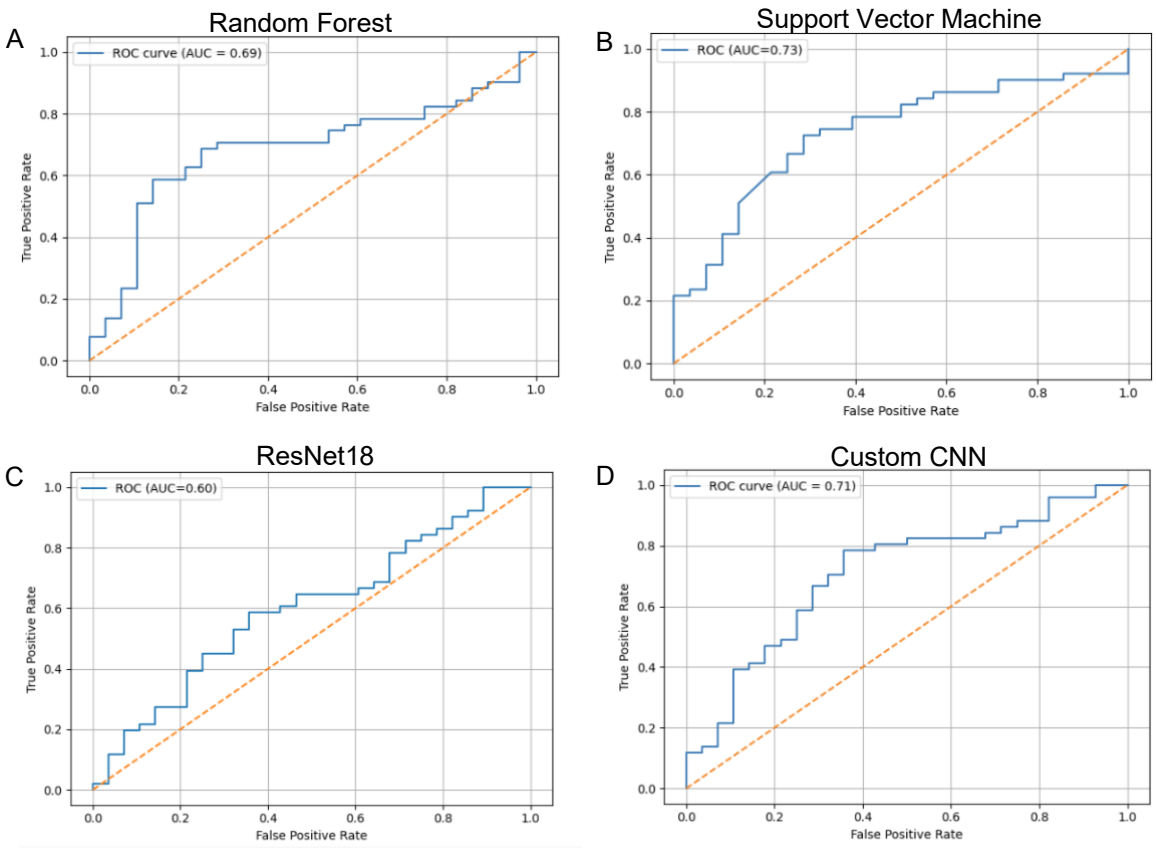

Figure 2. Receiver operating characteristic (ROC) curves for the four artificial intelligence models trained with HVF-only data, demonstrating their performance at various thresholds with true positive rates against false positive rates. From top left to bottom right, (A) Random Forest, (B) Support Vector Machine, (C) ResNet18 and (D) custom convolutional neural network.

SVM achieved the highest AUC (0.73), demonstrating superior classification ability to the other models with good specificity (0.84) but moderate sensitivity only (0.61). ResNet18 performed the worst (AUC=0.60), with particularly poor sensitivity (0.39).

Phase 2: HVF-OCT

Single Fused Input

Three models were evaluated with the validation set. RF had the best overall performance (AUC 0.64) compared to Logistic Regression (AUC 0.45) and SVM (AUC 0.52) and was chosen as the final model to evaluate the test set (Table 2).

Table 2. Summary metrics of the model performance of Random Forest (RF) with HVF-OCT fused input.

Model	**Accuracy**	**Precision**	**Recall**	**F1-Score**	**AUC**	**Confusion Matrix (TN, FP FN, TP)**
RF	0.70	0.68	0.94	0.79	0.64	4, 7 1, 15

Parallel Input

Parallel input was explored for the ML model RF and a DL model FusionNet (Table 3). FusionNet had better overall performance than RF with parallel input (AUC 0.66 vs 0.60), and better sensitivity (recall 0.81) but slightly poorer specificity (precision 0.68 vs 0.73). ROC curves for both the single fused-input and parallel input methods are summarised in Figure 3.

Table 3. Summary metrics of the model performance of machine learning model Random Forest (RF) and deep learning model FusionNet with HVF-OCT parallel inputs.

Model	Accuracy	Precision	Recall	F1-Score	AUC	Confusion Matrix (TN, FP FN, TP)
RF	0.59	0.73	0.50	0.59	0.60	8, 3 8, 8
FusionNet	0.67	0.68	0.81	0.74	0.66	5, 6 3,13

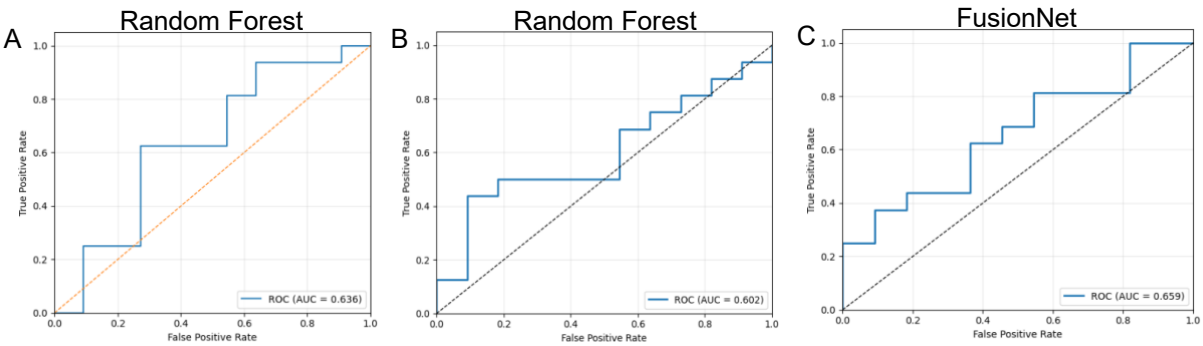

Figure 3. Receiver operating characteristic (ROC) curves for the three artificial intelligence models trained with HVF-OCT data, demonstrating their performance at various thresholds with true positive rates against false positive rates. From left to bottom right, (A) Random Forest trained with single fused input, (B) Random Forest trained with parallel inputs and (C) FusionNet trained with parallel inputs.

3.4 DISCUSSION

This study aimed to explore whether artificial intelligence models could predict a patient's CVD status based off 1) functional 24-2 HVF data and 2) structure-function data from fused HVF-OCT data.

For the models trained on HVF data only, we found that the ML model SVM performed the best with an AUC of 0.73, which falls into an 'acceptable' range of diagnostic accuracy (Mandrekar, 2010). Overall, the AUC ranged between 0.60 to 0.73, suggesting a better-than-chance discriminatory power across all models. Current literature proposes that systemic vascular risk factors are associated with POAG prevalence and disease progression. Some studies have shown that patients with higher genetic CVD risk scores are more likely to experience macular thinning and paracentral HVF defects (Marshall et al., 2022). Similarly, in *Chapter 2*, we found that specific HVF patterns are more likely to

be seen in patients with CVD than patients without CVD. Our results in this chapter further support this given that AUC >0.5 (better than chance), though it is possible that the heterogeneity of visual fields reduces the models' ability to predict CVD in this small dataset.

Within the key domains for our models, recall reflects sensitivity and is a marker of the model's ability to avoid false negatives. For screening tools, sensitivity is valued more than specificity (AlShawabkeh et al., 2024). RF performed better than SVM in terms of recall (0.71). F1 scores represent the balance between precision and recall (specificity and sensitivity), and RF and custom CNN had the most balanced F1 scores in Phase 1 of this study (0.72). ResNet18 performed the worst across all domains, with a recall of 0.39. This is likely due to ResNet18 performing better with image input, such as pattern deviation plots (Akter et al., 2022), rather than vectors containing pattern deviation sensitivity values. ResNet18 traditionally consists of pre-designed architecture created for ImageNet. In contrast, our custom CNN DL model was designed specifically for the 8x10 HVF matrices and performed on a comparable level to the two traditional ML models, suggesting that task-specific architecture design is more beneficial for DL model performance in identifying CVD-related HVF patterns.

Incorporating OCT ONH data did not improve discrimination beyond the performance of SVM with only HVF data. The FusionNet parallel-input architecture performed better than the RF parallel-input architecture, demonstrating a superior performance of DL models for parallel inputs. In contrast, the RF single-input model had similar AUC values with FusionNet (AUC 0.64 vs 0.66), indicating comparable overall discrimination. RF single input had higher sensitivity (recall = 0.94). The fusion of the multimodal data into a single input point appears to improve sensitivity but does not clearly enhance overall predictive balance.

The lack of improvement in model performance with multimodal input could be explained by several factors. First, the structural input involved disc-centred RNFL thickness maps, whereas the functional input involved macula-centred 24-2 HVFs. Any structure-function relationships therefore had to be inferred indirectly, without explicit one-to-one topographical mapping. The lack of improvement also raises the question whether RNFL data contains enough CVD-specific signals to differentiate between eyes with CVD and eyes without. Previous studies exploring the relationship between CVD and POAG have reported that patients with CVD tend to exhibit mGCIPL-dominant thinning, rather than pRNFL thinning (Marshall et al., 2021, 2022). This could explain why the addition of OCT ONH data did not improve our model performance. Secondly, the smaller sample size could also be a contributing factor.

Clinical Significance, Limitations and Future Directions

This chapter provides a proof-of-concept that systemic CVD influences HVF patterns in POAG, and this can be detected by ML models. Clinically, this creates an opportunity for a) opportunistic CVD risk identification through routine glaucoma assessment, particularly in patients who may not otherwise have had CVD workup, and b) identification of patients who may be at high risk of rapid glaucoma progression and would benefit from aggressive monitoring and therapy.

However, the current model performance is only modest and requires further optimisation. Our study is limited by a small sample size, which was even smaller for our HVF-OCT component, and lack of external validation. Although RF facilitated feature importance analysis, the use of PCA-transformed features meant that importance scores were assigned to principal components rather than individual test locations, limiting spatial interpretability. OCT scans did not undergo any manual grading for segmentation errors or other artefacts, which may introduce additional variability. Additionally, there is no direct topographical correspondence between the disc-centred OCT scans and macula-centred 24-HVFs.

Future studies should evaluate larger, multi-centre datasets and consider including OCT macula scans and vascular-specific imaging such as OCT angiography scans for more predictive modelling. OCT angiography can quantify peripapillary and macular vessel density loss in glaucoma, providing complementary information to structural OCT thickness measures. Multimodal models that include ONH, macular and vascular metrics may better capture CVD-related influences on ocular perfusion and improve prediction of cardiovascular status (WuDunn et al., 2021). They could focus on the ML models SVM and RF and DL models custom CNN and FusionNet. It would also be beneficial to explore SHAP analysis utilising spatially preserved HVF representations. If validated, this approach could expand the role of HVF testing from glaucoma assessment to broader CVD assessment and risk-stratification.

3.5 CONCLUSION

Traditional ML methods outperformed deep learning approaches, with SVM achieving higher AUC than both DL architectures. The custom CNN outperformed ResNet18 (AUC: 0.71 vs. 0.60). Overall, the modest AUC values (0.60–0.73) indicate that while the models can identify CVD signals from HVF data at above-chance levels, their discriminative performance remains limited and below thresholds typically regarded as clinically useful (AUC ≥ 0.7). Multimodal input with the addition of structural data in the form of OCT ONH scans did not improve model performance. Future directions include recruiting a larger patient population, with more structural information, to improve the ability of glaucoma assessment tools to screen for CVD.

Chapter 4. Artificial Intelligence Classification of 24-2 Visual Field Patterns in Glaucoma Rapid Progressors

ABSTRACT

PURPOSE

This study aims to use archetypal analysis to explore defect patterns across baseline visual fields in a longitudinal cohort of glaucoma patients, classified into rapid progressors and non-rapid progressors.

METHODS

Patients were recruited from a private glaucoma clinic if they had a) at least five 24-2 HVFs per eye, with the five latest HVFs spanning over at least two years and b) a diagnosis of POAG. Rapid progression was defined as a MD decline of at least 1dB/year over the five latest HVFs. An archetype model was fitted with the five latest HVFs from each eye and used to decompose each HVF into a combination of archetypal patterns. The dominant archetype at baseline and the mean weights of each archetypal pattern were recorded. Rapid progressors and non-rapid progressors were further categorised into disease severity baseline based on MD values (mild: MD > -6 dB, moderate: -12 < MD < -6 dB, severe: MD < -12 dB).

RESULTS

397 eyes met the inclusion criteria, including 89 rapid progressors and 308 non-rapid progressors. 1990 HVFs were used to fit the archetype model which obtained optimal performance at 17 archetypes. Rapid progressors most frequently had a normal pattern (53.9%), followed by superior altitudinal (7.9%) and inferior paracentral arcuate defects (6.7%). Non-rapid progressors most frequently had a normal pattern (72.5%), followed by superior arcuate (4.6%) and inferior paracentral arcuate defects (4.6%). Rapid progressors with severe disease at baseline were more likely to demonstrate a superior altitudinal defect while non-rapid progressors with severe disease demonstrated an inferior paracentral arcuate defect.

CONCLUSION

Rapid visual field progression may be associated with specific archetypal patterns at baseline, which may help clinicians identify and predict risk of progression.

4.1 INTRODUCTION

Glaucoma is the leading cause of irreversible blindness worldwide. While most patients maintain stable disease with appropriate management, there is a substantial subset of patients who experience rapid progression, commonly defined by a MD decline ≥1 dB of retinal sensitivity per year (Chauhan et al., 2014; Gordon et al., 2025; Jackson et al., 2023). Rapid progressors are at high risk of significant visual disability and subsequently reduced quality of life, highlighting the need to be able to identify these patients earlier to facilitate more aggressive treatment and monitoring.

Current glaucoma management relies on trend-based analyses of optical coherence tomography data and visual field indices to determine disease severity and progression rates (Scott et al., 2025). This requires several visits over months or years to collect sufficient longitudinal data for each individual, which could delay the identification of patients at high-risk for rapid progression. Furthermore, quantitative metrices may not fully capture pattern-specific changes in visual fields that could signal aggressive disease at an earlier age.

There is a growing body of research investigating risk factors associated with rapid progression, such as the presence of systemic cardiovascular disease (Chan et al., 2017), as well as analysing functional damage to predict future progression rates. Artificial intelligence approaches allow for objective and reproducible methods of analysing visual field data. Among these, archetypal analysis is an unsupervised learning approach that has been shown to be useful in extracting clinically significant glaucomatous patterns, glaucoma diagnosis, and detecting progression (Elze et al., 2015; Thakur et al., 2020; Wang et al., 2019, 2020). This method identifies a set of *k* archetypal patterns that lie on the extreme boundaries of the data space representing distinctive features of glaucomatous vision loss and decomposes visual fields into weighted combinations of these archetypes.

Archetypal analysis has been applied across different perimetric stimuli and optic neuropathies (such as glaucoma and non-arteritic anterior ischaemic optic neuropathy) and can generate consistent visual field archetypes (Szanto et al., 2024, 2025). These findings highlight the clinical utility of archetypes as standardised descriptors of functional loss across various testing conditions and diseases. Because each patient's visual field can be decomposed into weighted combinations of different archetypes, this approach allows clinicians to explore whether specific baseline patterns are associated with faster progression, thus allowing for pattern-based risk stratification.

Our study aims to use archetypal analysis to explore whether there are any differences in the baseline visual fields of rapid progressors compared to non-rapid progressors, to enhance risk stratification using initial functional data.

4.2 METHODOLOGY

Data Collection

A retrospective chart review was conducted on patients from a private ophthalmology clinic in New South Wales, Australia between the years 1991 to 2015. Ethics approval was obtained from the clinic's board, and the study was conducted according to the principles of the Declaration of Helsinki. Patients were included if they had a confirmed diagnosis of POAG, and if they had at least five 24-2 HVFs, with the five latest tests spanning at least two years. All HVFs were SITA fields performed on an HFA, as in *Chapter 2* and *Chapter 3*. HVFs with fixation loss >20% or false positives >15% were considered unreliable and excluded from analysis. To minimize bias from repeated measurements from the same patient, only the five most recent tests were included for each patient. If both eyes met the inclusion criteria, they were analysed separately.

MD and PSD values were extracted from each HVF and the annual rate of MD change was calculated for each eye. Eyes were classified into rapid progressors and non-rapid progressors, with rapid progression defined as an MD decline of ≥1 dB per year. Total deviation values were extracted using *Matlab2023b* to form 52-element vectors consisting of the deviation values from age-matched normative data at the 52 test locations, ordered by rows. Left eye matrices were horizontally flipped to align with right eye orientation to standardise the data.

Archetype Model Fitting

Archetypal analysis was performed using the *archetypes* package (version 2.2.0.2) in *R* (version 2025.09.0+387), following Elze et al's methodology for identifying patterns of functional vision loss in glaucoma (Elze et al., 2015). Models were fitted for k = 2 to 20 archetypes using the *stepArchetypes* function with the following parameters:

- Number of replications per k: 40
- Maximum iterations: 100
- Random seed: 42

For each value of k, the model with the lowest residual sum of squares (RSS) across all replications was retained as the best model. A scree plot was generated to display the RSS as a function of k, and the optimal number of archetypes was determined by identifying the 'elbow point' where the RSS curve flattens, indicating that additional archetypes provide diminishing improvements in model fit. Visual inspection of the scree plot revealed an elbow at k = 17 (Figure 1). The final archetype model at k = 17 was extracted and visualized by mapping each 52-element archetype vector back to a 24-2 VF layout (8×9 matrix with 2 blind spot locations).

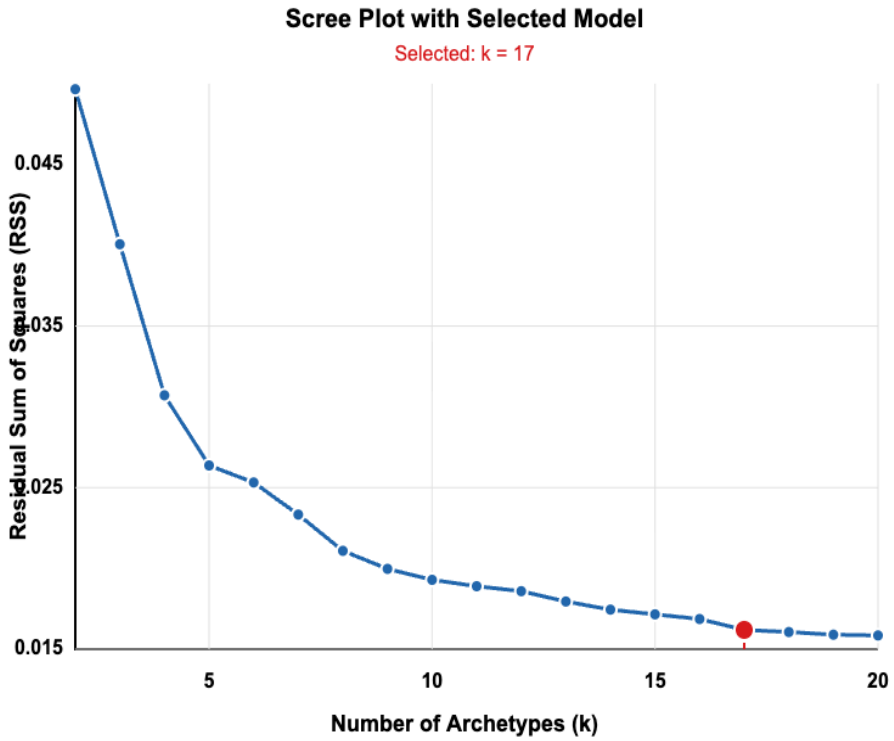

Figure 1. Scree plot of archetype model. Optimal number of archetypes and optimal model performance is determined by the 'elbow point', where the RSS curve flattens. The red datapoint indicates our optimal number of archetypes *k* = 17.

Archetype Distribution Analysis

For each eye, the first of the five included HVFs was considered the baseline HVF. Each baseline HVF was decomposed into archetype weights using the trained archetype model. This meant that each HVF is represented as a weighted combination of all 17 archetypes. The archetype with the highest weight for each HVF was identified as the dominant archetype and the frequency of each archetype appearing as the dominant pattern was calculated for rapid progressors and non-rapid progressors, allowing for descriptive comparison of pattern distributions between the two groups. To assess the average contribution of each archetype, the mean weight and standard deviation of each archetype were calculated across all baseline HVFs in each progression group. Mean archetypal weights represent the average contribution of each archetype within a group (rapid vs non-rapid progressors). Higher mean weight indicates that archetype contributes more strongly to the typical HVF seen in that group.

HVFs were further stratified by glaucoma severity based on MD values (mild: MD > -6 dB, moderate: -12 < MD < -6 dB, severe: MD < -12 dB) to facilitate subgroup analysis of both the dominant archetype and mean archetype weights across disease severity stages. For interest, archetypes were grouped according to the location of HVF damage (superior, inferior, central, circumferential, diffuse loss) and the dominant patterns assessed between rapid and non-rapid progressors.

4.3 RESULTS

Archetype Model Fitting and Identification

A total of 1990 HVFs from 397 eyes met the inclusion criteria. 89 eyes were classified as rapid progressors (MD decline ≥1 dB/year) and 308 eyes as non-rapid progressors. Within the baseline HVFs, there were 284 eyes with mild glaucoma (MD > -6 dB), 58 with moderate glaucoma (MD -6 to -12 dB), and 55 with severe glaucoma (MD < -12 dB). The distribution of included eyes stratified by progression and disease severity is summarised in Table 1.

Table 1. Distribution of included eyes by progression status and disease severity.

Glaucoma severity	**Rapid progressors**	**Non-rapid progressors**
Mild	60	224
Moderate	12	46
Severe	17	38
Total	89	308

Archetypal analysis identified 17 distinct archetypes in our patient population. These archetypes were reviewed with a glaucoma specialist and labelled (Figure 2). AT9 is a non-specific pattern along the outer edge rim points, which does not respect the horizontal meridian. Similar patterns have been deemed artifactual in other studies classifying visual fields (Ding et al., 2016; Galarza et al., 2021). AT9 was deemed to represent an artefact and excluded from the analysis. ATs 1 and 13 represent non-glaucomatous patterns (superotemporal quadrantanopia and temporal hemianopia respectively). HVFs with either AT1 or AT13 as their dominant pattern were identified and removed (*n* = 3 non-rapid progressors).

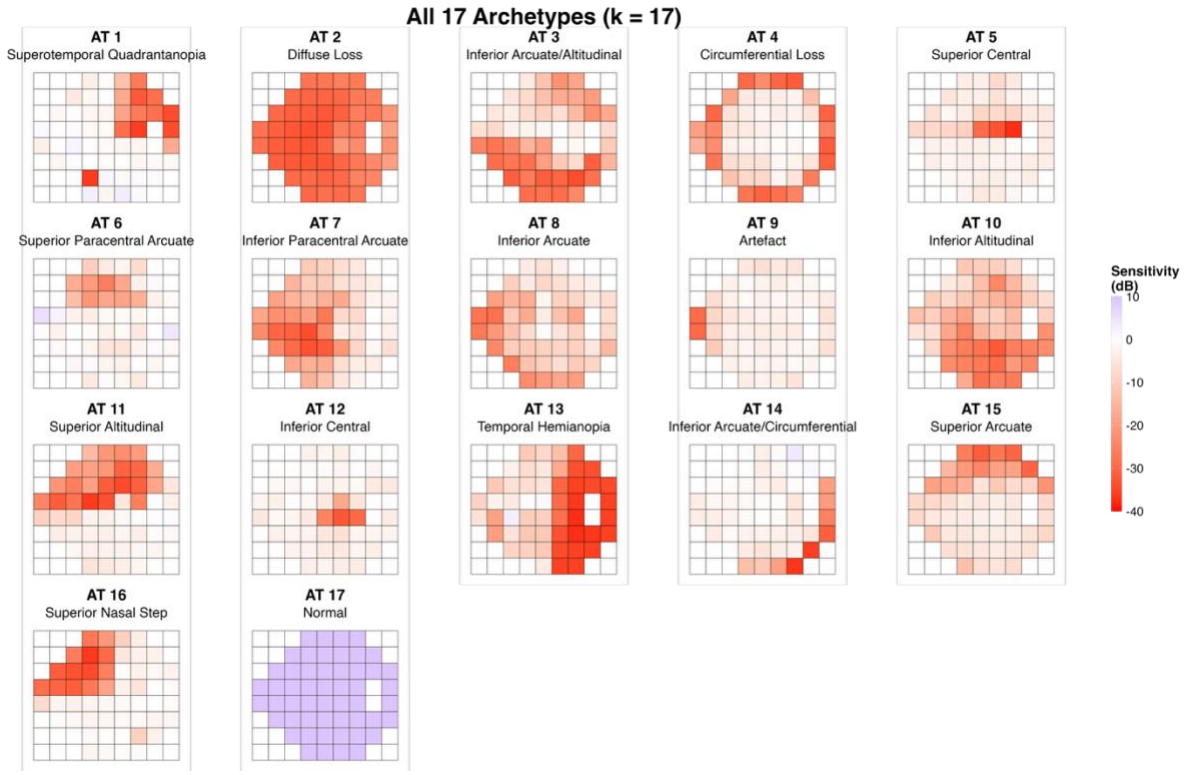

Figure 2. The 17 archetypes representing common patterns of vision loss in our patient population, as determined with archetypal analysis. All archetypes are plotted in right eye format. Sensitivity values extracted from Total Deviation plots (differences of thresholds against age-matched control values from a normative database) demonstrated in different colours; red, thresholds below norm, and blue, thresholds above norm). AT = archetype. Some archetypes share overlapping features; for example, both AT3 and AT10 show inferior altitudinal loss, but AT3 more closely resembles an inferior arcuate defect deepening into an altitudinal pattern.

Eyes with AT17 (normal) as the dominant pattern had the best MD values, indicating the least global severity and overall field loss, whereas eyes with AT2 (diffuse loss) had the worst MD values (Figure 3).

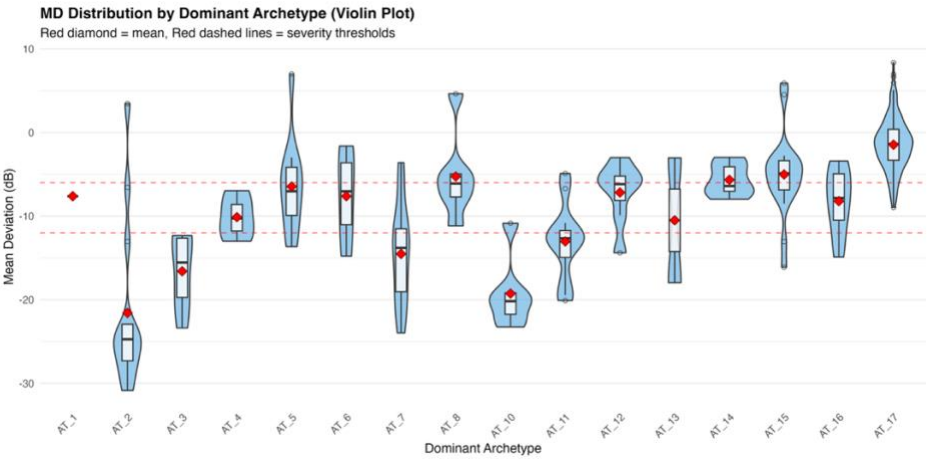

Figure 3. Violin plot of the mean deviation (MD) values corresponding to the 17 ATs identified in our study. Eyes with dominant AT17 (normal) had the least negative MD values and eyes with dominant AT2 (diffuse loss) had the most negative MD values, as expected.

Dominant Pattern Distribution

The most common dominant pattern in both rapid and non-rapid progressors was AT17, the normal pattern (Figure 4A; rapid progressors 53.9%, non-rapid progressors 72.5%). Among rapid progressors, the next most common patterns were AT11 (superior altitudinal defect; 7.9%) and AT7 (inferior paracentral arcuate; 6.7%). In non-rapid progressors, the next most common patterns were AT7 (inferior paracentral arcuate; 4.6%) and AT15 (superior arcuate; 4.6%). AT12 (inferior central), AT16 (superior nasal step) and AT17 (normal) were more common in non-rapid progressors compared to rapid progressors (Figure 4B).

To further evaluate the eyes with dominant AT17 pattern at baseline, the following parameters were collated: age, gender, baseline IOP, CDR and CCT and presence of vascular risk factors CVD, HTN and DM. There were no significant differences between rapid progressors (*n* = 48) and non-rapid progressors (*n* = 221) (Table 2).

A

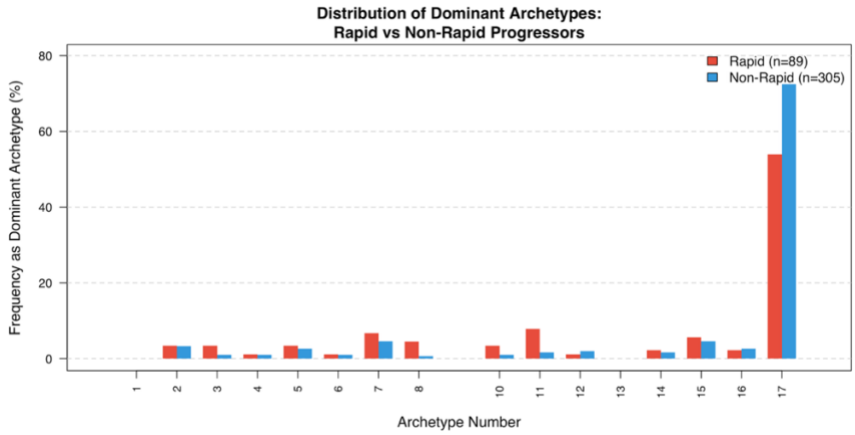

B

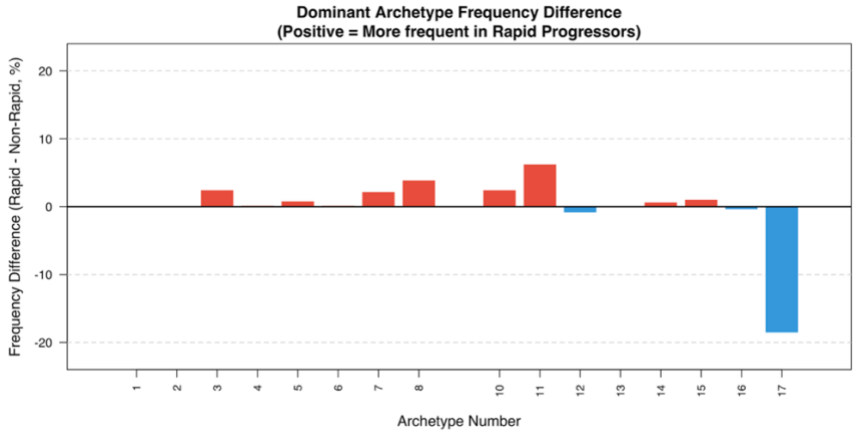

Figure 4. (A) Distribution of the dominant archetypes across both rapid and non-rapid progressors, represented as percentages within each group. AT9 was excluded from the list of archetypes. HVFs with ATs 1 and 13 as their dominant archetype were excluded from the analysis owing to their non-glaucomatous nature (*n* = 3 non-rapid progressors). (B) Differences in the proportion of eyes assigned each dominant archetype between rapid and non-rapid progressors. Positive (red) bars indicate dominant archetypes that have a higher within-group proportion in rapid progressors than non-rapid progressors.

Table 2. Demographics and ocular characteristics of eyes who were rapid progressors and non-rapid progressors with normal archetype AT17 at baseline. Note: categorical variables analysed using Chi-square test. Continuous variables analysed using Mann Whitney test owing to a non-normal distribution. Figures rounded to 2 decimal points. * indicates statistical significance (*p<0.05*).

	Rapid	**Non-rapid**	***p***
Total (number of eyes)	48	221	
Male (%)	18 (37.5%)	86 (38.9%)	0.86
Average age (in years)	64	62	0.36
Hypertension (%)	29 (60.4%)	140 (63.3%)	0.70
Diabetes (%)	11 (22.9%)	45 (20.4%)	0.70
Cardiovascular disease (%)	29 (60.4%)	130 (58.8%)	0.84
Average baseline IOP (mmHg ± SD)	21.4±3.3	20.8±4.6	0.25
Average baseline CDR	0.38	0.43	0.33
Average baseline CCT (µm ± SD)	538.4±28.2	537.1±35.9	0.67

Mean Archetype Weights Analysis

When assessing the mean archetype weights, ATs 12, 16 and 17 remained more common in non-rapid progressors. Interestingly, ATs 2 (diffuse loss), 4 (circumferential), 6 (superior paracentral arcuate) and 15 (superior arcuate) had higher weight in non-rapid progressors than rapid progressors (Figure 5).

A

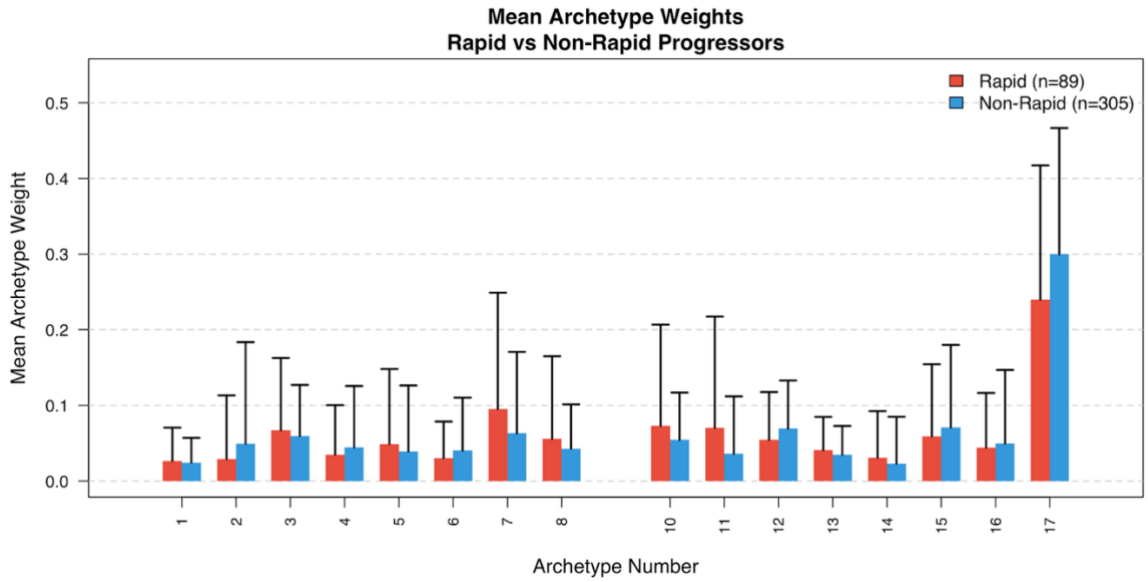

B

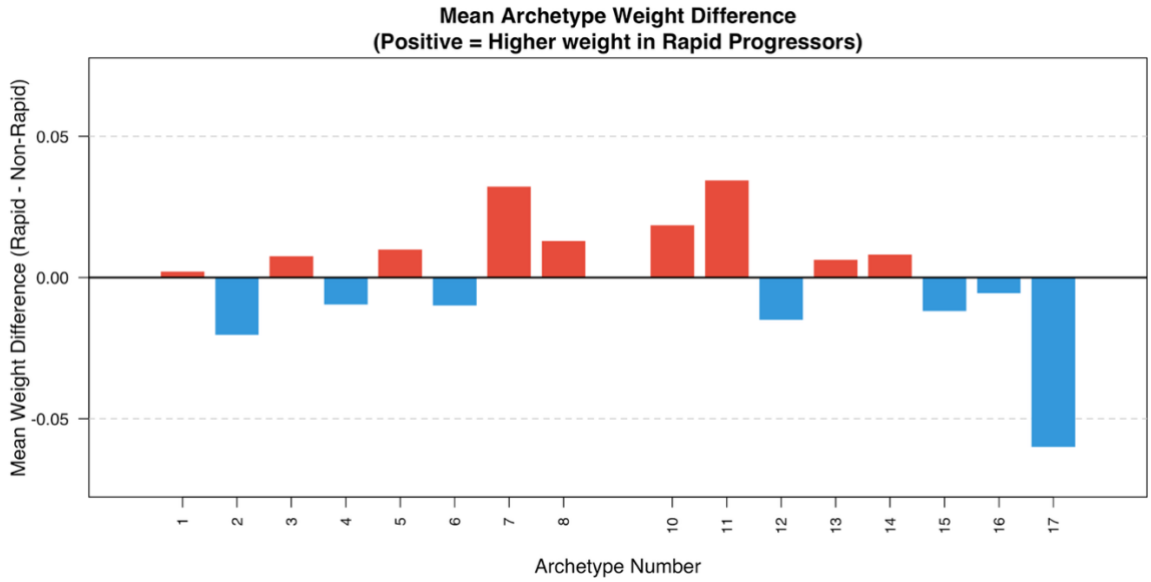

Figure 5. (A) Distribution of the mean archetype weights +/- standard deviation across both rapid and non-rapid progressors. (B) Differences in mean archetype weights between rapid and non-rapid progressors. Positive (red) bars indicate archetypes that contribute a higher within-group weight in rapid progressors compared to non-rapid progressors.

Stratification by Disease Severity

When stratified by disease severity (Figure 6), different patterns emerged. In eyes with mild glaucoma, both rapid and non-rapid progressors tended to have normal (AT17; rapid 76.7%; non-rapid 89.7%) and superior nasal step (AT15; rapid 6.7%; non-rapid 3.6%) patterns. Apart from the normal AT17 and inferior central AT12 patterns, all other patterns were more common in rapid progressors than non-rapid progressors.

In eyes with moderate glaucoma, rapid progressors predominantly demonstrated normal (AT17; 16.7%) and inferior (AT7 and AT8, each 16.7%) patterns whereas

non-rapid progressors had normal (AT17; 43.5%) and superior (AT15; 10.9% and AT16; 8.7%) patterns. Non-rapid progressors in this group also started to exhibit a higher prevalence of specific VF defects than rapid progressors, including diffuse loss (AT2), superior paracentral (AT6), superior arcuate and superior nasal step (ATs 15 and 16) and inferior altitudinal (AT10). Overall, inferior and central (ATs 5 and 12) patterns were more frequent in rapid progressors.

Conversely, in eyes with severe glaucoma, rapid progressors were most likely to have a superior altitudinal defect (AT11; 29.4%) while non-rapid progressors were more likely to have an inferior paracentral defect (AT7; 28.9%). The frequency of most archetypes was greater in non-rapid progressors than in rapid progressors within this population.

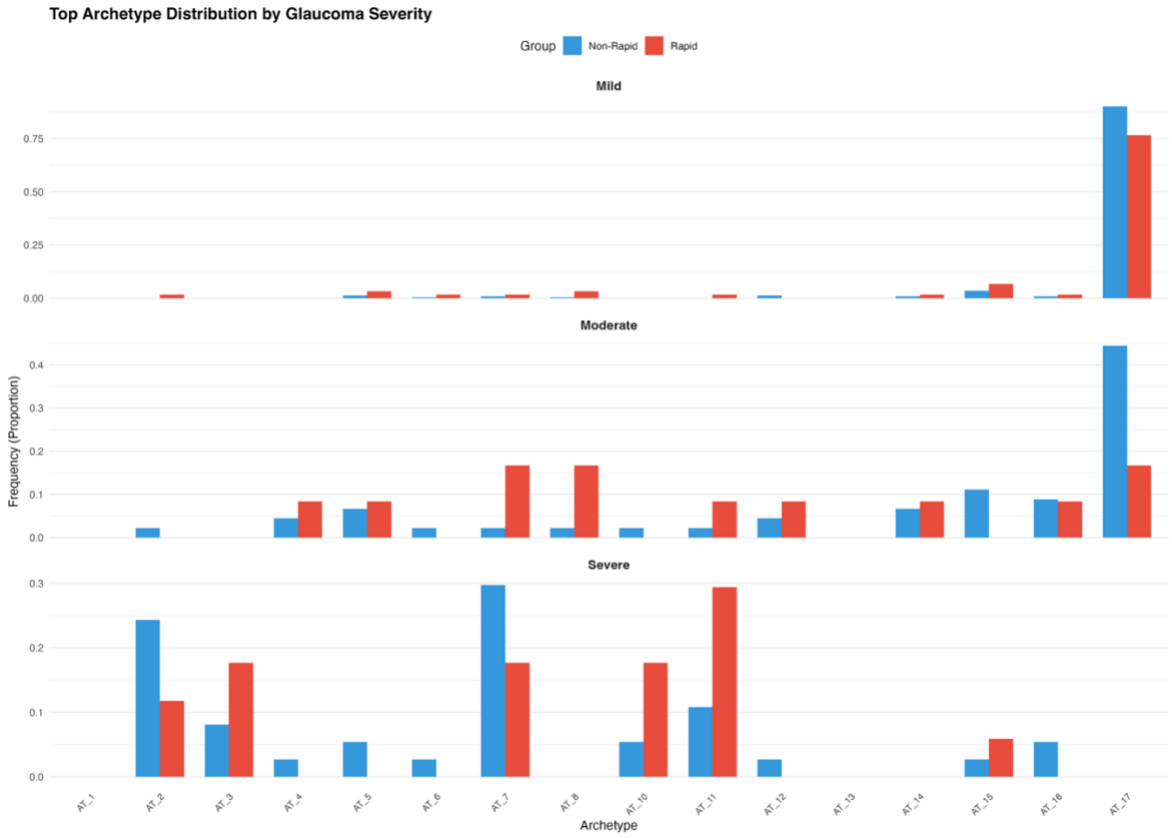

Figure 6. Distribution of the dominant archetype across rapid and non-rapid progressors, stratified by disease severity in the baseline field.

Grouped Analysis by Defect Location

Archetypes were further grouped by location of the defect to assess if there were any differences between general visual field pattern loss at baseline in rapid and non-rapid progressors (Table 3). Non-rapid progressors were more likely to have a normal VF pattern. Rapid progressors exhibited a greater frequency of defects across all locations when compared to non-rapid progressors (Figure 7).

Table 3. Classification of archetypes by location of functional visual field defect.

Group	**Included archetypes**
Superior	6, 11, 15, 16
Central	5, 12
Inferior	3, 7, 8, 10, 14
Diffuse loss	2
Circumferential loss	4
Normal	17

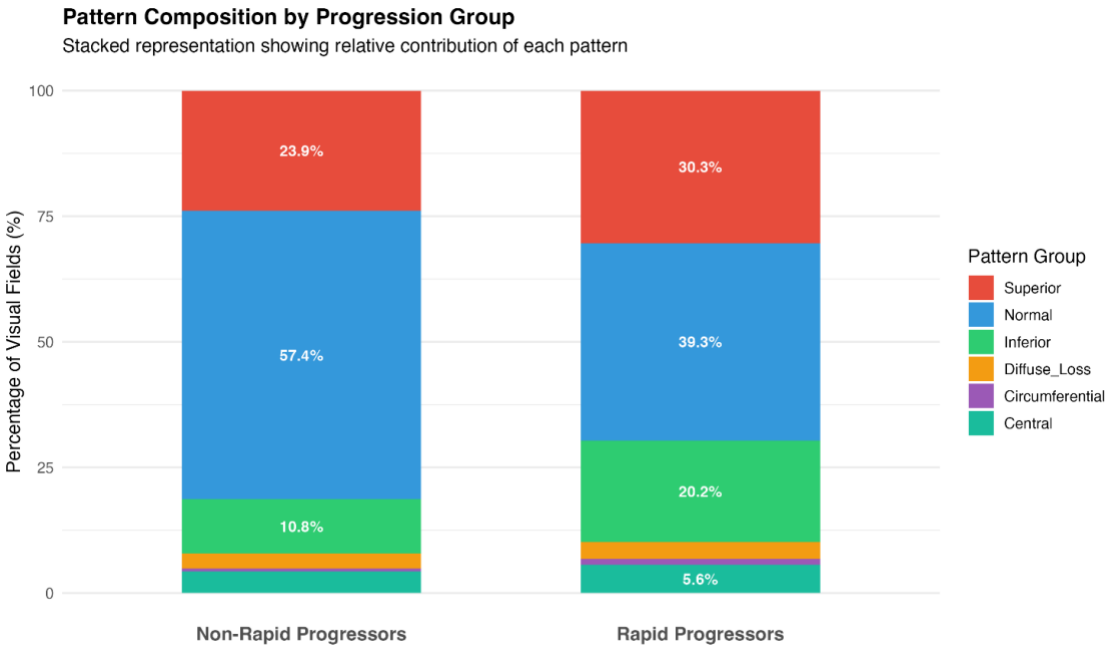

Figure 7. Distribution of the dominant pattern group among rapid and non-rapid progressors. Data is shown as stacked percentages.

4.4 DISCUSSION

This study utilised archetypal analysis to examine whether patients with rapid progression of their glaucomatous disease had different baseline visual field patterns compared to patients who did not progress rapidly. 17 distinct archetypes were identified in our analysis, similar to previous studies (Elze et al., 2015), demonstrating that we were able to utilise archetypal analysis to extract clinically significant phenotypes. We used real-world clinical data spanning a wide range of glaucoma severity, including standard 24-2 HVFs routinely used for glaucoma monitoring, thus supporting the clinical relevance of our findings.

We found that the normal archetype AT17 was the most frequent pattern in both groups, but the rapid progressors had lower frequencies and lower mean weights of AT17 compared to the non-rapid progressors. AT7 (inferior paracentral arcuate) and AT11 (superior altitudinal) patterns were more prevalent in rapid progressors and exhibited the greatest differences in mean weights (excluding AT17). AT12 (inferior central) and AT16 (superior nasal step) were more dominant in non-rapid

progressors compared to rapid progressors. When eyes were stratified by baseline severity, different archetypes were more prevalent in moderate and severe glaucoma for both rapid and non-rapid progressors. Overall, rapid progressors were more likely to have functional loss in any location compared to non-rapid progressors at baseline, as shown in the grouped analysis by location of defect.

Interpretation of Normal Archetype Findings
AT17 being the most common pattern is not unexpected, since we are investigating the 'baseline' visual fields. In another study using archetypal analysis to assess glaucoma progression, they found that 63% of their population had a normal pattern, and this normal pattern was one of the most frequently progressed patterns(M. Wang et al., 2019). AT17 being more common in non-rapid progressors, both in terms of frequency and mean weight, suggests that rapid progressors may exhibit subtle functional abnormalities at baseline. Similarly, patients from the Ocular Hypertension Treatment Study that were later diagnosed with glaucoma were found to have occult patterns of VF loss that were predictive of glaucoma conversion(R. K. Singh et al., 2024). Our study extends this from ocular hypertension patients to patients with an established diagnosis of glaucoma.

There were no significant differences between the baseline IOP, CDR, CCT or the age, gender, and presence of vascular risk factors CVD, HTN or DM between the rapid and non-rapid progressors with normal baseline patterns. This suggests that archetypal analysis can reveal subtle compositional differences between rapid and non-rapid progressors through mean weight analysis and can serve as a complementary tool for risk stratification. Further investigation is warranted to explore structural or clinical biomarkers that can facilitate early identification of rapid progressors with normal fields at baseline, in combination with archetypal analysis.

Clinical Significance of Specific Archetypes (AT7, AT11)
ATs 7 and 11 had the strongest overall association with rapid progressors in our study. Superior hemifield defects have been described as more common than inferior defects in glaucoma (Vandersnickt et al., 2024), with defects in the superior hemifield showing faster rates of visual field progression (Jo et al., 2019; Su et al., 2018; Takeo Fukuchi, 2010; Yousefi et al., 2018). Superior altitudinal loss has also been reported in previous studies using archetypal analysis as one of the most frequently progressed patterns in glaucoma (Wang et al., 2019), supporting our finding of AT11 being associated with rapid progression. In contrast, AT16 (superior nasal step) was more dominant in non-rapid progressors, which is in keeping with nasal steps being the most common visual field defect (Vandersnickt et al., 2024).

Though superior defects have been described as more common, inferior defects can also demonstrate rapid progression (Takeo Fukuchi, 2010). Specifically, our findings suggest that inferior paracentral arcuate patterns may be associated with rapid progression. This could be due to the paracentral involvement in AT7. Both ATs 7

and 11 demonstrate depression within the nasal portion of the central 4 points of the 24-2 HVF, which have been shown to be predictive of functional loss affecting the central 10 degrees of fixation (Chakravarti et al., 2021, 2022). Central visual field defects have been associated with more rapid progression of glaucomatous disease and poorer quality of life (Abe et al., 2016; Garg et al., 2018; Jackson et al., 2023). Previous archetypal analysis demonstrated an association between superonasal and inferonasal defects on 10-2 HVFs with more rapid disease progression (Wang et al., 2020a), which was proposed to be due to these locations falling in the more vulnerable macular zone described by Hood et al. (Hood et al., 2011, 2012).

In contrast to the central patterns AT5 (superior central) and AT12 (inferior central), ATs 7 and 11 appear to follow the nerve fibre bundle anatomy whereas ATs 5 and 12 are more diffuse, without clear arcuate-like patterns. These patterns have been described as not typically glaucomatous (Yousefi et al., 2018), and could represent papillomacular bundle damage in glaucoma or non-glaucomatous macular pathology. Arcuate patterns were reported as the most common central defect in 10-2 HVFs (Wang et al., 2020a). For this reason, the central loss in ATs 7 and 11 may be more associated with rapid glaucoma progression than the diffuse central defects ATs 5 and 12.

The Role of Baseline Disease Severity

We further explored how the distribution of archetypes changes across glaucoma severity within each progression group. As expected, the proportion of normal fields reduces as the disease severity increases in both groups. Interestingly, inferior archetypes were more common in rapid progressors with moderate glaucoma at baseline whereas the superior altitudinal defect was more common in rapid progressors with severe glaucoma. For non-rapid progressors, the frequencies of all archetypes increased as the disease severity increased – of note, non-rapid progressors tended to have greater proportions of diffuse loss (AT2 diffuse loss and AT4 circumferential loss) as disease severity increased. Non-rapid progressors with severe disease also had a higher frequency of AT7 dominant patterns, though AT7 was still more common in rapid progressors as shown by the overall frequency and mean weight.

These findings suggest a relationship between the baseline disease severity and the pattern of functional loss. Patients with moderate glaucoma and inferior defects may progress rapidly, suggesting that inferior arcuate bundles may be more susceptible to early damage. Patients with severe glaucoma and superior altitudinal loss may not have ‘burnt out’ but may continue to progress rapidly and require aggressive treatment. Non-rapid progressors may have more diffuse patterns as disease severity increases, suggesting a different pathway of functional loss (expanding rather than deepening) (Vandersnickt et al., 2024), or perhaps co-existing non-glaucomatous pathology such as cataracts. The increased frequency of an inferior paracentral arcuate in non-rapid progressors with severe disease may suggest that

this pattern has reached a floor effect in eyes with MD <-12 dB and therefore would not experience further rapid progression. Further work comparing longitudinal progression within each subject could elucidate whether this represents a true staging pattern or is influenced by sampling and cohort composition.

Limitations

There are several limitations to this exploratory study. First, the sample size was modest, with only 12 rapid progressors with moderate glaucoma and 17 rapid progressors with severe glaucoma, thus limiting statistical power and generalisability. All analyses were descriptive cross-sectional comparisons without formal statistical testing to establish significance of observed differences.

Secondly, this was a retrospective study. Due to the training requirements of our archetype model, the first field of the latest five was set as the 'baseline' and may not represent true disease onset. We utilised the most recent five fields to categorise each eye into rapid or non-rapid progressors, though progression rates may fluctuate over time and patients could transition between either category. This cross-sectional design limited the ability to track progression trajectories for individual eyes. Only 24-2 HVFs were available with no 10-2 fields to supplement our data, which would have provided clearer insight on the extent of central involvement in the archetypes associated with rapid progression.

Another important limitation of this HFA-based archetypal analysis is the nonlinear relationship between RGC loss and visual field sensitivity decline (Hood et al., 2007). Up to 30-40% of RGCs may be lost before functional patterns of vision loss emerge – therefore, eyes with predominantly normal archetypes may include those with insufficient RGC loss to manifest functionally on HFA testing.

Lastly, this was an exploratory study assessing the utility of archetypal analysis to explore baseline visual field phenotypes between rapid and non-rapid progressors without incorporating other variables such as ocular demographics (baseline IOP, presence of disc haemorrhages, treatment intensity, changes in treatment at each field visit) or systemic demographics (migraine, hypertension or hypotension, sleep apnoea, vascular risk factors). Future prospective studies with larger cohorts, longitudinal data, central field assessment and multivariate analysis would be useful to validate these exploratory studies and create a comprehensive risk stratification model.

4.5 CONCLUSION

This study demonstrates that unsupervised archetypal analysis can extract consistent patterns of visual field defects to explore differences between rapid and non-rapid progressors. Eyes with inferior paracentral arcuate or superior altitudinal defects at baseline may warrant closer monitoring as they may progress more rapidly. Disease severity at baseline can further help distinguish rapid from non-rapid

progressors in conjunction with the observed visual field pattern. These preliminary findings provide a framework on which further studies can build upon to establish comprehensive risk stratification models using a patient's baseline visual field to guide clinical management.

Chapter 5. Concluding Thoughts

5.1 THESIS OVERVIEW

This thesis utilised HVF data from POAG patients to examine the relationship between POAG and CVD as well as other vascular risk factors, and to examine disease progression. We conducted three original studies, which a) characterised baseline phenotypes in POAG patients with and without CVD and other vascular risk factors b) explored the use of artificial intelligence to predict CVD from HVF data (and HVF-OCT data) and c) used unsupervised archetypal analysis to analyse baseline HVF patterns in rapid and non-rapid progressors. Specific HVF patterns may be associated with CVD and other vascular risk factors in POAG patients, or with rapid disease progression. Artificial intelligence models performed modestly at predicting CVD from HVF data.

5.2 KEY FINDINGS

In *Chapter 2*, we demonstrated that baseline superior arcuate and central defects were associated with CVD and other vascular risk factors. *Chapter 3* showed that a traditional ML model SVM was able to achieve modest performance in predicting CVD status from HVF data alone, though further optimisation is needed for clinical use. *Chapter 4* identified clinically relevant archetypal patterns and revealed differing archetype weight distributions between rapid and non-rapid progressors and across baseline disease severity. Rapid progressors with moderate disease tended to have baseline inferior defects while those with severe disease had a baseline superior altitudinal defect.

These findings highlight areas of functional loss that are over-represented in POAG patients with vascular comorbidities and in those that tend to progress rapidly. The above-chance performance of our artificial intelligence models further supports a relationship between POAG and CVD. It is likely that this relationship is part of a broader and more complex dynamic interplay of systemic and ocular risk factors as outlined in *Chapter 1* (i.e., dyslipidaemia, BP, OPP, vascular dysfunction and oxidative stress). Overall, our findings suggest that specific arcuate nerve fibre bundles and the macula may be particularly susceptible to glaucomatous damage and progression when there is underlying vascular dysregulation.

A potential conceptual framework to integrate these findings is that systemic vascular disease contributes to vascular dysfunction and results in impaired or unstable OPP at the ONH and macula. This reduced microvascular reserve may predispose the RGCs at these regions to glaucomatous damage at IOP levels traditionally considered normal. Within this framework, the HVF patterns reported in this thesis could represent a ‘vascularly vulnerable’ POAG subgroup (with some similarities to NTG patients but remaining pathologically distinct) that experiences a combination of both IOP-independent and IOP-dependent mechanisms.

5.3 VISUAL FIELD PATTERNS

A recurring theme in this thesis is the use of spatial patterns of visual field loss to better characterise a relationship between CVD and glaucoma, and differences between non-rapid and rapid progressors. *Chapter 2* employed a set of clinician-defined visual field phenotypes informed by prior published work on common glaucomatous field loss, with simplification to allow for standardised classification between non-glaucoma clinicians. In contrast, *Chapter 4* used unsupervised archetypal analysis to derive data-driven patterns from available, real-world fields.

The resulting archetypes differ in appearance to the phenotypes defined in *Chapter 2*, reflecting differences in methodology between a) supervised, clinician-led classification and unsupervised, convex combinations of extremes b) focus on associations with cardiovascular risk factor profiles versus risk of rapid progression and c) inclusion of fields with an initial defect versus baseline field from a progression series. By including both *Chapter 2* and *Chapter 4* findings, we demonstrate that both clinician-led and data-driven visual field representations can capture meaningful aspects of functional loss in glaucoma that are relevant to cardiovascular risk and progression.

This thesis used sensitivity loss measured through SAP as the primary measure of functional loss in glaucoma, which mirrors the standard clinical practice in glaucoma. As discussed in *Chapter 1* however, emerging work suggests that sensitivity loss alone may not fully capture functional vision change and that delay abnormalities can occur in regions with apparently normal SAP sensitivity. If there was a relationship between CVD and delay in POAG, alternative perimetric methods could complement our SAP data and improve our CVD-prediction performance in *Chapter 3*.

With the limited response windows in SAP, slow responses are recorded as missed stimuli and thus delay defects may also sometimes masquerade as sensitivity loss (Nowomiejska et al., 2010). Some of the sensitivity signal in our HVFs may be mixed sensitivity and delay signals, which could affect how cleanly our phenotypes and archetypes map to CVD status or progression risk in Chapters 2 through 4.

An alternate explanation to why rapid progressors with moderate and severe disease tended to have different spatial distribution of defects at baseline in *Chapter 4* could be that the superior and inferior bundles are both vulnerable to rapid progression but suffer different functional losses over time. Superior nerve fibre bundles may be more prone to demonstrating sensitivity loss detectable with SAP in moderate disease, while inferior nerve bundles may be predominantly delay-compromised with slowed responses but preserved SAP sensitivities. As damage accumulates, these bundles may then develop sensitivity loss and manifest as superior defects on the SAP. However, this explanation remains speculative as our archetypes capture only the sensitivity-weight summaries of functional loss. Any CVD- or progression-related

effects that primarily affect delay, or cause delay defects to masquerade as sensitivity loss, may not be fully captured by our phenotypes and archetypes.

5.4 TRANSLATIONAL SIGNIFICANCE

The findings in this thesis have several clinical implications. First, baseline HVF patterns may play a larger role in clinical decision-making and risk stratification for rapid progression, particularly in patients with known CVD or vascular risk factors. This would support more individualised management strategies, such as closer surveillance intervals and stricter IOP targets. Second, our findings highlight the importance of a systemic and more integrated approach to the evaluation of POAG, with a focus on CVD and other vascular comorbidities. With further optimisation, routine HVF testing used for glaucoma monitoring may also serve a secondary function of identifying patients who warrant referral for cardiovascular assessment.

5.5 STRENGTHS, LIMITATIONS AND FUTURE DIRECTIONS

This thesis has several strengths such as the use of real-world clinical data, strict inclusion criteria for reliable fields and longitudinal follow-up for progression analysis.

Limitations include the reliance on self-reported medical history, its retrospective nature, and use of single-centre data with a resulting small dataset. Specifically, this limited the power for multivariate analysis in *Chapter 2* to address possible confounders. For the work in *Chapter 3*, the modest performance of the ML and DL models may reflect a combination of noisy CVD labels, heterogeneity within the CVD group and constraints imposed by sample size. In *Chapter 4*, the similarity in archetypal weights between rapid and non-rapid progressors may also be attributed to the constraints of our sample size. Because this thesis only utilises SAP, we are unable to comment on the relationship between CVD and delay changes in POAG, if any.

Future work should prioritise larger prospective, multi-centre studies with standardised CVD phenotyping. Specifics such as BP or OPP measurements and duration of systemic disease or therapy, and integration of other imaging modalities such as OCT angiography or 10-2 HVFs could further elucidate mechanisms of vascular dysfunction. Larger datasets would facilitate multivariate analysis to adjust for confounders and provide more robust training and testing datasets for our artificial intelligence models and archetypal analysis. Rather than collapsing vascular risk factors into a small number of predefined phenotypes, future studies could retain individual CVD variables (e.g. BP, lipid profile, cardiac history, systemic therapy) and apply singular value decomposition-based factor analysis to derive a smaller set of latent cardiovascular components such as BP-related vascular risk, metabolic risk, cardiac structural disease etc. With larger datasets, we could collect more visual field descriptors e.g. archetypal weights and global indices, then use multivariate techniques such as canonical correlation analysis to jointly decompose the cardiovascular and visual field domains to identify the principal hidden dimensions

linking systemic vascular status to patterns of glaucomatous functional loss. If feasible, perimetric measures of response delay could be integrated alongside sensitivity measures through objective or saccadic perimetry platforms.

Further work is necessary to create and validate HVF-based risk scores that integrate HVF phenotypes, archetypal weights and systemic data to identify POAG patients at increased risk of rapid progression and blindness. Interventional studies that assess the effect of optimising vascular disease and IOP on glaucoma progression would provide strong evidence for a causal role of vascular dysregulation in POAG and support the development of more comprehensive vascular models of care.

References

Abe, R. Y., Diniz-Filho, A., Costa, V. P., Gracitelli, C. P. B., Baig, S., & Medeiros, F. A. (2016). The Impact of Location of Progressive Visual Field Loss on Longitudinal Changes in Quality of Life of Patients with Glaucoma. *Ophthalmology*, *123*(3), 552–557. https://doi.org/10.1016/j.ophtha.2015.10.046

Akter, N., Fletcher, J., Perry, S., Simunovic, M. P., Briggs, N., & Roy, M. (2022). Glaucoma diagnosis using multi-feature analysis and a deep learning technique. *Scientific Reports*, *12*, 8064. https://doi.org/10.1038/s41598-022-12147-y

Aldarrab, A., Jarallah, O. J. A., & Balawi, H. B. A. (2023). Association of diabetes, fasting glucose, and the risk of glaucoma: a systematic review and meta-analysis. *Eur Rev Med Pharmacol* Sci, 27(6):2419-2427. *https://doi.org/10.26355/eurrev_202303_31776*

AlShawabkeh, M., AlRyalat, S. A., Al Bdour, M., Alni'mat, A., & Al-Akhras, M. (2024). The utilization of artificial intelligence in glaucoma: Diagnosis versus screening. *Frontiers in Ophthalmology*, *4*, 1368081. https://doi.org/10.3389/fopht.2024.1368081

Arish, M., Momeni-Moghaddam, H., Alborzi, M., Maleki, A., Daneshvar, R., & Heidari, H.-R. (2024). Peripapillary vessel density in healthy people, primary open-angle glaucoma, and normal-tension glaucoma. *European Journal of Ophthalmology*, *34*(1), 161–167. https://doi.org/10.1177/11206721231181929

Artes, P. H., Iwase, A., Ohno, Y., Kitazawa, Y., & Chauhan, B. C. (2002). Properties of Perimetric Threshold Estimates from Full Threshold, SITA Standard, and

SITA Fast Strategies. *Investigative Ophthalmology & Visual Science*, *43*(8), 2654–2659.

Ballae Ganeshrao, S., Senthil, S., Choudhari, N., Sri Durgam, S., & Garudadri, C. S. (2019). Comparison of Visual Field Progression Rates Among the High Tension Glaucoma, Primary Angle Closure Glaucoma, and Normal Tension Glaucoma. *Investigative Ophthalmology & Visual Science*, *60*(4), 889–900. https://doi.org/10.1167/iovs.18-25421

Bata, A. M., Fondi, K., Witkowska, K. J., Werkmeister, R. M., Hommer, A., Vass, C., Resch, H., Schmidl, D., Popa-Cherecheanu, A., Chua, J., Garhöfer, G., & Schmetterer, L. (2019). Optic nerve head blood flow regulation during changes in arterial blood pressure in patients with primary open-angle glaucoma. *Acta Ophthalmologica*, *97*(1), e36–e41. https://doi.org/10.1111/aos.13850

Benoist d'Azy, C., Pereira, B., Chiambaretta, F., & Dutheil, F. (2016). Oxidative and Anti-Oxidative Stress Markers in Chronic Glaucoma: A Systematic Review and Meta-Analysis. *PLOS ONE*, *11*(12), e0166915. https://doi.org/10.1371/journal.pone.0166915

Bhagat, P., Shah, A. H., & Rana, Y. (2022). *A comparative study of ocular blood flow in untreated patients of primary open-angle glaucoma, normal-tension glaucoma, and ocular hypertension*. *5*.

Bowe, A., Grünig, M., Schubert, J., Demir, M., Hoffmann, V., Kütting, F., Pelc, A., & Steffen, H.-M. (2015). Circadian Variation in Arterial Blood Pressure and Glaucomatous Optic Neuropathy—A Systematic Review and Meta-Analysis. *American Journal of Hypertension*, *28*(9), 1077–1082. https://doi.org/10.1093/ajh/hpv016

Carle, C. F., James, A. C., Kolic, M., Loh, Y.-W., & Maddess, T. (2011). High-resolution multifocal pupillographic objective perimetry in glaucoma. *Investigative Ophthalmology & Visual Science*, *52*(1), 604–610. https://doi.org/10.1167/iovs.10-5737

Chakravarti, T., Moghimi, S., De Moraes, C. G., & Weinreb, R. N. (2021). Central-most Visual Field Defects in Early Glaucoma. *Journal of Glaucoma*, *30*(3), e68–e75. https://doi.org/10.1097/IJG.0000000000001747

Chakravarti, T., Moghimi, S., & Weinreb, R. N. (2022). Prediction of Central Visual Field Severity in Glaucoma. *Journal of Glaucoma*, *31*(6), 430–437. https://doi.org/10.1097/IJG.0000000000002031

Chan, K. K. W., Tang, F., Tham, C. C. Y., Young, A. L., & Cheung, C. Y. (2017). Retinal vasculature in glaucoma: A review. *BMJ Open Ophthalmology*, *1*(1). https://doi.org/10.1136/bmjophth-2016-000032

Chan, T. C. W., Bala, C., Siu, A., Wan, F., & White, A. (2017). Risk Factors for Rapid Glaucoma Disease Progression. *American Journal of Ophthalmology*, *180*, 151–157. https://doi.org/10.1016/j.ajo.2017.06.003

Chauhan, B. C., Garway-Heath, D. F., Goñi, F. J., Rossetti, L., Bengtsson, B., Viswanathan, A. C., & Heijl, A. (2008). Practical recommendations for measuring rates of visual field change in glaucoma. *The British Journal of Ophthalmology*, *92*(4), 569–573. https://doi.org/10.1136/bjo.2007.135012

Chauhan, B. C., Malik, R., Shuba, L. M., Rafuse, P. E., Nicolela, M. T., & Artes, P. H. (2014). Rates of Glaucomatous Visual Field Change in a Large Clinical Population. *Investigative Ophthalmology & Visual Science*, *55*(7), 4135–4143. https://doi.org/10.1167/iovs.14-14643

Chen, C., Bojikian, K. D., Wen, J. C., Zhang, Q., Xin, C., Mudumbai, R. C., Johnstone, M. A., Chen, P. P., & Wang, R. K. (2017). Peripapillary retinal nerve fiber layer vascular microcirculation in eyes with glaucoma and Single-Hemifield visual field loss. *JAMA Ophthalmology*, *135*(5), 461. https://doi.org/10.1001/jamaophthalmol.2017.0261

Chen, D., Ran, E. A., Tan, T. F., Ramachandran, R., Li, F., Cheung, C., Yousefi, S., Tham, C. C. Y., Ting, D. S. W., Zhang, X., & Al-Aswad, L. A. (2023). Applications of Artificial Intelligence and Deep Learning in Glaucoma. *Asia-Pacific Journal of Ophthalmology*, *12*(1), 80–93. https://doi.org/10.1097/APO.0000000000000596

Chen, Y.-Y., Hu, H.-Y., Chu, D., Chen, H.-H., Chang, C.-K., & Chou, P. (2016). Patients with Primary Open-Angle Glaucoma May Develop Ischemic Heart Disease More Often than Those without Glaucoma: An 11-Year Population-Based Cohort Study. *PLOS ONE*, *11*(9), e0163210. https://doi.org/10.1371/journal.pone.0163210

Chen, Z., Yang, W., Yang, Y., Jiang, Y., Zhang, Y., Zhang, X., Luo, C., Wang, M., Fan, Y., Liu, P., Nathwani, N., Gazzard, G., & Yu, M. (2025). Comparison of baseline clinical characteristics and patterns of visual field defects between high-tension and normal-tension glaucoma. *British Journal of Ophthalmology*, *109*(5), 587–593. https://doi.org/10.1136/bjo-2023-324852

Cherecheanu, A. P., Garhofer, G., Schmidl, D., Werkmeister, R., & Schmetterer, L. (2013). Ocular perfusion pressure and ocular blood flow in glaucoma. *Current Opinion in Pharmacology, Neurosciences*, *13*(1), 36–42. https://doi.org/10.1016/j.coph.2012.09.003

Ch'ng, T., Chua, C., Kalsom, M. U., Azhany, Y., Gong, V., Rasool, A., & Liza-Sharmini, A. (2021). Ocular Perfusion Pressure and Severity of Glaucoma: Is There a Link? *Journal of Current Glaucoma Practice*, *15*(2), 78–85. https://doi.org/10.5005/jp-journals-10078-1305

Choi, J. A., Lee, S.-N., Jung, S.-H., Won, H.-H., & Yun, J.-S. (2023). Association of glaucoma and lifestyle with incident cardiovascular disease: A longitudinal prospective study from UK Biobank. *Scientific Reports*, *13*(1), 2712. https://doi.org/10.1038/s41598-023-29613-w

Collaborative Normal-Tension Glaucoma Study Group. The effectiveness of intraocular pressure reduction in the treatment of normal-tension glaucoma. (1998). *American Journal of Ophthalmology*, *126*(4), 498–505. https://doi.org/10.1016/S0002-9394(98)00272-4

Cutler, A., & Breiman, L. (1994). Archetypal Analysis. *Technometrics*. (world). https://www.tandfonline.com/doi/abs/10.1080/00401706.1994.10485840

Dascalu, A. M., Stana, D., Nicolae, V. A., Cirstoveanu, C., Vancea, G., Serban, D., & Socea, B. (2021). Association between vascular comorbidity and glaucoma progression: A four-year observational study. *Experimental and Therapeutic Medicine*, *21*(3), 283. https://doi.org/10.3892/etm.2021.9714

De La Cruz, N., Shabaneh, O., & Appiah, D. (2021). The Association of Ideal Cardiovascular Health and Ocular Diseases Among US Adults. *The American Journal of Medicine*, *134*(2), 252-259.e1. https://doi.org/10.1016/j.amjmed.2020.06.004

Dervenis, N., Coleman, A. L., Harris, A., Wilson, M. R., Yu, F., Anastasopoulos, E., Founti, P., Pappas, T., Kilintzis, V., & Topouzis, F. (2019). Factors Associated With Retinal Vessel Diameters in an Elderly Population: The Thessaloniki Eye

Study. *Investigative Ophthalmology & Visual Science*, *60*(6), 2208–2217. https://doi.org/10.1167/iovs.18-26276

Di Russo, F., Martínez, A., Sereno, M. I., Pitzalis, S., & Hillyard, S. A. (2002). Cortical sources of the early components of the visual evoked potential. *Human Brain Mapping*, *15*(2), 95–111. https://doi.org/10.1002/hbm.10010

Diabetes and risk of glaucoma: Systematic review and a Meta-analysis of prospective cohort studies. (2017). *International Journal of Ophthalmology*. https://doi.org/10.18240/ijo.2017.09.16

Ding, X., Chang, R. T., Guo, X., Liu, X., Johnson, C. A., Holden, B. A., & He, M. (2016). Visual field defect classification in the Zhongshan Ophthalmic Center–Brien Holden Vision Institute High Myopia Registry Study. *British Journal of Ophthalmology*, *100*(12), 1697–1702. https://doi.org/10.1136/bjophthalmol-2015-307942

Elze, T., Pasquale, L. R., Shen, L. Q., Chen, T. C., Wiggs, J. L., & Bex, P. J. (2015). Patterns of functional vision loss in glaucoma determined with archetypal analysis. *Journal of the Royal Society Interface*, *12*(103), 20141118. https://doi.org/10.1098/rsif.2014.1118

Funk, R. O., Hodge, D. O., Kohli, D., & Roddy, G. W. (2022). Multiple Systemic Vascular Risk Factors Are Associated With Low-Tension Glaucoma. *Journal of Glaucoma*, *31*(1), 15–22. https://doi.org/10.1097/IJG.0000000000001964

Galarza, P., Parnasa, E., Guttmann, N., & Kruger, J. M. (2021). Artifactual Visual Field Defects Identified on Technically Reliable Visual Field Studies in a Neuro-Ophthalmology Practice. *Eye and Brain*, *13*, 79–88. https://doi.org/10.2147/EB.S274523

Gardiner, S. K., Swanson, W. H., Goren, D., Mansberger, S. L., & Demirel, S. (2014). Assessment of the reliability of standard automated perimetry in regions of glaucomatous damage. *Ophthalmology*, *121*(7), 1359–1369. https://doi.org/10.1016/j.ophtha.2014.01.020

Garg, A., De Moraes, C. G., Cioffi, G. A., Girkin, C. A., Medeiros, F. A., Weinreb, R. N., Zangwill, L., & Liebmann, J. M. (2018). Baseline 24-2 Central Visual Field Damage is Predictive of Global Progressive Field Loss. *American Journal of Ophthalmology*, *187*, 92–98. https://doi.org/10.1016/j.ajo.2018.01.001

Garhöfer, G., Bata, A. M., Popa-Cherecheanu, A., Hommer, A., Vass, C., Resch, H., Schmidl, D., Werkmeister, R. M., & Schmetterer, L. (2022). Retinal Oxygen Extraction in Patients with Primary Open-Angle Glaucoma. *International Journal of Molecular Sciences*, *23*(17), 10152. https://doi.org/10.3390/ijms231710152

Garway-Heath, D. F., Poinoosawmy, D., Fitzke, F. W., & Hitchings, R. A. (2000). Mapping the visual field to the optic disc in normal tension glaucoma eyes. *Ophthalmology*, *107*(10), 1809–1815. https://doi.org/10.1016/s0161-6420(00)00284-0

Gerber, A. L., Harris, A., Siesky, B., Lee, E., Schaab, T. J., Huck, A., & Amireskandari, A. (2015). Vascular Dysfunction in Diabetes and Glaucoma: A Complex Relationship Reviewed. *J Glaucoma*, *24*(6).

Germano, R. A. S., Germano, C. S., Susanna, F. N., & Susanna, R. (2022). Patterns of Visual Field Loss in Early, Moderate, and Severe Stages of Open Angle Glaucoma. *Journal of Glaucoma*, *31*(7), 609. https://doi.org/10.1097/IJG.0000000000001986

Gordon, M. O., Heuer, D. K., Higginbotham, E. J., Parrish, R. K., Liu, L., Brandt, J. D., Huecker, J. B., Miller, J. P., Perera, C., Xie, C., Keltner, J. L., Johnson, C. A., Gardiner, S. K., Liebmann, J. M., & Kass, M. A. (2025). Visual Field Progression in the Ocular Hypertension Treatment Study. *American Journal of Ophthalmology*, *271*, 360–370. https://doi.org/10.1016/j.ajo.2024.11.017

Harada, T., Harada, C., Nakamura, K., Quah, H.-M. A., Okumura, A., Namekata, K., Saeki, T., Aihara, M., Yoshida, H., Mitani, A., & Tanaka, K. (2007). The potential role of glutamate transporters in the pathogenesis of normal tension glaucoma. *The Journal of Clinical Investigation*, *117*(7), 1763–1770. https://doi.org/10.1172/JCI30178

Heijl, A. (2012). *The Field Analyzer Primer: Effective Perimetry*. Carl Zeiss Meditec Incorporated.

Hodapp, E., Parrish, R. K., & Anderson, D. R. (1993). *Clinical decisions in glaucoma*. Mosby.

Hood, D. C., Anderson, S. C., Wall, M., & Kardon, R. H. (2007). Structure versus function in glaucoma: An application of a linear model. *Investigative Ophthalmology & Visual Science*, *48*(8), 3662–3668. https://doi.org/10.1167/iovs.06-1401

Hood, D. C., Bach, M., Brigell, M., Keating, D., Kondo, M., Lyons, J. S., Marmor, M. F., McCulloch, D. L., & Palmowski-Wolfe, A. M. (2012). ISCEV standard for clinical multifocal electroretinography (mfERG) (2011 edition). *Documenta Ophthalmologica. Advances in Ophthalmology*, *124*(1), 1–13. https://doi.org/10.1007/s10633-011-9296-8

Hood, D. C., Raza, A. S., De Moraes, C. G. V., Odel, J. G., Greenstein, V. C., Liebmann, J. M., & Ritch, R. (2011). Initial Arcuate Defects within the Central

10 Degrees in Glaucoma. *Investigative Opthalmology & Visual Science*, *52*(2), 940. https://doi.org/10.1167/iovs.10-5803

Hood, D. C., Raza, A. S., De Moraes, C. G. V., Liebmann, J. M., & Ritch, R. (2012). Glaucomatous damage of the macula. *Progress in Retinal and Eye Research*, *32*, 1–21. https://doi.org/10.1016/j.preteyeres.2012.08.003

Horani, A., Frenkel, S., & Blumenthal, E. Z. (2007). Test-Retest Variability in Visual Field Testing Using Frequency Doubling Technology. *European Journal of Ophthalmology*, *17*(2), 203–207. https://doi.org/10.1177/112067210701700209

Horwitz, A., Klemp, M., Jeppesen, J., Tsai, J. C., Torp-Pedersen, C., & Kolko, M. (2017). Antihypertensive Medication Postpones the Onset of Glaucoma: Evidence From a Nationwide Study. *Hypertension*, *69*(2), 202–210. https://doi.org/10.1161/HYPERTENSIONAHA.116.08068

Hu, W., Lin, Z., Clark, M., Henwood, J., Shang, X., Chen, R., Kiburg, K., Zhang, L., Ge, Z., van Wijngaarden, P., Zhu, Z., & He, M. (2025). Real-world feasibility, accuracy and acceptability of automated retinal photography and AI-based cardiovascular disease risk assessment in Australian primary care settings: A pragmatic trial. *NPJ Digital Medicine*, *8*(1), 122. https://doi.org/10.1038/s41746-025-01436-1

Huang, X., Islam, M. R., Akter, S., Ahmed, F., Kazami, E., Serhan, H. A., Abd-alrazaq, A., & Yousefi, S. (2023). Artificial intelligence in glaucoma: Opportunities, challenges, and future directions. *BioMedical Engineering OnLine*, *22*, 126. https://doi.org/10.1186/s12938-023-01187-8

Hulsman, C. A. A., Vingerling, J. R., Hofman, A., Witteman, J. C. M., & de Jong, P. T. V. M. (2007). Blood Pressure, Arterial Stiffness, and Open-angle

Glaucoma: The Rotterdam Study. *Archives of Ophthalmology*, *125*(6), 805–812. https://doi.org/10.1001/archopht.125.6.805

Hwang, J. C., Konduru, R., Zhang, X., Tan, O., Francis, B. A., Varma, R., Sehi, M., Greenfield, D. S., Sadda, S. R., & Huang, D. (2012). Relationship among Visual Field, Blood Flow, and Neural Structure Measurements in Glaucoma. *Investigative Ophthalmology & Visual Science*, *53*(6), 3020–3026. https://doi.org/10.1167/iovs.11-8552

Jackson, A. B., Martin, K. R., Coote, M. A., Medeiros, F. A., Girkin, C. A., Fazio, M. A., Liebmann, J. M., De Moraes, C. G., Weinreb, R. N., Zangwill, L. M., & Wu, Z. (2023). Fast Progressors in Glaucoma: Prevalence Based on Global and Central Visual Field Loss. *Ophthalmology*, *130*(5), 462–468. https://doi.org/10.1016/j.ophtha.2023.01.008

Jiang, J., Ye, C., Zhang, C., Ye, W., Wang, X., Shang, X., Xu, X., Zhang, H., Zhang, S., Zheng, J., Zuo, J., Hu, J., Congdon, N., Lu, F., & Liang, Y. (2021). Intraocular asymmetry of visual field defects in primary angle-closure glaucoma, high-tension glaucoma, and normal-tension glaucoma in a Chinese population. *Scientific Reports*, *11*, 11674. https://doi.org/10.1038/s41598-021-91173-8

Jimenez-Aragon, F., Garcia-Martin, E., Larrosa-Lopez, R., Artigas-Martín, J. M., Seral-Moral, P., & Pablo, L. E. (2013). Role of Color Doppler Imaging in Early Diagnosis and Prediction of Progression in Glaucoma. *BioMed Research International*, *2013*(1), 871689. https://doi.org/10.1155/2013/871689

Jo, Y. H., Kwon, J., Jeong, D., Shon, K., & Kook, M. S. (2019). Rapid Central Visual Field Progression Rate in Eyes with Open-Angle Glaucoma and Choroidal

Microvasculature Dropout. *Scientific Reports*, *9*(1), 8525. https://doi.org/10.1038/s41598-019-44942-5

Jonas, J. B., Aung, T., Bourne, R. R., Bron, A. M., Ritch, R., & Panda-Jonas, S. (2017). Glaucoma. *The Lancet*, *390*(10108), 2183–2193. https://doi.org/10.1016/S0140-6736(17)31469-1

Kamalzadeh, H., Khorrami, F., Ahmadi, A., Mirlohi, S. R., Vatankhah, M., & Choobin, N. (2025). Through the eye to the heart: A scoping review of artificial intelligence in retinal imaging for cardiovascular disease assessment. *BMC Medical Informatics and Decision Making*, *25*, 453. https://doi.org/10.1186/s12911-025-03300-4

Kang, J.-W., Park, B., & Cho, B. J. (2015). Comparison of Risk Factors for Initial Central Scotoma versus Initial Peripheral Scotoma in Normal-tension Glaucoma. *Korean Journal of Ophthalmology : KJO*, *29*(2), 102–108. https://doi.org/10.3341/kjo.2015.29.2.102

Keltner, J. L., Johnson, C. A., Cello, K. E., Edwards, M. A., Bandermann, S. E., Kass, M. A., Gordon, M. O., & for the Ocular Hypertension Treatment Study Group. (2003). Classification of Visual Field Abnormalities in the Ocular Hypertension Treatment Study. *Archives of Ophthalmology*, *121*(5), 643–650. https://doi.org/10.1001/archopht.121.5.643

Kim, H., & Choi, B. (2019). Nonlinear Relationship Between Blood Pressure and Glaucoma in US Adults. *American Journal of Hypertension*, *32*(3), 308–316. https://doi.org/10.1093/ajh/hpy186

Kim, H. K., Lee, W., Ryu, I. H., Kim, J. K., Kim, H., & Yoo, T. K. (2024). Association between metformin use and the risk of developing open-angle glaucoma among patients with diabetes: A retrospective cohort study and meta-analysis.

International Ophthalmology, *44*(1), 6. https://doi.org/10.1007/s10792-024-02945-w

Kim, J. H., Lee, T. Y., Lee, J. W., & Lee, K. W. (2014). Comparison of the Thickness of the Lamina Cribrosa and Vascular Factors in Early Normal-tension Glaucoma with Low and High Intraocular Pressures. *Korean Journal of Ophthalmology*, *28*(6), 473. https://doi.org/10.3341/kjo.2014.28.6.473

Kim, J., Kennedy Neary, M. T., Aschard, H., Palakkamanil, M. M., Do, R., Wiggs, J. L., Khawaja, A. P., Pasquale, L. R., Kang, J. H., & for the International Glaucoma Genetics Consortium (IGGC), UK Biobank Eye and Vision Consortium, and Modifiable Risk Factors for Glaucoma Collaboration. (2022). Statin Use in Relation to Intraocular Pressure, Glaucoma, and Ocular Coherence Tomography Parameters in the UK Biobank. *Investigative Opthalmology & Visual Science*, *63*(5), 31. https://doi.org/10.1167/iovs.63.5.31

Kim, J. M., Kim, M. S., Jang, H. J., Park, K. H., & Caprioli, J. (2012). The Association between Retinal Vessel Diameter and Retinal Nerve Fiber Layer Thickness in Asymmetric Normal Tension Glaucoma Patients. *Investigative Ophthalmology & Visual Science*, *53*(9), 5609. https://doi.org/10.1167/iovs.12-9783

Kim, J. M., Kyung, H., Shim, S. H., Azarbod, P., & Caprioli, J. (2015). Location of Initial Visual Field Defects in Glaucoma and Their Modes of Deterioration. *Investigative Ophthalmology & Visual Science*, *56*(13), 7956–7962. https://doi.org/10.1167/iovs.15-17297

Kim, K. E., Oh, S., Baek, S. U., Ahn, S. J., Park, K. H., & Jeoung, J. W. (2020). Ocular Perfusion Pressure and the Risk of Open-Angle Glaucoma: Systematic

Review and Meta-analysis. *Scientific Reports*, *10*(1), 10056. https://doi.org/10.1038/s41598-020-66914-w

Kolli, A., Sekimitsu, S., Wang, J., Segre, A., Friedman, D., Elze, T., Pasquale, L. R., Wiggs, J., & Zebardast, N. (2023). Background polygenic risk modulates the association between glaucoma and cardiopulmonary diseases and measures: An analysis from the UK Biobank. *British Journal of Ophthalmology*, *107*(8), 1112–1118. https://doi.org/10.1136/bjophthalmol-2021-320305

Kosior-Jarecka, E., Wróbel-Dudzińska, D., Łukasik, U., & Żarnowski, T. (2017). Ocular and Systemic Risk Factors of Different Morphologies of Scotoma in Patients with Normal-Tension Glaucoma. *Journal of Ophthalmology*, *2017*, 1–6. https://doi.org/10.1155/2017/1480746

Kumar, R. S., Anegondi, N., Chandapura, R. S., Sudhakaran, S., Kadambi, S. V., Rao, H. L., Aung, T., & Roy, A. S. (2016). Discriminant function of optical coherence tomography angiography to determine disease severity in glaucoma. *Investigative Ophthalmology & Visual Science*, *57*(14), 6079. https://doi.org/10.1167/iovs.16-19984

Kwon, Y. H., Fingert, J. H., Kuehn, M. H., & Alward, W. L. M. (2009, March 12). *Primary Open-Angle Glaucoma* [Review-article]. Massachusetts Medical Society. (world). The New England Journal of Medicine. https://doi.org/10.1056/NEJMra0804630

Lee, A., Shin, J. W., Lee, J. Y., Baek, M. S., & Kook, M. S. (2022). Vasculature–function relationship in open-angle glaucomatous eyes with a choroidal microvasculature dropout. *Scientific Reports*, *12*(1), 19507. https://doi.org/10.1038/s41598-022-23109-9

Lee, E. B., Hu, W., Singh, K., & Wang, S. Y. (2022). The Association among Blood Pressure, Blood Pressure Medications, and Glaucoma in a Nationwide Electronic Health Records Database. *Ophthalmology*, *129*(3), 276–284. https://doi.org/10.1016/j.ophtha.2021.10.018

Lee, E. J., Kim, T.-W., Kim, J.-A., & Kim, J.-A. (2018). Central Visual Field Damage and Parapapillary Choroidal Microvasculature Dropout in Primary Open-Angle Glaucoma. *Ophthalmology*, *125*(4), 588–596. https://doi.org/10.1016/j.ophtha.2017.10.036

Lee, J. S., Bae, H. W., Park, S., Kim, C. Y., & Lee, S. Y. (2022). Systemic Arterial Stiffness Is Associated With Structural Progression in Early Open-Angle Glaucoma. *Investigative Opthalmology & Visual Science*, *63*(3), 28. https://doi.org/10.1167/iovs.63.3.28

Lee, J. Y., Shin, J. W., Song, M. K., Hong, J. W., & Kook, M. S. (2021). An Increased Choroidal Microvasculature Dropout Size is Associated With Progressive Visual Field Loss in Open-Angle Glaucoma. *American Journal of Ophthalmology*, *223*, 205–219. https://doi.org/10.1016/j.ajo.2020.10.018

Lee, N. Y., Jung, Y., Han, K., & Park, C. K. (2017). Fluctuation in systolic blood pressure is a major systemic risk factor for development of primary open-angle glaucoma. *Scientific Reports*, *7*(1), 43734. https://doi.org/10.1038/srep43734

Lee, N. Y., Shin, D. Y., & Park, C. K. (2024). Associations of long-term fluctuation in blood pressure and ocular perfusion pressure with visual field progression in normal-tension glaucoma. *BMC Ophthalmology*, *24*(1), 209. https://doi.org/10.1186/s12886-024-03454-1

Lee, S. H., Kim, G. A., Lee, W., Bae, H. W., Seong, G. J., & Kim, C. Y. (2017). Vascular and metabolic comorbidities in open-angle glaucoma with low- and high-teen intraocular pressure: A cross-sectional study from South Korea. *Acta Ophthalmologica*, *95*(7), e564–e574. https://doi.org/10.1111/aos.13487

Lee, T., Bae, H. W., Seong, G. J., Kim, C. Y., & Lee, S. Y. (2021). High Pulse Wave Velocity Is Associated With Decreased Macular Vessel Density in Normal-Tension Glaucoma. *Investigative Ophthalmology & Visual Science*, *62*(10), 12. https://doi.org/10.1167/iovs.62.10.12

Lee, Y., & Seo, J. H. (2024). Potential Causal Association Between Atrial Fibrillation/Flutter and Primary Open-Angle Glaucoma: A Two-Sample Mendelian Randomisation Study. *Journal of Clinical Medicine*, *13*(24), 7670. https://doi.org/10.3390/jcm13247670

Leske, M. C., Heijl, A., Hyman, L., & Bengtsson, B. (1999). Early manifest glaucoma trial. *Ophthalmology*, *106*(11), 2144–2153. https://doi.org/10.1016/S0161-6420(99)90497-9

Leung, G., Grant, A., Garas, A. N., Li, G., & Freeman, E. E. (2023). A Systematic Review and Meta-analysis of Systemic Antihypertensive Medications With Intraocular Pressure and Glaucoma. *American Journal of Ophthalmology*, *255*, 7–17. https://doi.org/10.1016/j.ajo.2023.03.014

Lindemann, F., Kuerten, D., Koch, E., Fuest, M., Fischer, C., Voss, A., & Plange, N. (2018). Blood Pressure and Heart Rate Variability in Primary Open-Angle Glaucoma and Normal Tension Glaucoma. *Current Eye Research*, *43*(12), 1507–1513. https://doi.org/10.1080/02713683.2018.1506036

Loo, J. H., Wang, Z., & Chong, R. S. (2023). Caveolin-1 in vascular health and glaucoma: A critical vascular regulator and potential therapeutic target. *Frontiers in Medicine*, *10*. https://doi.org/10.3389/fmed.2023.1087123

Maddess, T. (2011). The influence of sampling errors on test-retest variability in Perimetry. *Investigative Ophthalmology and Visual Science*, *52*(2), 1014–1022. https://doi.org/10.1167/iovs.10-6014

Maddess, T. (2014). Modeling the relative influence of fixation and sampling errors on retest variability in perimetry. *Graefe's Archive for Clinical and Experimental Ophthalmology = Albrecht Von Graefes Archiv Fur Klinische Und Experimentelle Ophthalmologie*, *252*(10), 1611–1619. https://doi.org/10.1007/s00417-014-2751-y

Maddess, T., Carle, C. F., Kolic, M., Saraç, Ö., Essex, R. W., Rohan, E. M. F., Sabeti, F., & van Kleef, J. P. (2024). Diagnostic Power and Reproducibility of Objective Perimetry in Glaucoma. *Journal of Glaucoma*, *33*(12), 940–950. https://doi.org/10.1097/IJG.0000000000002485

Madjedi, K. M., Stuart, K. V., Chua, S. Y., Luben, R. N., Warwick, A., Pasquale, L. R., Kang, J. H., Wiggs, J. L., Lentjes, M. A., Aschard, H., Sattar, N., Foster, P. J., Khawaja, A. P., Chia, M., Do, R., Kastner, A., Kim, J., Montesano, G., Atan, D., Zheng, Y. (2022). The Association between Serum Lipids and Intraocular Pressure in 2 Large United Kingdom Cohorts. *Ophthalmology*, *129*(9), 986–996. https://doi.org/10.1016/j.ophtha.2022.04.023

Mahmoudinezhad, G., Moghimi, S., Nishida, T., Latif, K., Yamane, M., Micheletti, E., Mohammadzadeh, V., Wu, J.-H., Kamalipour, A., Li, E., Liebmann, J. M., Girkin, C. A., Fazio, M. A., Zangwill, L. M., & Weinreb, R. N. (2023). Association Between Rate of Ganglion Cell Complex Thinning and Rate of

Central Visual Field Loss. *JAMA Ophthalmology*, *141*(1), 33. https://doi.org/10.1001/jamaophthalmol.2022.4973

Mandrekar, J. N. (2010). Receiver Operating Characteristic Curve in Diagnostic Test Assessment. *Journal of Thoracic Oncology*, *5*(9), 1315–1316. https://doi.org/10.1097/JTO.0b013e3181ec173d

Manz, K. C., Mocek, A., Höer, A., Simantiri, C., Heuck, A., Eberhardt, A., Mrosowsky, T., Zander, S., Fritz, B., Schuster, A. K., & Erb, C. (2024). Epidemiology and Treatment of Patients With Primary Open Angle Glaucoma in Germany: A Health Claims Data Analysis. *Journal of Glaucoma*. https://doi.org/10.1097/IJG.0000000000002420

Marshall, H. N., Andrew, N. H., Hassall, M., Qassim, A., Souzeau, E., Ridge, B., Nguyen, T., Fitzgerald, J., Awadalla, M. S., Burdon, K. P., Healey, P. R., Agar, A., Galanopoulos, A., Hewitt, A. W., Graham, S. L., Landers, J., Casson, R. J., & Craig, J. E. (2019). Macular Ganglion Cell–Inner Plexiform Layer Loss Precedes Peripapillary Retinal Nerve Fiber Layer Loss in Glaucoma with Lower Intraocular Pressure. *Ophthalmology*, *126*(8), 1119–1130. https://doi.org/10.1016/j.ophtha.2019.03.016

Marshall, H., Mullany, S., Han, X., Berry, E. C., Hassall, M. M., Qassim, A., Nguyen, T., Hollitt, G. L., Knight, L. S. W., Ridge, B., Schmidt, J., Crowley, C., Schulz, A., Mills, R. A., Agar, A., Galanopoulos, A., Landers, J., Healey, P. R., Graham, S. L., … Craig, J. E. (2022). Genetic Risk of Cardiovascular Disease Is Associated with Macular Ganglion Cell-Inner Plexiform Layer Thinning in an Early Glaucoma Cohort. *Ophthalmology Science*, *2*(1), 100108. https://doi.org/10.1016/j.xops.2021.100108

Marshall, H., Mullany, S., Qassim, A., Siggs, O., Hassall, M., Ridge, B., Nguyen, T., Awadalla, M., Andrew, N. H., Healey, P. R., Agar, A., Galanopoulos, A., Hewitt, A. W., MacGregor, S., Graham, S. L., Mills, R., Shulz, A., Landers, J., Casson, R. J., & Craig, J. E. (2021). Cardiovascular Disease Predicts Structural and Functional Progression in Early Glaucoma. *Ophthalmology*, *128*(1), 58–69. https://doi.org/10.1016/j.ophtha.2020.06.067

McKendrick, A. M., & Turpin, A. (2024). Understanding and identifying visual field progression. *Clinical and Experimental Optometry*, *107*(2), 122–129. https://doi.org/10.1080/08164622.2024.2316002

Meier, N. F., Lee, D.-C., Sui, X., & Blair, S. N. (2018). Physical Activity, Cardiorespiratory Fitness, and Incident Glaucoma. *Medicine & Science in Sports & Exercise*, *50*(11), 2253. https://doi.org/10.1249/MSS.0000000000001692

Melgarejo, J. D., Eijgen, J. V., Wei, D., Maestre, G. E., Al-Aswad, L. A., Liao, C.-T., Mena, L. J., Vanassche, T., Janssens, S., Verhamme, P., Zhang, Z.-Y., Keer, K. V., & Stalmans, I. (2023). Effect of 24-h blood pressure dysregulations and reduced ocular perfusion pressure in open-angle glaucoma progression. *Journal of Hypertension*, *41*(11).

Melgarejo, J. D., Lee, J. H., Petitto, M., Yépez, J. B., Murati, F. A., Jin, Z., Chávez, C. A., Pirela, R. V., Calmón, G. E., Lee, W., Johnson, M. P., Mena, L. J., Al-Aswad, L. A., Terwilliger, J. D., Allikmets, R., Maestre, G. E., & De Moraes, C. G. (2018). Glaucomatous Optic Neuropathy Associated with Nocturnal Dip in Blood Pressure. *Ophthalmology*, *125*(6), 807–814. https://doi.org/10.1016/j.ophtha.2017.11.029

Memarzadeh, F., Ying-Lai, M., Chung, J., Azen, S. P., & Varma, R. (2010). Blood Pressure, Perfusion Pressure, and Open-Angle Glaucoma: The Los Angeles Latino Eye Study. *Investigative Opthalmology & Visual Science*, *51*(6), 2872. https://doi.org/10.1167/iovs.08-2956

Midgett, D. E., Pease, M. E., Jefferys, J. L., Patel, M., Franck, C., Quigley, H. A., & Nguyen, Thao. D. (2017). The Pressure-Induced Deformation Response of the Human Lamina Cribrosa: Analysis of Regional Variations. *Acta Biomaterialia*, *53*, 123–139. https://doi.org/10.1016/j.actbio.2016.12.054

Mitchell, P., Lee, A. J., Rochtchina, E., & Wang, J. J. (2004). Open-Angle Glaucoma and Systemic Hypertension: The Blue Mountains Eye Study. *Journal of Glaucoma*, *13*(4), 319–326. https://doi.org/10.1097/00061198-200408000-00010

Mitchell, P., Leung, H., Wang, J. J., Rochtchina, E., Lee, A. J., Wong, T. Y., & Klein, R. (2005). Retinal vessel diameter and open-angle glaucoma: The Blue Mountains Eye Study. *Ophthalmology*, *112*(2), 245–250. https://doi.org/10.1016/j.ophtha.2004.08.015

Montesano, G., Rabiolo, A., Garway-Heath, D. F., Fu, D. J., Gazzard, G., Ometto, G., Crabb, D. P., & Khawaja, A. P. (2025). Association of Systemic Calcium Channel Blocker Use with Visual Field Progression in a Large Real-World Cohort from Glaucoma Clinics. *Ophthalmology Glaucoma*, *8*(4), 333–342. https://doi.org/10.1016/j.ogla.2025.03.002

Mwanza, J.-C., Oakley, J. D., Budenz, D. L., Chang, R. T., Knight, O. J., & Feuer, W. J. (2011). Macular ganglion cell-inner plexiform layer: Automated detection and thickness reproducibility with spectral domain-optical coherence

tomography in glaucoma. *Investigative Ophthalmology & Visual Science*, *52*(11), 8323–8329. https://doi.org/10.1167/iovs.11-7962

National Academies of Sciences, Engineering, and Medicine (2025). Visual Field Assessment and Disability Evaluation. *Washington, DC: The National Academies Press.*

Nislawati, R., Taufik Fadillah Zainal, A., Ismail, A., Waspodo, N., Kasim, F., & Gunawan, A. M. A. K. (2021). Role of hypertension as a risk factor for open-angle glaucoma: A systematic review and meta-analysis. *BMJ Open Ophthalmology*, *6*(1), e000798. https://doi.org/10.1136/bmjophth-2021-000798

Nowomiejska, K., Vonthein, R., Paetzold, J., Zagorski, Z., Kardon, R., & Schiefer, U. (2010). Reaction time during semi-automated kinetic perimetry (SKP) in patients with advanced visual field loss. *Acta Ophthalmologica*, *88*(1), 65–69. https://doi.org/10.1111/j.1755-3768.2008.01407.x

Nusinovici, S. (2022). *High-Density Lipoprotein 3 Cholesterol and Primary Open-Angle Glaucoma*. *129*(3).

Omodaka, K., Fujioka, S., An, G., Udagawa, T., Tsuda, S., Shiga, Y., Morishita, S., Kikawa, T., Pak, K., Akiba, M., Yokota, H., & Nakazawa, T. (2020). Structural Characterization of Glaucoma Patients with Low Ocular Blood Flow. *Current Eye Research*, *45*(10), 1302–1308. https://doi.org/10.1080/02713683.2020.1736306

Park, S. C., De Moraes, C. G., Teng, C. C. W., Tello, C., Liebmann, J. M., & Ritch, R. (2011). Initial parafoveal versus peripheral scotomas in glaucoma: Risk factors and visual field characteristics. *Ophthalmology*, *118*(9), 1782–1789. https://doi.org/10.1016/j.ophtha.2011.02.013

Park, Y. M., Park, J. W., Bae, H. W., Kim, C. Y., & Lee, K. (2023). Optic Nerve Head Morphology is Associated with the Initial Location of Structural Progression in Early Open Angle Glaucoma. *Journal of Glaucoma*, *32*(11), e145–e150. https://doi.org/10.1097/IJG.0000000000002274

Pham, V. Q., Nishida, T., Moghimi, S., Girkin, C. A., Fazio, M. A., Liebmann, J. M., Zangwill, L. M., & Weinreb, R. N. (2025). Long-Term Blood Pressure Variability and Visual Field Progression in Glaucoma. *JAMA Ophthalmology*, *143*(1), 25. https://doi.org/10.1001/jamaophthalmol.2024.4868

Plotnikov, D., Huang, Y., Khawaja, A. P., Foster, P. J., Zhu, Z., Guggenheim, J. A., & He, M. (2022). High Blood Pressure and Intraocular Pressure: A Mendelian Randomization Study. *Investigative Opthalmology & Visual Science*, *63*(6), 29. https://doi.org/10.1167/iovs.63.6.29

Posch-Pertl, L., Michelitsch, M., Wagner, G., Wildner, B., Silbernagel, G., Pregartner, G., & Wedrich, A. (2022). Cholesterol and glaucoma: A systematic review and meta-analysis. *Acta Ophthalmologica*, *100*(2), 148–158. https://doi.org/10.1111/aos.14769

Rai, B. B., Sabeti, F., Carle, C. F., & Maddess, T. (2024). Visual Field Tests: A Narrative Review of Different Perimetric Methods. *Journal of Clinical Medicine*, *13*(9), 2458. https://doi.org/10.3390/jcm13092458

Russell, M. W., Kumar, M., Li, A., Singh, R. P., & Talcott, K. E. (2024). Incidence of ocular pathology following bariatric surgery for with morbid obesity across a large United States National Database. *Eye*. https://doi.org/10.1038/s41433-024-03088-z

Sabeti, F., James, A. C., Carle, C. F., Essex, R. W., Bell, A., & Maddess, T. (2017). Comparing multifocal pupillographic objective perimetry (mfPOP) and

multifocal visual evoked potentials (mfVEP) in retinal diseases. *Scientific Reports*, *7*(1), 45847. https://doi.org/10.1038/srep45847

Sabeti, F., van Kleef, J. P., Iyer, R. M., Carle, C. F., Nolan, C. J., Chia, R. H., & Maddess, T. (2024). Discriminating early-stage diabetic retinopathy with subjective and objective perimetry. *Frontiers in Endocrinology*, *14*. https://doi.org/10.3389/fendo.2023.1333826

Saccà, S. C., Vernazza, S., Iorio, E. L., Tirendi, S., Bassi, A. M., Gandolfi, S., & Izzotti, A. (2020). Molecular changes in glaucomatous trabecular meshwork. Correlations with retinal ganglion cell death and novel strategies for neuroprotection. *Progress in Brain Research*, *256*(1), 151–188. https://doi.org/10.1016/bs.pbr.2020.06.003

Saks, D. G., Schulz, A., Qassim, A., Marshall, H., Hewitt, A. W., MacGregor, S., Craig, J. E., & Graham, S. L. (2023). Genetic risk of glaucoma is associated with vascular and retinal nerve fibre wedge defects. *Acta Ophthalmologica*, *102*(2), e185–e194. https://doi.org/10.1111/aos.15775

Schiefer, U., Papageorgiou, E., Sample, P. A., Pascual, J. P., Selig, B., Krapp, E., & Paetzold, J. (2010). Spatial Pattern of Glaucomatous Visual Field Loss Obtained with Regionally Condensed Stimulus Arrangements. *Investigative Ophthalmology & Visual Science*, *51*(11), 5685–5689. https://doi.org/10.1167/iovs.09-5067

Scott, T. D., Guzman Aparicio, M. A., Ratanawongphaibul, K., Lee, H., Zemplenyi, M., Tsikata, E., Margeta, M. A., Ondeck, C. L., Coleman, A. L., Yu, F., de Boer, J. F., & Chen, T. C. (2025). Comparison of Event-based Analysis Versus Trend-based Analysis in the Detection of Glaucoma Progression by

Optical Coherence Tomography 3-Dimensional Rim Measurements. *Journal of Glaucoma*, *34*(8), 616–624. https://doi.org/10.1097/IJG.0000000000002573

Shin, D. Y., Hong, K. E., Lee, N. Y., Park, C. K., & Park, H. Y. L. (2022). Association of choroidal blood flow with autonomic dysfunction in patients with normal tension glaucoma. *Scientific Reports*, *12*(1), 5136. https://doi.org/10.1038/s41598-022-09162-4

Shoji, T., Zangwill, L. M., Akagi, T., Saunders, L. J., Yarmohammadi, A., Manalastas, P. I. C., Penteado, R. C., & Weinreb, R. N. (2017). Progressive Macula Vessel Density Loss in Primary Open-Angle Glaucoma: A Longitudinal Study. *American Journal of Ophthalmology*, *182*, 107–117. https://doi.org/10.1016/j.ajo.2017.07.011

Shoshani, Y., Harris, A., Shoja, M. M., Arieli, Y., Ehrlich, R., Primus, S., Ciulla, T., Cantor, A., Wirostko, B., & Siesky, B. A. (2012). Impaired ocular blood flow regulation in patients with open-angle glaucoma and diabetes. *Clinical and Experimental Ophthalmology*.

Singh, P., & Rijal, A. (2020). Pattern of Visual Field Defects in Newly Diagnosed Primary Open Angle Glaucoma Patients Attending Tertiary Care Hospital, Kathmandu, Nepal. *Nepal Medical College Journal*, *22*(4), 203–210. https://doi.org/10.3126/nmcj.v22i4.34181

Singh, R. K., Smith, S., Fingert, J., Gordon, M., Kass, M., Scheetz, T., Segrè, A. V., Wiggs, J., Elze, T., & Zebardast, N. (2024). Machine Learning–Derived Baseline Visual Field Patterns Predict Future Glaucoma Onset in the Ocular Hypertension Treatment Study. *Investigative Ophthalmology & Visual Science*, *65*(2), 35. https://doi.org/10.1167/iovs.65.2.35

Singh, S., Patel, N. A., Soundararajan, A., & Pattabiraman, P. P. (2024). High Glucose-Induced Transcriptomic Changes in Human Trabecular Meshwork Cells. *Research Square*, rs.3.rs-5690041. https://doi.org/10.21203/rs.3.rs-5690041/v1

Stein, J. D., Newman-Casey, P. A., Talwar, N., Nan, B., Richards, J. E., & Musch, D. C. (2012). The Relationship Between Statin Use and Open-Angle Glaucoma. *Ophthalmology*, *119*(10), 2074–2081. https://doi.org/10.1016/j.ophtha.2012.04.029

Su, W.-W., Hsieh, S.-S., Cheng, S.-T., Su, C.-W., Wu, W.-C., & Chen, H. S.-L. (2018). Visual Subfield Progression in Glaucoma Subtypes. *Journal of Ophthalmology*, *2018*, 7864219. https://doi.org/10.1155/2018/7864219

Sugisaki, K., Inoue, T., Yoshikawa, K., Kanamori, A., Yamazaki, Y., Ishikawa, S., Uchida, K., Iwase, A., Araie, M., Araie, M., Tomidokoro, A., Sugisaki, K., Ryo, A., Murata, H., Tanihara, H., Inatani, M., Inoue, T., Yoshikawa, K., Negi, A., … Iwase, A. (2022). Factors Threatening Central Visual Function of Patients with Advanced Glaucoma. *Ophthalmology*, *129*(5), 488–497. https://doi.org/10.1016/j.ophtha.2021.11.025

Suzuki, Y., & Kiyosawa, M. (2022). Cardiac Hypertrophy May Be a Risk Factor for the Development and Severity of Glaucoma. *Biomedicines*, *10*(3), 677. https://doi.org/10.3390/biomedicines10030677

Szanto, D., Linton, E., & Wall, M. (2025). Archetypal Analysis Reveals Consistent Visual Field Patterns for Stimulus Size III and Size Modulation Perimetry in Glaucoma. *Translational Vision Science & Technology*, *14*(10), 12. https://doi.org/10.1167/tvst.14.10.12

Szanto, D., Wall, M., Chong, L. X., Woods, B., Elze, T., Wang, J.-K., Garvin, M., Kardon, R., & Kupersmith, M. J. (2024). Archetypal Analysis Reveals Consistent Visual Field Patterns for Stimulus Sizes III and V in Glaucoma and NAION. *Translational Vision Science & Technology*, *13*(12), 15. https://doi.org/10.1167/tvst.13.12.15

Takeo Fukuchi. (2010). Progression rate of total, and upper and lower visual field defects in open-angle glaucoma patients. *Clinical Ophthalmology*, 1315. https://doi.org/10.2147/OPTH.S13101

Takeuchi, R., Enomoto, N., Ishida, K., Anraku, A., & Tomita, G. (2019). Factors Related to Superior and Inferior Hemifield Defects in Primary Open-Angle Glaucoma. *Journal of Ophthalmology*, *2019*, 4705485. https://doi.org/10.1155/2019/4705485

Tan, J. C. K., Yohannan, J., Ramulu, P. Y., Kalloniatis, M., Crabb, D. P., Crowston, J., & Phu, J. (2025). Visual field testing in glaucoma using the Swedish Interactive Thresholding Algorithm (SITA). *Survey of Ophthalmology*, *70*(1), 141–152. https://doi.org/10.1016/j.survophthal.2024.09.005

Tang, B., Li, S., Cao, W., & Sun, X. (2019). The Association of Oxidative Stress Status with Open-Angle Glaucoma and Exfoliation Glaucoma: A Systematic Review and Meta-Analysis. *Journal of Ophthalmology*, *2019*, 1–14. https://doi.org/10.1155/2019/1803619

Tao, A., Liang, Y., Chen, J., Hu, H., Huang, Q., Zheng, J., Ye, C., & Lu, F. (2020). Structure-function correlation of localized visual field defects and macular microvascular damage in primary open-angle glaucoma. *Microvascular Research*, *130*, 104005. https://doi.org/10.1016/j.mvr.2020.104005

Tatham, A. J., Miki, A., Weinreb, R. N., Zangwill, L. M., & Medeiros, F. A. (2014). Defects of the lamina cribrosa in eyes with localized retinal nerve fiber layer loss. *Ophthalmology*, *121*(1), 110–118. https://doi.org/10.1016/j.ophtha.2013.08.018

Thakur, A., Goldbaum, M., & Yousefi, S. (2020). Convex Representations Using Deep Archetypal Analysis for Predicting Glaucoma. *IEEE Journal of Translational Engineering in Health and Medicine*, *8*, 1–7. https://doi.org/10.1109/JTEHM.2020.2982150

Tham, Y.-C., Li, X., Wong, T. Y., Quigley, H. A., Aung, T., & Cheng, C.-Y. (2014). Global Prevalence of Glaucoma and Projections of Glaucoma Burden through 2040: A Systematic Review and Meta-Analysis. *Ophthalmology*, *121*(11), 2081–2090. https://doi.org/10.1016/j.ophtha.2014.05.013

Tham, Y.-C., Lim, S.-H., Gupta, P., Aung, T., Wong, T. Y., & Cheng, C.-Y. (2018). Inter-relationship between ocular perfusion pressure, blood pressure, intraocular pressure profiles and primary open-angle glaucoma: The Singapore Epidemiology of Eye Diseases study. *British Journal of Ophthalmology*, *102*(10), 1402–1406. https://doi.org/10.1136/bjophthalmol-2017-311359

Thepass, G., Lemij, H. G., Vermeer, K. A., van der Steen, J., & Pel, J. J. M. (2021). Slowed Saccadic Reaction Times in Seemingly Normal Parts of Glaucomatous Visual Fields. *Frontiers in Medicine*, *8*. https://doi.org/10.3389/fmed.2021.679297

Thiermeier, N., Lämmer, R., Mardin, C., & Hohberger, B. (2021). *Erlanger Glaucoma Registry: Effect of a Long-Term Therapy with Statins and Acetyl Salicylic Acid on Glaucoma Conversion and Progression*.

Thonginnetra, O., Greenstein, V. C., Chu, D., Liebmann, J. M., Ritch, R., & Hood, D. C. (2010). Normal Versus High Tension Glaucoma: A Comparison of Functional and Structural Defects. *Journal of Glaucoma*, *19*(3), 151–157. https://doi.org/10.1097/IJG.0b013e318193c45c

Tian, Y., Zang, M., Sharma, A., Gu, S. Z., Leshno, A., & Thakoor, K. A. (2023). Glaucoma Progression Detection and Humphrey Visual Field Prediction Using Discriminative and Generative Vision Transformers. In B. Antony, H. Chen, H. Fang, H. Fu, C. S. Lee, & Y. Zheng (Eds), *Ophthalmic Medical Image Analysis* (pp. 62–71). Springer Nature Switzerland. https://doi.org/10.1007/978-3-031-44013-7_7

Trott, M. (2022). *Eye disease and mortality, cognition, disease, and modifiable risk factors: An umbrella review of meta-analyses of observational studies*.

Ueda, Y., Suda, K., Kameda, T., Ikeda, H., Miyake, M., Hasegawa, T., Numa, S., & Tsujikawa, A. (2024). Risk factors for progression of primary open angle glaucoma with lower normal intraocular pressure. *Ophthalmic Research*. https://doi.org/10.1159/000536314

Ung, L., Pattamatta, U., Carnt, N., Wilkinson-Berka, J. L., Liew, G., & White, A. J. R. (2017). Oxidative stress and reactive oxygen species: A review of their role in ocular disease. *Clinical Science*.

Valera-Cornejo, D. A., Loayza-Gamboa, W., Herrera-Quiroz, J., Alvarado-Villacorta, R., Córdova-Crisanto, L., Valderrama-Albino, V., & Pantoja-Dávalos, N. (2019). *Changes on Confocal Scanning Laser Ophthalmoscopy with the Heidelberg Retinal Tomography after a Cardiac Catheterism in a Patient with Progressive Glaucoma*.

Vandersnickt, M. F., Van Eijgen, J., Lemmens, S., Stalmans, I., Pinto, L. A., & Vandewalle, E. M. (2024). Visual field patterns in glaucoma: A systematic review. *Saudi Journal of Ophthalmology*, *38*(4), 306–315. https://doi.org/10.4103/sjopt.sjopt_143_24

Vergroesen, J. E., Thee, E. F., Ahmadizar, F., Van Duijn, C. M., Stricker, B. H., Kavousi, M., Klaver, C. C. W., & Ramdas, W. D. (2022). Association of Diabetes Medication With Open-Angle Glaucoma, Age-Related Macular Degeneration, and Cataract in the Rotterdam Study. *JAMA Ophthalmology*, *140*(7), 674. https://doi.org/10.1001/jamaophthalmol.2022.1435

Von Hanno, T., Hareide, L. L., Småbrekke, L., Morseth, B., Sneve, M., Erke, M. G., Mathiesen, E. B., & Bertelsen, G. (2022). Macular Layer Thickness and Effect of BMI, Body Fat, and Traditional Cardiovascular Risk Factors: The Tromsø Study. *Investigative Opthalmology & Visual Science*, *63*(9), 16. https://doi.org/10.1167/iovs.63.9.16

Vrijling, A. C. L., De Boer, M. J., Renken, R. J., Marsman, J. B. C., Grillini, A., Petrillo, C. E., Heutink, J., Jansonius, N. M., & Cornelissen, F. W. (2023). Stimulus contrast, pursuit mode, and age strongly influence tracking performance on a continuous visual tracking task. *Vision Research*, *205*, 108188. https://doi.org/10.1016/j.visres.2023.108188

Vrijling, A. C. L., de Boer, M. J., Renken, R. J., Marsman, J.-B. C., Heutink, J., Cornelissen, F. W., & Jansonius, N. M. (2025). Detecting and Quantifying Glaucomatous Visual Function Loss With Continuous Visual Stimulus Tracking: A Case-Control Study. *Translational Vision Science & Technology*, *14*(2), 3. https://doi.org/10.1167/tvst.14.2.3

Wang, M., Shen, L. Q., Pasquale, L. R., Boland, M. V., Wellik, S. R., De Moraes, C. G., Myers, J. S., Nguyen, T. D., Ritch, R., Ramulu, P., Wang, H., Tichelaar, J., Li, D., Bex, P. J., & Elze, T. (2020a). Artificial Intelligence Classification of Central Visual Field Patterns in Glaucoma. *Ophthalmology*, *127*(6), 731–738. https://doi.org/10.1016/j.ophtha.2019.12.004

Wang, M., Shen, L. Q., Pasquale, L. R., Boland, M. V., Wellik, S. R., De Moraes, C. G., Myers, J. S., Nguyen, T., Ritch, R., Ramulu, P., Wang, H., Tichelaar, J., Li, D., Bex, P. J., & Elze, T. (2020b). Artificial Intelligence Classification of Central Visual Field Patterns in Glaucoma. *Ophthalmology*, *127*(6), 731–738. https://doi.org/10.1016/j.ophtha.2019.12.004

Wang, M., Shen, L. Q., Pasquale, L. R., Petrakos, P., Formica, S., Boland, M. V., Wellik, S. R., De Moraes, C. G., Myers, J. S., Saeedi, O., Wang, H., Baniasadi, N., Li, D., Tichelaar, J., Bex, P. J., & Elze, T. (2019). An Artificial Intelligence Approach to Detect Visual Field Progression in Glaucoma Based on Spatial Pattern Analysis. *Investigative Ophthalmology & Visual Science*, *60*(1), 365–375. https://doi.org/10.1167/iovs.18-25568

Wang, S., & Bao, X. (2019). Hyperlipidemia, Blood Lipid Level, and the Risk of Glaucoma: A Meta-Analysis. *Investigative Opthalmology & Visual Science*, *60*(4), 1028. https://doi.org/10.1167/iovs.18-25845

Wang, Y., Hou, X.-W., Liang, G., & Pan, C.-W. (2021). Metabolomics in Glaucoma: A Systematic Review. *Investigative Ophthalmology & Visual Science*, *62*(6), 9. https://doi.org/10.1167/iovs.62.6.9

Wareham, L. K., & Calkins, D. J. (2020). The Neurovascular Unit in Glaucomatous Neurodegeneration. *Frontiers in Cell and Developmental Biology*, *8*. https://doi.org/10.3389/fcell.2020.00452

Weinreb, R. N., Aung, T., & Medeiros, F. A. (2014). The Pathophysiology and Treatment of Glaucoma: A Review. *JAMA*, *311*(18), 1901–1911. https://doi.org/10.1001/jama.2014.3192

Wen, J. C., Lee, C. S., Keane, P. A., Xiao, S., Rokem, A. S., Chen, P. P., Wu, Y., & Lee, A. Y. (2019). Forecasting future Humphrey Visual Fields using deep learning. *PloS One*, *14*(4), e0214875. https://doi.org/10.1371/journal.pone.0214875

WuDunn, D., Takusagawa, H. L., Sit, A. J., Rosdahl, J. A., Radhakrishnan, S., Hoguet, A., Han, Y., & Chen, T. C. (2021). OCT Angiography for the Diagnosis of Glaucoma: A Report by the American Academy of Ophthalmology. *Ophthalmology*, *128*(8), 1222–1235. https://doi.org/10.1016/j.ophtha.2020.12.027

Ye, S., Chang, Y., Kim, C.-W., Kwon, M.-J., Choi, Y., Ahn, J., Kim, J. M., Kim, H. S., Shin, H., & Ryu, S. (2015). Intraocular pressure and coronary artery calcification in asymptomatic men and women. *The British Journal of Ophthalmology*, *99*(7), 932–936. https://doi.org/10.1136/bjophthalmol-2014-305925

Ye, S.-T., Shang, X.-W., Huang, Y., Zhu, S., Zhu, Z.-T., Zhang, X.-L., Wang, W., Tang, S.-L., Ge, Z.-Y., Yang, X.-H., & He, M.-G. (2024). Association of age at diagnosis of diabetes with subsequent risk of age-related ocular diseases and vision acuity. *World Journal of Diabetes*, *15*(4), 697–711. https://doi.org/10.4239/wjd.v15.i4.697

Yibekal, B. T., Rai, B. B., van Kleef, J. P., Sabeti, F., Rohan, E. M. F., Nolan, C. J., & Maddess, T. (2026). Objective perimetry and diabetic retinopathy progression:

A 10-year follow-up study. *Frontiers in Endocrinology*, *16*. https://doi.org/10.3389/fendo.2025.1755262

Yoo, E., Yoo, C., Lee, T.-E., & Kim, Y. Y. (2017). Comparison of Retinal Vessel Diameter Between Open-Angle Glaucoma Patients With Initial Parafoveal Scotoma and Peripheral Nasal Step. *American Journal of Ophthalmology*, *175*, 30–36. https://doi.org/10.1016/j.ajo.2016.11.012

Yousefi, S., Sakai, H., Murata, H., Fujino, Y., Garway-Heath, D., Weinreb, R., & Asaoka, R. (2018). Asymmetric Patterns of Visual Field Defect in Primary Open-Angle and Primary Angle-Closure Glaucoma. *Investigative Ophthalmology & Visual Science*, *59*(3), 1279–1287. https://doi.org/10.1167/iovs.17-22980

Yu, E., Mercer, J., & Bennett, M. (2012). Mitochondria in vascular disease. *Cardiovascular Research*, *95*(2), 173–182. https://doi.org/10.1093/cvr/cvs111

Yuan, Y., Wang, W., Shang, X., Xiong, R., Ha, J., Zhang, L., Zhu, Z., & He, M. (2021). Association between statin use and the risks of glaucoma in Australia: a 10-year cohort study. *British Journal of Ophthalmology*, *107*(1), 66–71. https://doi.org/10.1136/bjophthalmol-2021-318789

Zhang, N., Wang, J., Li, Y., & Jiang, B. (2021). Prevalence of primary open angle glaucoma in the last 20 years: A meta-analysis and systematic review. *Scientific Reports*, *11*(1), 13762. https://doi.org/10.1038/s41598-021-92971-w

Zhao, D., Cho, J., Kim, M. H., Friedman, D. S., & Guallar, E. (2015). Diabetes, Fasting Glucose, and the Risk of Glaucoma. *Ophthalmology*, *122*(1), 72–78. https://doi.org/10.1016/j.ophtha.2014.07.051

Zhao, D., Cho, J., Kim, M. H., & Guallar, E. (2014). The Association of Blood Pressure and Primary Open-Angle Glaucoma: A Meta-analysis. *American*

Journal of Ophthalmology, *158*(3), 615-627.e9. https://doi.org/10.1016/j.ajo.2014.05.029

Zhao, Y., & Chen, X. (2017). Diabetes and risk of glaucoma: systematic review and a Meta-analysis of prospective cohort studies. *International Journal of Ophthalmology*, *10*(9), 1430–1435. https://doi.org/10.18240/ijo.2017.09.16

Zhou, B., & Tian, R. (2018). Mitochondrial dysfunction in pathophysiology of heart failure. *The Journal of Clinical Investigation*, *128*(9).

Zhou, M., Wang, W., Huang, W., & Zhang, X. (2014). Diabetes Mellitus as a Risk Factor for Open-Angle Glaucoma: A Systematic Review and Meta-Analysis. *PLOS ONE*, *9*(8), e102972. https://doi.org/10.1371/journal.pone.0102972

Appendices

Appendix 1. Demographics and ocular characteristics of eyes with and without CVD and a single observed visual field defect. Note: continuous variables age, CDR and CCT analysed using independent samples t-test. IOP, VFI, MD analysed using Mann Whitney test. * indicates statistical significance (*p<0.05*)

	CVD	No CVD	*p*
Total (number of eyes)	180	117	
Male (%)	75 (41.7%)	48 (41.0%)	0.85
Average age (in years)	66	60	<0.00*
Hypertension (%)	138 (78.0%)	50 (42.5%)	<0.00*
Diabetes (%)	43 (24.3%)	5 (4.4%)	<0.00*
Range of baseline IOP (mmHg)	13-36	14-30	
Average baseline IOP (mmHg ± SD)	20.7±4.3	20.6±3.8	0.77
Average baseline CDR	0.44	0.42	0.71
Average baseline CCT (µm ± SD)	534.7±35.2	537.9±39.0	0.01
Average VFI of included field	92.3	95.4	<0.00*
Average MD of included field (dB ± SD)	-4.4±3.0	-2.8±2.8	<0.00*

Appendix 2. 'Per defect' analysis. Odds ratios (ORs) as calculated using multinomial logistic regression for each observed visual field phenotype relative to 'no defect', for each combination of vascular risk factors compared to eyes with no risk factors. Although this analysis is limited due to the lack of independence, it is interesting to see that similar results were obtained compared to our 'per eye' analysis. Note: "na" not applicable because there were zero patients in the 'All 3" risk group.

Pattern (compared to No defect)	Risk category (compared to Nil risk)	Odds Ratio	95% CI for OR		p-value
			Lower	Upper	
Any SA	**All 3 vs Nil**	4.4	1.5	13.1	**<0.01**
	(HTN and/or DM, no CVD) vs Nil	4.0	1.6	10.5	**<0.01**
	(CVD+HTN or CVD+DM) vs Nil	9.0	3.9	20.8	**<0.01**
	(CVD only) vs Nil	6.3	1.7	22.7	**<0.01**
	Nil (reference)	1	reference category		
Any IA	**All 3 vs Nil**	3.4	1.2	9.5	**0.02**
	(HTN and/or DM, no CVD) vs Nil	1.9	0.7	4.9	0.20
	(CVD+HTN or CVD+DM) vs Nil	5.8	2.6	12.8	**<0.01**
	(CVD only) vs Nil	3.5	1.0	12.5	0.06
	Nil (reference)	1	reference category		
Any Central	**All 3 vs Nil**	4.5	1.6	12.5	**<0.01**
	(HTN and/or DM, no CVD) vs Nil	2.4	0.9	6.1	0.07
	(CVD+HTN or CVD+DM) vs Nil	6.1	2.7	13.4	**<0.01**
	(CVD only) vs Nil	4.1	1.2	14.7	**0.03**
	Nil (reference)	1	reference category		
Any Superior NS	**All 3 vs Nil**	4.1	0.2	75	0.34
	(HTN and/or DM, no CVD) vs Nil	5.3	0.4	64	0.19
	(CVD+HTN or CVD+DM) vs Nil	11.6	1.3	105	**0.03**
	(CVD only) vs Nil	36.3	3.3	395	**<0.01**
	Nil (reference)	1	reference category		
Any Inferior NS	**All 3 vs Nil**	4.1	0.2	75	0.34
	(HTN and/or DM, no CVD) vs Nil	5.3	0.4	64	0.19
	(CVD+HTN or CVD+DM) vs Nil	5.8	0.6	61	0.14
	(CVD only) vs Nil	7.3	0.4	140	0.19
	Nil (reference)	1	reference category		
Any EBS	**All 3 vs Nil**	3.6	0.9	13.9	0.07

	(HTN and/or DM, no CVD) vs Nil	0.8	0.1	4.2	0.75
	(CVD+HTN or CVD+DM) vs Nil	1.7	0.5	5.8	0.43
	(CVD only) vs Nil	4.1	0.8	20.8	0.08
	Nil (reference)	1	reference category		
Any Non-Specific	**All 3 vs Nil**	0	na		na
	(HTN and/or DM, no CVD) vs Nil	2.6	0.3	21.1	0.36
	(CVD+HTN or CVD+DM) vs Nil	2.9	0.4	19.3	0.27
	(CVD only) vs Nil	0	na		na
	Nil (reference)	1	reference category		